

USING EXPERIMENTAL DESIGN AND RESPONSE SURFACE METHODOLOGY TO
MODEL INDUCED FRACTURE GEOMETRY IN SHUBLIK SHALE

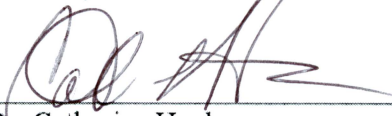
By

Venkatasai Sri Chand Poludasu



RECOMMENDED:

Dr. Obadare Awoleke
Advisory Committee Member



Dr. Catherine Hanks
Advisory Committee Member



Dr. Mohabbat Ahmadi
Advisory Committee Chair

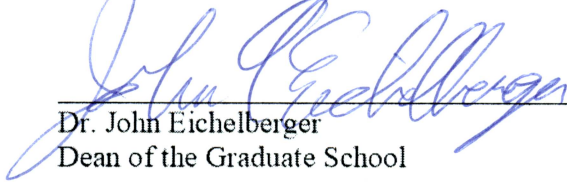


Dr. Abhijit Dandekar,
Chair, Department of Petroleum Engineering

APPROVED:



Dr. Douglas Goering
Dean, College of Engineering and Mines



Dr. John Eichelberger
Dean of the Graduate School

12/7/14

Date

USING EXPERIMENTAL DESIGN AND RESPONSE SURFACE METHODOLOGY TO
MODEL INDUCED FRACTURE GEOMETRY IN SHUBLIK SHALE

A
THESIS

Presented to the Faculty
of the University of Alaska Fairbanks

in Partial Fulfillment of the Requirements

for the Degree of

MASTER OF SCIENCE

By

Venkatasai Sri Chand Poludasu, B.Tech.

Fairbanks, Alaska

December 2014

Abstract

The Triassic Shublik Formation of the Alaska North Slope is a world-class resource rock and has been identified as the major source of many of the conventional hydrocarbon accumulations on the North Slope, including Prudhoe Bay. Recent interest in the Shublik as a potential shale resource play has highlighted the need for robust hydraulic fracture modeling and simulation of the interval, but little geologic information is available because of the remote nature of the region and the complex character of the Shublik. In this study, a methodology was developed for identifying the critical variables needed for accurate planning of a hydraulic fracturing treatment in a play like the Shublik where much of the geology remains unconstrained. These identified critical variables can be used to develop a proxy model that can be used in lieu of a numerical simulator.

This study was conducted in two stages. The first stage used 2-level fractional factorial design to identify the statistical significance of the input variables on the simulated fracture geometry. This stage was conducted in three phases, each phase incorporating progressively more complex assumptions about geology. Using the three most significant variables identified from first stage, the second stage of this study applies Box-Behnken experimental design and response surface methodology for quantifying functional relationships between input variables and the predicted fracture geometry. A pseudo 3D numerical simulator (Fracpro PT) and MATLAB were used to develop proxy models. These proxy models, typically a polynomial equation, are an easier alternative to Fracpro PT and can predict the fracture geometry with very less computational time.

The use of experimental design drastically reduces the number of simulations required to evaluate large number of variables. With only 137 simulations, 26 variables were ranked based on their statistical significance and a non-linear proxy model was developed. Predicted values of the fracture geometry obtained using the proxy models were in good agreement with the simulated values of the fracture geometry (R^2 value of 99.39% for fracture length, R^2 value of 99.54% for fracture height and R^2 value of 98.17% for fracture width).

Dedicated to:

My Family and Friends

Table of Contents

	Page
Signature Page	i
Title Page	iii
Abstract	v
Table of Contents	ix
List of Figures	xiii
List of Tables	xvii
Acknowledgments	xix
CHAPTER 1 INTRODUCTION	1
1.1 Unconventional resources	1
1.2 Shale resources.....	2
1.3 Shale resource potential in Alaska	5
1.4 Hydraulic fracturing and application to shale resource plays	8
1.5 Objective of the study	9
CHAPTER 2 LITERATURE REVIEW	11
2.1 Shublik geology	11
2.2 Data availability and geologic analog of Shublik.....	13
2.3 Conventional hydraulic fracturing theory.....	14
2.3.1 Fracture mechanics fundamentals.....	15
2.3.2 Fracturing fluid mechanics.....	17
2.3.3 Fracture propagation models	18

2.3.3.1	PKN model	19
2.3.3.2	KGD model.....	21
2.3.3.3	Radial model.....	22
2.3.3.4	3D models.....	24
2.3.3.4.1	Pseudo 3D models.....	24
2.3.3.4.2	Planar 3D models	24
2.3.3.4.3	General 3-D models.....	25
2.4	Special concerns for fracturing design in shale reservoirs	26
2.4.1	Reservoir characterization	26
2.4.2	Presence and interaction of natural fractures.....	26
2.4.3	Multi-stage hydraulic fracturing.....	28
2.4.3.1	Horizontal well design.....	28
2.4.3.2	Completion techniques.....	28
2.4.4	Fracturing fluid selection.....	30
2.4.5	Proppant selection.....	31
2.4.5.1	Proppant availability	31
2.4.5.2	Conductivity requirements.....	31
2.5	Current methodology to select optimum hydraulic fracture design.....	32
2.5.1	Pre-treatment prediction	32

2.5.2	Post-treatment evaluation.....	33
2.6	Experimental design and response surface concepts	35
2.6.1	Factorial design.....	35
2.6.2	Fractional factorial design.....	35
2.6.3	Box-Behnken design.....	36
2.6.4	Regression analysis.....	37
CHAPTER 3 Using Experimental Design and Response Surface Methodology to Model Induced Fracture Geometry of Shublik Shale.....		39
3.1	Methodology.....	39
3.2	Stage 1: Significant parameter identification.....	43
3.2.1	Phase I.....	43
3.2.2	Phase II	47
3.2.3	Phase III	50
3.3	Stage 2: Proxy model development	54
3.3.1	Box-Behnken design.....	56
3.3.2	Stage 2: Results.....	57
3.3.2.1	Fracture width at the top of the fracture	57
3.3.2.2	Fracture width at the middle of the fracture	58
3.3.2.3	Fracture width at the bottom of the fracture	60

3.3.2.4	Fracture length.....	61
3.3.2.5	Propped length.....	63
3.3.2.6	Fracture height.....	64
3.3.2.7	Propped height.....	66
3.3.2.8	Upper fracture outgrowth.....	67
3.3.2.9	Lower fracture outgrowth.....	69
3.4	Discussions.....	70
3.4.1	Stage 1.....	70
3.4.1.1	Phases I and II.....	70
3.4.1.2	Phase III.....	71
3.4.2	Stage 2.....	72
3.4.2.1	Analysis of response surfaces.....	72
3.4.2.2	Applications of proxy models.....	73
CHAPTER 4 CONCLUSIONS AND RECOMMENDATIONS.....		75
4.1	Conclusions.....	75
4.2	Recommendations.....	76
REFERENCES.....		77
Appendix A Design and Planning tables for all the three phases in Stage 1.....		83

List of Figures

	Page
Figure 1.1: Resource triangle concept for hydrocarbon resources	2
Figure 1.2: US dry gas production forecast by U.S. Energy Information Administration's AEO 2013	3
Figure 1.3: US shale gas and shale oil plays by U.S. Energy Information Administration's US shale report, 2011	4
Figure 1.4: US shale gas production estimated by U.S. Energy Information Administration	4
Figure 1.5: USGS estimates of undiscovered oil in shale resource plays, showing the potential of the Alaska North Slope shales	7
Figure 1.6: A typical hydraulic fracturing job	8
Figure 1.7: Typical multi-stage hydraulic fracturing operation in shales	9
Figure 2.1: Lithostratigraphy and corresponding gamma ray log response for Shublik shale based from one of the wells in Prudhoe Bay	12
Figure 2.2: Components of a conventional hydraulic fracture model	14
Figure 2.3: Typical rheological curve	17
Figure 2.4: Basic notation of PKN model.....	20
Figure 2.5: Basic notation of KGD model.....	22
Figure 2.6: Crossing scenario for natural fracture interaction	27
Figure 2.7: Opening scenario for natural fracture interaction.....	27
Figure 2.8: Single-stage-at-once completion system	29

Figure 2.9: Multiple-stages-at-once completion system	29
Figure 2.10: Methodology for selecting optimum fracture design	34
Figure 2.11: Box-Behnken design	36
Figure 3.1: Flowchart describing the workflow used in this study	41
Figure 3.2: Output variables estimation from the simulator fracture profile	42
Figure 3.3: Geological assumptions made in Phase I	44
Figure 3.4: Geological assumptions made in Phase II	47
Figure 3.5: Geological assumptions made in Phase III.....	51
Figure 3.6: 3D response surface plot showing the effect of krC and h_u on $width_top$	58
Figure 3.7: 3D response surface plot showing the effect of krC and h_l on $width_top$	58
Figure 3.8: 3D response surface plot showing the effect of h_l and h_u on $width_top$	58
Figure 3.9: Relationship between $width_top$ predicted by the simulator and the non-linear model from this study	58
Figure 3.10: 3D response surface plot showing the effect of krC and E_u on $width_mid$	59
Figure 3.11: 3D response surface plot showing the effect of h_r and E_u on $width_mid$	59
Figure 3.12: 3D response surface plot showing the effect of krC and h_r on $width_mid$	60
Figure 3.13: Relationship between $width_mid$ predicted by the simulator and the non-linear model from this study	60
Figure 3.14: 3D response surface plot showing the effect of v_l and E_rA on $width_bot$	61
Figure 3.15: 3D response surface plot showing the effect of E_rA and P_t on $width_bot$	61
Figure 3.16: 3D response surface plot showing the effect of P_t and v_l on $width_bot$	61
Figure 3.17: Relationship between $width_bot$ predicted by the simulator and the non-linear model.....	61

Figure 3.18: 3D response surface plot showing the effect of k_rC and h_u on *fracture_length* 62

Figure 3.19: 3D response surface plot showing the effect of h_r and h_u on *fracture_length* 62

Figure 3.20: 3D response surface plot showing the effect of k_rC and h_r on *fracture_length* 62

Figure 3.21: Relationship between *fracture_length* predicted by the simulator and the non-linear model 62

Figure 3.22: 3D response surface plot showing the effect of k_rC and h_u on *propped_length* 63

Figure 3.23: 3D response surface plot showing the effect of h_r and h_u on *propped_length* 63

Figure 3.24: 3D response surface plot showing the effect of k_rC and h_r on *propped_length* 64

Figure 3.25: Relationship between *propped_length* predicted by the simulator and the non-linear model from this study 64

Figure 3.26: 3D response surface plot showing the effect of E_rA and h_r *fracture_height* 65

Figure 3.27: 3D response surface plot showing the effect of h_r and D on *fracture_height* 65

Figure 3.28: 3D response surface plot showing the effect of E_rA and D on *fracture_height* 65

Figure 3.29: Relationship between *fracture_height* predicted by the simulator and the non-linear model from this study 65

Figure 3.30: 3D response surface plot showing the effect k_rC and E_rA on *propped_height* 66

Figure 3.31: 3D response surface plot showing the effect of h_r and E_rA on *Propped_height* 66

Figure 3.32: 3D response surface plot showing the effect of k_rC and h_r on *propped_height* 67

Figure 3.33: Relationship between *upper_outgrowth* predicted by the simulator and the non-linear model from this study 67

Figure 3.34: 3D response surface plot showing the effect of h_r and W_p *upper_outgrowth* 68

Figure 3.35: 3D response surface plot showing the effect h_r and E_rA on *upper_outgrowth* 68

Figure 3.36: 3D response surface plot showing the effect of ErA and Wp on <i>upper_outgrowth</i>	68
Figure 3.37: Relationship between <i>upper_outgrowth</i> predicted by the simulator and the non-linear model from this study	68
Figure 3.38: 3D response surface plot showing the effect of hr and Wp on <i>lower_outgrowth</i>	69
Figure 3.39: 3D response surface plot showing the effect hr and ErA on <i>lower_outgrowth</i>	69
Figure 3.40: 3D response surface plot showing the effect of ErA and Wp on <i>lower_outgrowth</i>	70
Figure 3.41: Relationship between <i>lower_outgrowth</i> predicted by the simulator and the non-linear model from this study	70

List of Tables

	Page
Table 1.1: Potential of Alaska North Slope shales compared to other major U.S. shale plays.....	6
Table 1.2: USGS Shublik Formation shale oil and shale gas assessment results.....	7
Table 2.1: Geologic characteristics of Eagle Ford Shale and Shublik Shale	13
Table 2.2: Pressure drop for Newtonian fluid in laminar flow	18
Table 3.1: Nine fracture geometry variables modeled in this study	42
Table 3.2: Variables investigated by this study in Phase I.....	45
Table 3.3: p-values of the variables evaluated in Phase I	46
Table 3.4: Variables investigated by this study in Phase II	48
Table 3.5: p-values of the variables evaluated in Phase II	49
Table 3.6: Variables investigated by this study in Phase III.....	52
Table 3.7: p-values of the variables evaluated in Phase III.....	53
Table 3.8: Three most important input variables affecting the modeled fracture geometry identified in Stage 1 of study.....	55
Table 3.9: Box-Behnken design for three variables	56
Table A.1: Factorial planning table for the 16 variables chosen in Phase I.....	83
Table A.2: Factorial design table for the 16 variables chosen in Phase I (1 being the higher and -1 being the lower end of parameter range).....	84
Table A.3: Factorial planning table for the 18 variables chosen in Phase II	85

Table A.4: Factorial design table for the 18 variables chosen in Phase II 86

Table A.5: Factorial planning table for the 26 variables chosen in Phase III 87

Table A.6: Factorial design table for the 26 variables chosen in Phase III 88

Acknowledgments

First of all, I express my sincere thanks to my principal advisor, Dr. Mohabbat Ahmadi, for his constant support, encouragement, and invaluable guidance during my graduate studies. I also greatly appreciate my advisory committee members Dr. Obadare Awoleke and Dr. Catherine Hanks for their valuable suggestions and commitment to this thesis.

The financial support from the Dean of the Graduate School at the University of Alaska Fairbanks and Alaska Department of Natural Resources are gratefully acknowledged. Special thanks to CARBO for providing the Fracpro software.

I express my deepest gratitude to my parents, Mr. Gopichand and Mrs. Kusuma Poludasu, for their unconditional love and support. Finally, I would like to thank my faculty and friends for their support during my time at UAF.

CHAPTER 1 INTRODUCTION

1.1 Unconventional resources

Due to the exponential increase in world energy consumption, the focus has shifted from conventional resources (formations which can economically produce without requiring any specialized techniques) to unconventional resources. Unconventional reservoirs can be defined as the hydrocarbon accumulations that cannot produce economic volumes of hydrocarbons without specialized extraction technologies like massive stimulation techniques. Typical unconventional reservoirs are tight sands, coalbed methane, heavy oil, gas hydrates, oil shales and shale reservoirs.

The resource triangle concept published by Masters (1979) states that all the natural resources are distributed log-normally in nature. **Figure 1.1** presents the concept of resource triangle as applied to hydrocarbon resources. The top of the resource triangle consists of the highest quality, easy to extract hydrocarbons, but these accumulations are often small in size and difficult to identify. As we go lower in the resource triangle, the reservoir quality deteriorates due to decreasing permeability and/or increasing hydrocarbon viscosity. These low quality deposits of hydrocarbons require improved technology and higher commodity prices before they can be developed and produced economically. However, the size of the deposits can be large when compared to conventional, high quality reservoirs (Rahim et al., 2012).

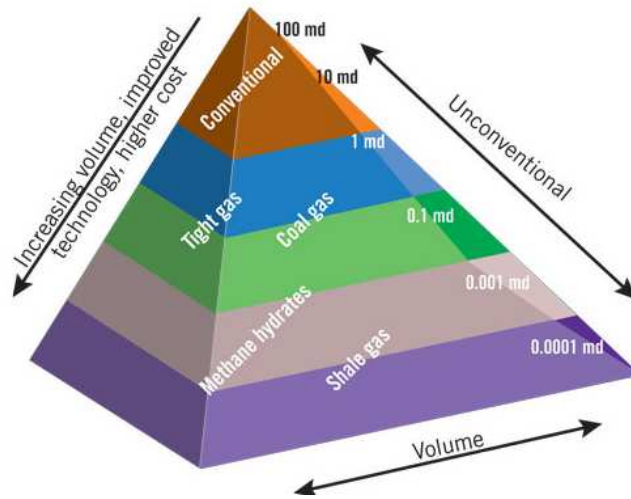


Figure 1.1: Resource triangle concept for hydrocarbon resources (Rahim et al., 2012)

1.2 Shale resources

Organic-rich shale formations are traditionally regarded as source rocks for conventional hydrocarbon accumulations. Recently, shales have been recognized as potential unconventional reservoirs for hydrocarbons, although with much lower permeability. The low permeability and porosity of shale reservoirs require specialized completions techniques to enable commercial production. Recent technological advances in horizontal drilling and hydraulic fracturing (multi-stage hydraulic fracturing) have made natural gas and oil production from low permeability shale formations a reality.

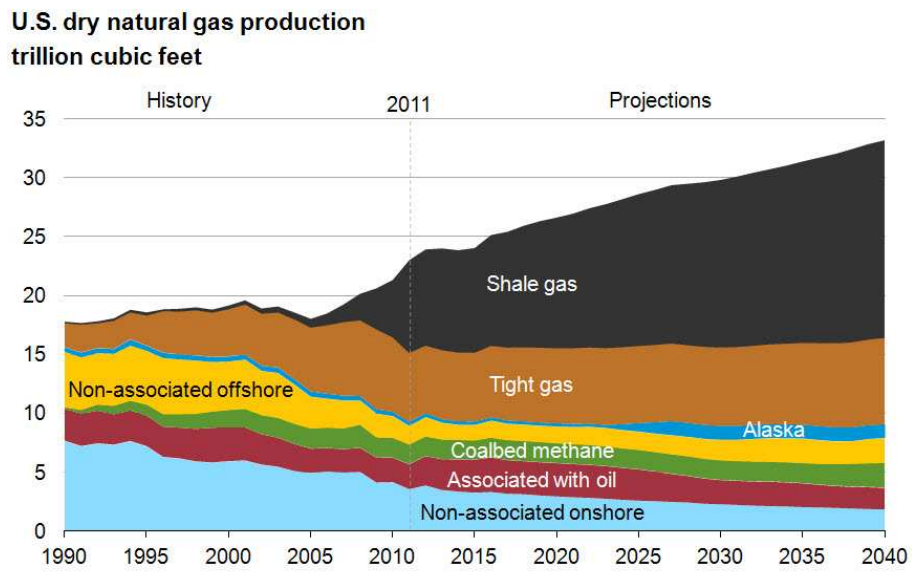


Figure 1.2: US dry gas production forecast by U.S. Energy Information Administration's AEO 2013

The first large-scale shale gas production started during the 1980s and 1990s when Mitchell Energy and Development Corporation started production from Barnett Shale in North-Central Texas (King, 2012). By the end of 2005, the Barnett shale alone was producing 0.5 trillion cubic feet of natural gas per year. The success of the Barnett Shale and its geologic equivalent, the Fayetteville Shale in Arkansas, resulted in development of other shale plays including Marcellus, Bakken, Haynesville, Woodford and the Eagle Ford (**Figure 1.3**).

The production of shale gas has grown exponentially from year 2000 onwards (**Figure 1.4**). During 2000 to 2006 production of natural gas from shale in the United States grew by an average of 17 percent per year. From 2006 to 2011, U.S. shale gas production grew by an average of 48 percent per year (AEO 2013). The U.S. Energy Information Administration's Annual Energy Outlook 2013 (AEO 2013 Early Release) projects U.S. natural gas production to increase from 23.0 trillion cubic feet in 2011 to 33.1 trillion cubic feet in 2040, a 44% increase. Almost all of this increase in domestic natural gas production is due to projected growth in shale gas production (**Figure 1.2**), which is projected to grow from 7.8 trillion cubic feet in 2011 to 16.7 trillion cubic feet in 2040.

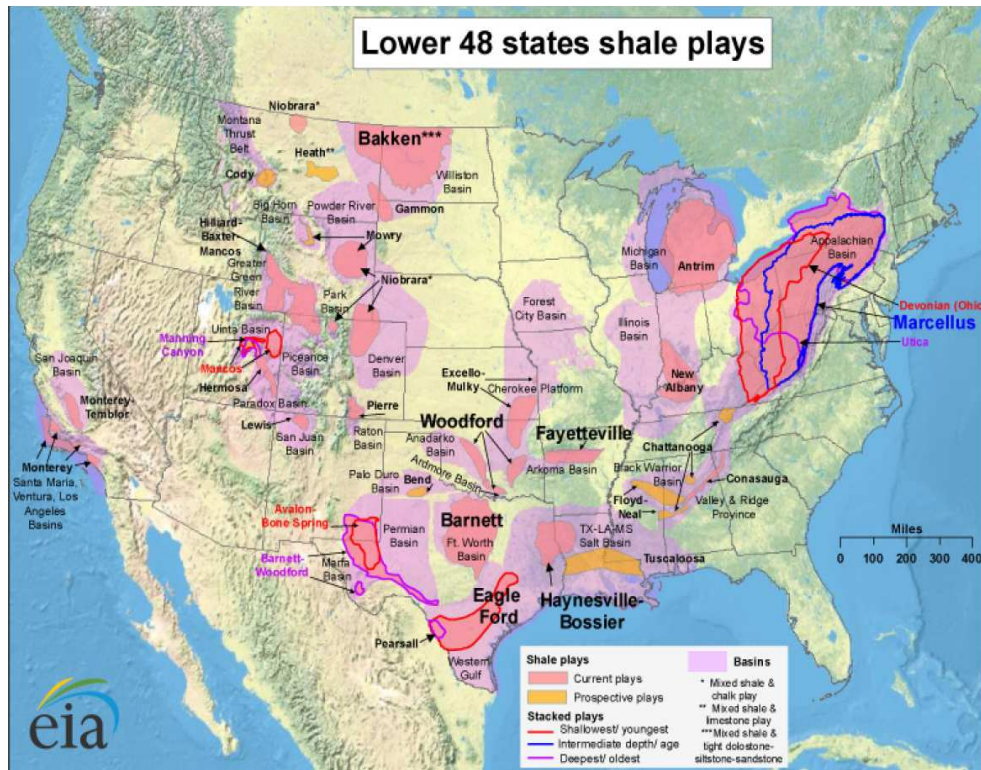


Figure 1.3: US shale gas and shale oil plays by U.S. Energy Information Administration's US shale report, 2011

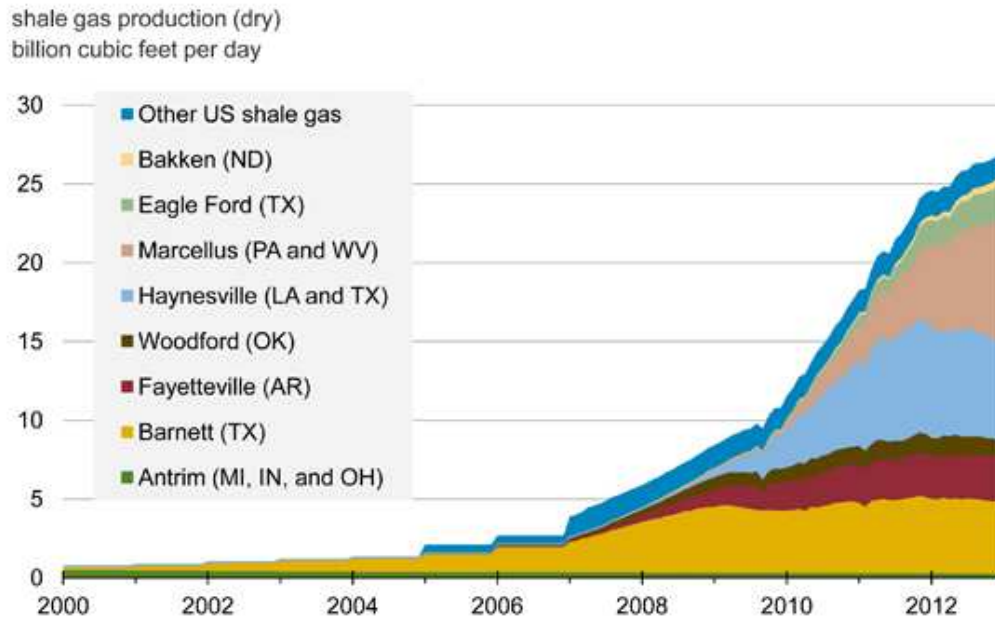


Figure 1.4: US shale gas production estimated by U.S. Energy Information Administration

1.3 Shale resource potential in Alaska

The first major discovery of oil in Alaska was in 1957 on the Kenai Peninsula at Swanson River. However, it was the discovery of the massive hydrocarbon accumulations in the Prudhoe Bay of the Alaskan North Slope in 1967 that confirmed Alaska's position as a major hydrocarbon producer. Currently, Alaska's oil production accounts for approximately 10 percent of U.S. Domestic production consists of conventional hydrocarbon accumulations (four of the ten largest oilfields in the U.S. to date are located on the Alaskan North Slope). Even though the production rate is declining at the Alaskan oil fields, there is a high prospect of discovering new oil fields in Alaska (Retrieved from <http://globalwarming-arclein.blogspot.com/2011/03/alaska-could-be-eighth-largest-oil.html> on October 31, 2014).

The Alaskan North Slope has three major source rock intervals that are potential unconventional shale resource plays. These are the shales of the Cretaceous Brookian sequence, the Jurassic Kingak Shale, and the Triassic Shublik shale (Decker, 2011). As seen in **Table 1.1**, the combined potential of these three shales of the Alaskan North Slope was estimated by the US Geological Survey (USGS) as 940 million barrels of undiscovered oil and 42 trillion cubic feet of undiscovered gas. **Figure 1.5** compares the estimated undiscovered oil of major shale plays in US. Note that the North Slope's potential shale oil resources are greater than that of the Eagle Ford Shale of Texas. Development of the North Slope shale resources may be crucial in sustaining Alaska's oil production in the future. However, this development will be subject to operational constraints.

The Shublik shale, one of the three potential unconventional shale reservoirs in Alaskan North Slope, is the focus of the current study. The USGS assessment for Shublik Formation has, on average, 463 million barrels of oil of undiscovered oil, with 462 billion cubic feet of gas of associated gas and 12 million barrels of natural gas liquids as seen in **Table 1.2**.

Table 1.1: Potential of Alaska North Slope shales compared to other major U.S. shale plays
(Houseknecht et al., 2012)

Shale Oil	USGS Estimated Undiscovered Oil (MMBO)
Bakken	3,645
North Slope	940
Eagle Ford	853
Woodford	393
Niobrara	227

Shale Gas	USGS Estimated Undiscovered Gas (BCFG)
Marcellus	81,374
Haynesville	60,734
Eagle Ford	50,219
North Slope	42,006
Woodford	15,105

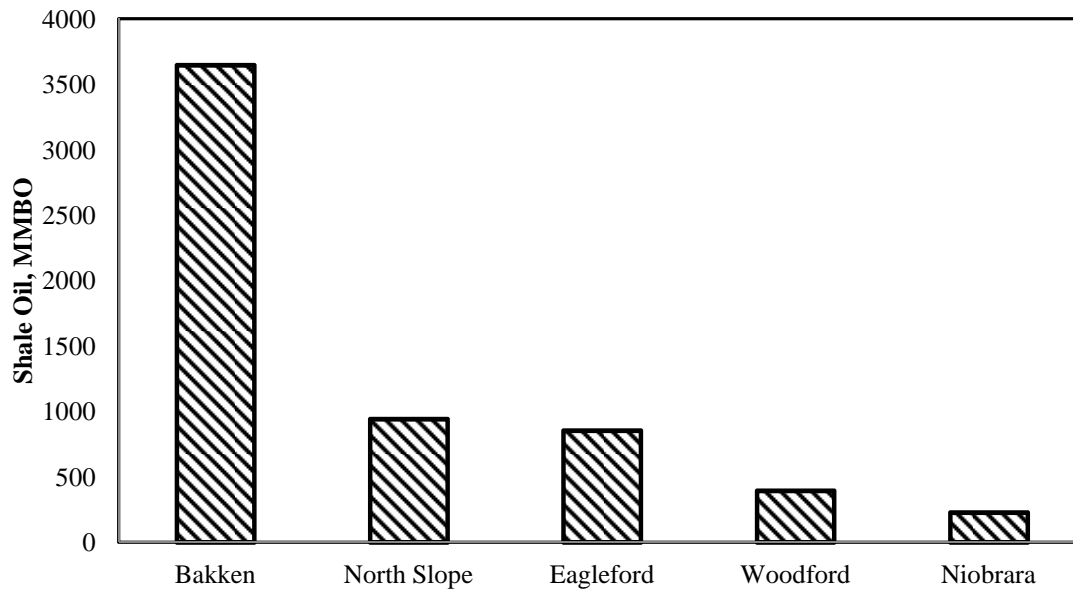


Figure 1.5: USGS estimates of undiscovered oil in shale resource plays, showing the potential of the Alaska North Slope shales in comparison to major U.S. shale oil plays (modified from Houseknecht et al., 2012)

Table 1.2: USGS Shublik Formation shale oil and shale gas assessment results (Houseknecht et al., 2012)

Assessment Units (AU)	Field Type	Total Undiscovered Resources		
		Oil (MMBO)	Gas (BCFG)	NGL (MMBNGL)
Shublik Shale Oil AU	Oil	463	462	12
Shublik Shale Gas AU	Gas	-	38,405	205

1.4 Hydraulic fracturing and application to shale resource plays

Hydraulic fracturing is a process in which a fluid is pumped at a high rate into a formation until the fluid pressure is raised above the minimum horizontal in situ stress of the formation, causing a fracture to form. It was first performed in 1947 by Halliburton and Stanolind Oil in the Hugoton gas field in Grant County of southwestern Kansas (King, 2012). The permeability enhancement caused by the increased area of contact due to these induced fractures significantly improves the production performance (from http://en.wikipedia.org/wiki/Hydraulic_fracturing).

Since its inception, hydraulic fracturing has been widely used in stimulation of conventional reservoirs for improved production rates. Several technical advancements like hybrid fracturing fluids and high pumping power made fracturing one of the most efficient stimulation techniques (King, 2010).

A conventional fracturing process consists of three stages (**Figure 1.6**; Beard, 2011). First, in the pad stage the fracturing fluid is pumped with high injection rates. This stage is mainly responsible for creating the desired fracture length. Once the pumping stops in the pad stage, the closure stress of the formation causes the fracture to close. To avoid the fracture closure, a slurry is created with proppants and injected. These proppants get embedded into the fracture and prevent it from closing. In the third stage, clean fracturing fluid is flushed into the wellbore in order to clean the wellbore and initiate production.

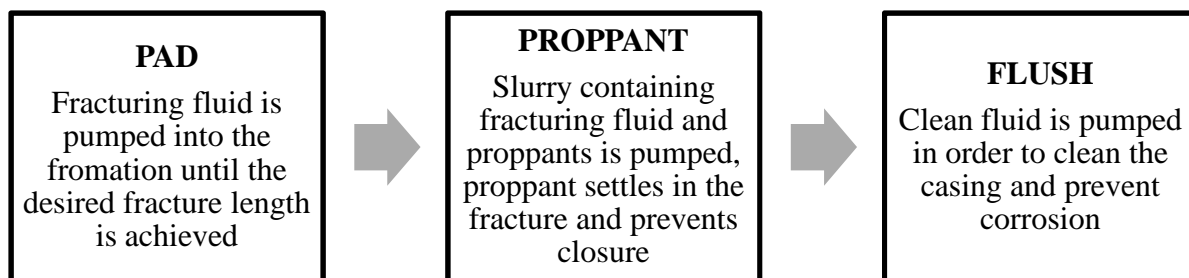


Figure 1.6: A typical hydraulic fracturing job (Modified from Beard, 2011)

Unconventional reservoirs like shales have permeability of the order of nanodarcies (10^{-9} Darcy). Production at economic rates is not possible using conventional methods. Horizontal drilling

coupled with hydraulic fracturing has proven to improve the economic viability of unconventional reservoirs by increasing the volume of the reservoir contacted by an individual well bore.

To enhance flow from the nanodarcies rocks/shales, a large area needs to be stimulated. This is possible using multi-stage fracturing. The horizontal well is placed in the target shale and it is fractured at regular intervals in order to attain maximum Stimulated Reservoir Volume (SRV) as seen in **Figure 1.7**. The higher the SRV, the greater will be the area of permeability enhancement. Consequently determining an optimum multi-stage hydraulic fracturing design is crucial for development of any shale reservoir.

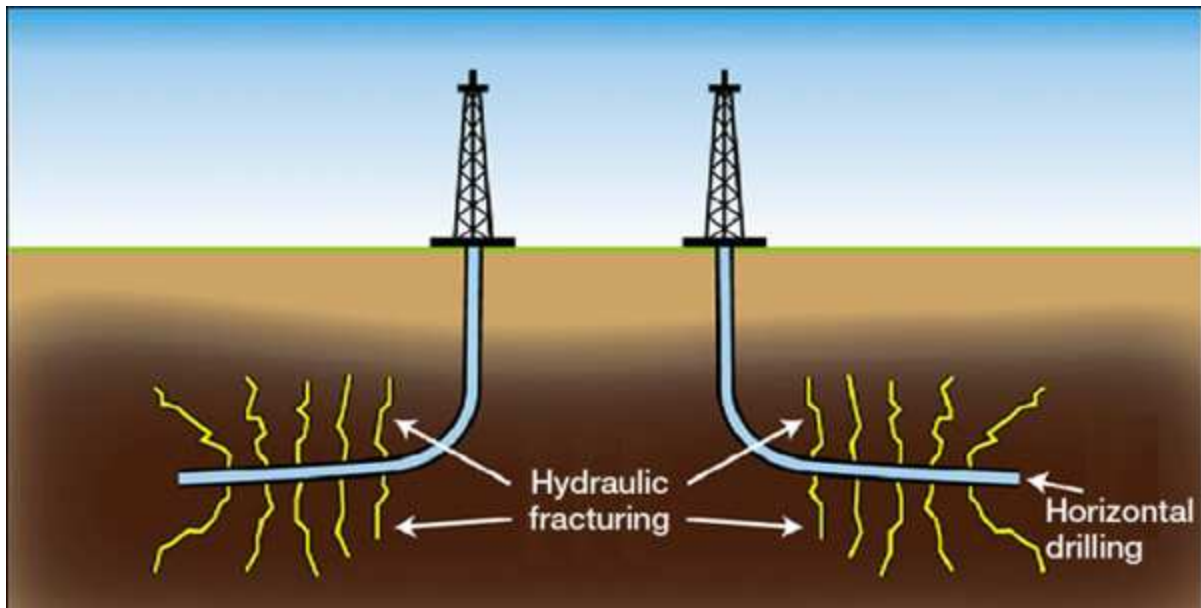


Figure 1.7: Typical multi-stage hydraulic fracturing operation in shales
(<http://thetyee.ca/News/2013/01/08/Shale-Gas-Hard-On-Landscape/>)

1.5 Objective of the study

The economic viability of developing a shale reservoir greatly depends on the efficiency of the hydraulic fracturing treatments among other factors. Understanding the effect of various reservoir and fracture design variables on the induced fracture dimensions is of utmost importance for designing fracturing treatments in shale reservoirs, especially in the early

development phase. For a new shale play like Shublik shale, the scarcity of representative reservoir and geologic data leads to uncertainties in simulated fracture dimensions. This thesis presents a methodology to identify the statistically significant reservoir and treatment properties, and develop functional relationships between the significant properties and fracture dimensions. This study is conducted in two stages. The first stage mainly focuses on identifying the significant variables affecting the simulated fracture dimensions. This stage was conducted in three phases, each phase incorporating progressively more complex assumptions about geology. Using the three most significant variables identified from first stage, the second stage of this study applies Box-Behnken experimental design and response surface methodology for quantifying functional relationships between input variables and the predicted fracture geometry.

The main objectives of this study are:

- Present a workflow for an efficient screening strategy to identify the optimum hydraulic fracture design in the Shublik shale
- Identify the significant reservoir, geologic, mechanical, and treatment properties affecting the induced fracture dimensions in Shublik
- Vary the geologic assumptions and observe the changes in statistical significance of the significant properties, and finally,
- Develop mathematical models which can predict the induced fracture dimensions in the Shublik shale

CHAPTER 2 LITERATURE REVIEW

2.1 Shublik geology

The Triassic Shublik Formation is a heterogeneous phosphatic limestone and calcareous shale interval, and it is a major source rock for hydrocarbon accumulations on the North Slope. At Prudhoe Bay, the Shublik Formation is thin (varying between 0-585 ft) and is bounded by the Eileen and the Sag River Sandstones (Parrish and Hulm, 2001; Kelly, 2004). The Shublik is subdivided into four distinct zones in the subsurface (**Figure 2.1**; Kupecz, 1995; Hulm, 1999). These zones are labeled A through D, from the top to base of the section. Zones A and C are organic rich, consist of black shale and dark grey limestone and are the target zones for stimulation. The thicknesses of zones A and C range from 0-83 ft and 0-46 ft, respectively. Zone B varies from 0-28 ft in thickness and is mainly composed of phosphorite, phosphatic carbonates and siliciclastic rocks. Lastly, Zone D is fine-to-medium-grained phosphatic sandstone with thicknesses ranging from 0-24 ft (Hulm, 1999).

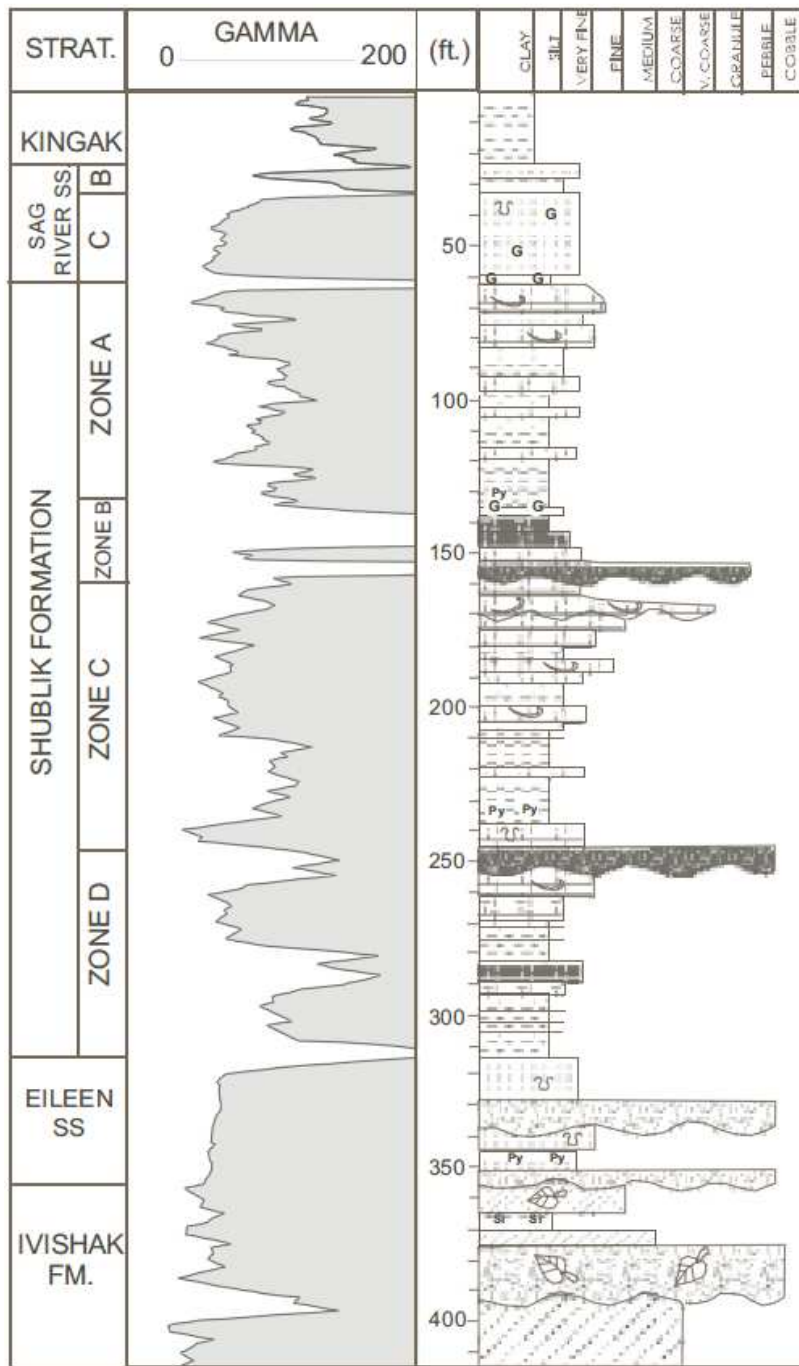


Figure 2.1: Lithostratigraphy and corresponding gamma ray log response for Shublik shale based from one of the wells in Prudhoe Bay (Hulm, 1999)

2.2 Data availability and geologic analog of Shublik

Development of the Shublik as a shale resource play has been hindered partly because of the unavailability of accurate estimates of reservoir and mechanical properties. For this reason, when the reservoir and mechanical properties of Shublik needed for simulation were unavailable, the properties of Eagle Ford shale, a geologic analog were used.

The Eagle Ford shale is a Cretaceous-age heterogeneous calcareous shale formation that is the source rock for the Austin Chalk Formation and the East Texas oil fields (Jiang, 1989). As seen in **Table 2.1**, Eagle Ford and Shublik appear to have similar Total Organic Carbon (TOC) values and kerogen types. Both Eagle Ford and Shublik shales are calcareous shales, are brittle and have natural fractures. These similarities make the Eagle Ford a reasonable geologic analog for the Shublik, suggesting that hydraulic fracture treatments effective in the Eagle Ford could also be effective in the Shublik (Decker, 2011). These similarities also suggest that well and production data from the Eagle Ford can be used to investigate the Shublik’s response to a simulated fracture treatments (Hutton et al., 2012).

Table 2.1: Geologic characteristics of Eagle Ford Shale and Shublik Shale (Decker, 2011)

	Eagle Ford	Shublik
Total Organic Carbon	2-7 %	2.40%
Main Kerogen types	I/II (oil)	I/II-S (oil)
Oil Gravity, API	30 - 50 API	24 API
Thickness	50 - 250 ft	0 - 600 ft
Thermal Maturity	Imm-Oil-Gas	Imm-Oil-Gas
Lithology and Variability	Sh-Slts-Sh	Sh-Slts-Ls
Brittleness	Yes - Quartz	Yes – Calcite
Natural Fractures	Yes	Yes
Overpressure	Yes	Locally

2.3 Conventional hydraulic fracturing theory

Fracturing models typically consists of three basic components: a fluid flow model; a rock deformation model; and a fracture propagation criterion (**Figure 2.2**). The fluid flow model describes the pressure losses and pressure distribution along the fracture, and leak-off into the surrounding porous media when a fracturing fluid is injected. The rock deformation model predicts the response of the fractured surface to hydraulic loading. The fracture propagation criterion establishes a combination of loading and deformation conditions that result in propagation of the fracture into the intact rock volume (Martinez, 2012).

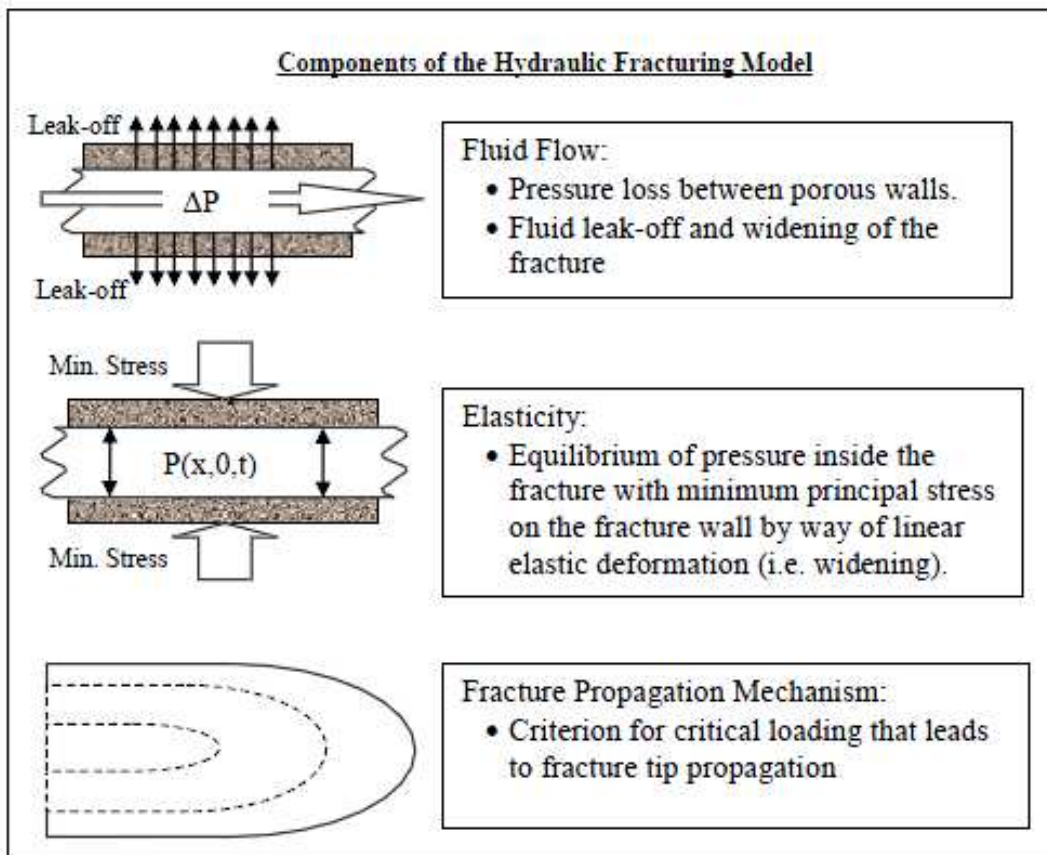


Figure 2.2: Components of a conventional hydraulic fracture model (Martinez, 2012)

2.3.1 Fracture mechanics fundamentals

Most failure criteria theories derive from the work done by Griffith (1921), who proposed that the existence of minute cracks in the material act as stress concentrators. When a crack propagates in a medium, a part of the elastic energy of the medium is released to create new fractures. Subsequent modifications of Griffith's theory led to more general loading conditions in terms of measurable parameters called "stress intensity factors" (Martinez, 2012). These studies, along with many other following contributions led to the origin of the classic theory of fracture mechanics. In the case of fracture propagation in a rock, it is assumed that loading and deformations have a linear relation, and that propagation of the fracture occurs in brittle fashion before considerable non-linear features are apparent. This assumption of linear elasticity is combined with the principles of classic fracture mechanics in what is known as Linear Elastic Fracture Mechanics (LEFM). In LEFM, the concept of plane strain is often used to reduce the dimensionality of the problem. This concept assumes that the body is infinite in at least one direction, and external forces are applied parallel to this direction.

The concept of plane strain is a reasonable approximation in a rock, but the main problem is how to select the infinite plane. Two possibilities arise, leading to two different approaches to fracture modeling. The plane strain is assumed to be in the horizontal plane by Khristianovitch and Zheltov (1955) and by Geertsma and de Klerk (1969) (KGD), while the plane strain is assumed to be in the vertical plane by Perkins and Kern (1961) and Nordgren (1972) (PKN).

From the work done by Sneddon (1973), it is well known that the pressurized crack in the state of plane strain has an elliptical width distribution.

$$w(x) = \frac{4p_0}{E'} \sqrt{c^2 - x^2} \quad (1)$$

Where x is the distance from the center of the crack, c is the crack half length, and p_0 is the constant pressure exerted on the rock. From the above equation, the maximum width at the center can be solved as shown below.

$$w(x) = \frac{4cp_0}{E'} \quad (2)$$

This indicates a linear relationship between crack opening induced and the pressure exerted. When the concept of a pressurized crack is applied to hydraulic fracturing, p_0 is replaced by net pressure, p_n , which is the difference between the pressure inside the fracture and the minimum principle stress acting from outside, trying to close the fracture (Economides et al., 2002).

According to Griffith (1921), the presence of defects in the rock (cracks, soft inclusions, etc.), have the effect of intensifying the magnitude of any applied load. The intensification effect is the result of a compromise between the surrounding loads, the geometry of the defect, and the mechanical properties of the medium and is called a stress intensity factor. The stress intensity factor for a pressurized line crack is given by

$$K_I = p_0 c^{1/2} \quad (3)$$

Where c is the crack half length, and p_0 is the constant pressure exerted on the rock. It can be observed that the stress intensity factor at tip of the fracture is proportional to pressure opening the fracture and the square root of fracture half length (Martinez, 2012).

LEFM states that, for a given material, there exists a critical value of the stress intensity factor, K_{IC} , called fracture toughness. It can be understood that as long as the stress intensity factor at the tip of the fracture is greater than the fracture toughness, the fracture will propagate (Economides et al., 2002).

2.3.2 Fracturing fluid mechanics

Compared to solids, fluids are more compressible and will deform continuously when subjected to a constant pressure. The most important property of fracturing fluids is apparent viscosity. Apparent viscosity is defined as the ratio of shear stress to shear rate. The material function that relates the shear stress to shear rate is called a rheological curve. Based on the trend of the rheological curve, we can classify the types of fluids (**Figure 2.3**). These rheological curves can be used to calculate the pressure drop for a given flow conditions. Rheological properties of the fracturing fluids are mainly dependent on chemical composition, temperature, and several other factors like shear history (Economides et al., 2002).

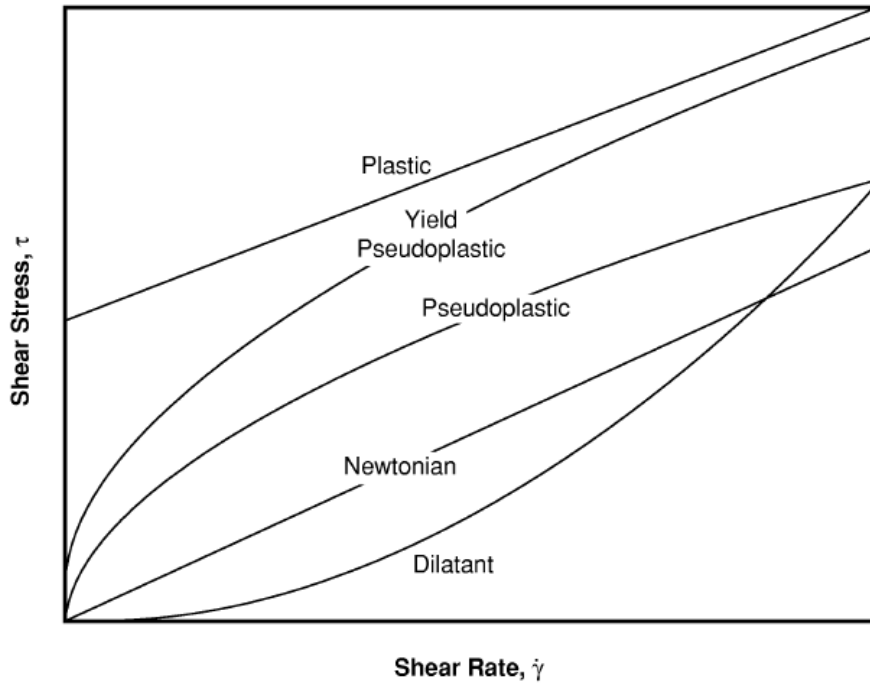


Figure 2.3: Typical rheological curve (Economides et al., 2002)

Typically, the flow condition of fracturing fluids is laminar flow with two limiting geometries. Slot flow occurs in a channel of rectangular cross section when the ratio of the major dimension to the minor dimension is extremely large. Ellipsoid flow occurs for an elliptical cross section with extremely large aspect ratio. Slot flow corresponds to horizontal plane strain. Ellipsoid flow corresponds to vertical plane strain. **Table 2.2** gives the solutions commonly used in hydraulic

fracturing to calculate pressure drop for Newtonian fluids where μ is the apparent viscosity, u_{avg} is the average fluid velocity, w/w_0 is the fracture width/maximum width, and Δp is the pressure drop.

Table 2.2: Pressure drop for Newtonian fluid in laminar flow (Economides et al., 2002)

Rheological model	Newtonian $\tau = \mu\gamma$
Slot flow	$\frac{\Delta p}{L} = \frac{12 \mu u_{avg}}{w^2}$
Ellipsoid flow	$\frac{\Delta p}{L} = \frac{16 \mu u_{avg}}{w_0^2}$

As the fracture fluid is injected and the fracture is propagated, a part of the injected fracturing fluid is lost into the reservoir. This fluid loss is called leak-off volume. According to Carter (1957), leak-off velocity, v_L , is given by the Carter equation:

$$v_L = \frac{C_L}{\sqrt{t}} \quad (4)$$

Where C_L is the leak-off coefficient and t is the time elapsed since the start of the leak-off process. The integrated form of the Carter's equation is:

$$\frac{V_{Lost}}{A_L} = 2C_L \sqrt{t} + S_p \quad (5)$$

Where V_{Lost} is the fluid volume that passes through the surface area A_L from time 0 to t . The constant S_p is called the spurt loss coefficient, which is the width of the fluid body passing through the surface instantaneously at the beginning of the leak-off process. As the fracture propagates, the fracturing fluid-reservoir contact area increases, this leads to larger volume of fluid leak-off and decreased efficiency.

2.3.3 Fracture propagation models

Fracture propagation models combine elasticity, fluid flow, material balance, and any additional propagation criterion. If the fluid injection schedule is known, the fracture propagation should

predict the evolution of fracture geometry with time and wellbore pressure. Initially there were two original 2-D models: the PKN and KGD models. Each represents a set of different assumptions in deriving the analytical solutions. Based on these models, several other models were developed.

2.3.3.1 PKN model

The PKN model was first developed by Perkins and Kern (1961), and later modified with the leak-off effect by Nordgren (1972). This model assumes the plane strain to be in a vertical plane normal to the direction of fracture propagation. This model assumes constant net pressure in the vertical coordinate that varies with the change in the lateral coordinate. This assumption leads to an elliptical fracture cross-section as seen in **Figure 2.4**. The formulae for calculating the fracture geometry (width, w) and the net pressure, P_{net} , from the PK model can be seen below.

$$P_{net}(x,t) = \left[\frac{16\eta q_i E'^3 (L-x)}{\pi h_f^4} \right]^{\frac{1}{4}} \quad (6)$$

$$w(x,t) = 3 \left[\frac{\mu q_i E'^3 (L-x)}{E'} \right]^{\frac{1}{4}} \quad (7)$$

Where t is the total pumping time, L is the fracture length at t , $w(x,t)$ is the fracture width, $P_{net}(x,t)$ is the net pressure, q_i is the total pump rate, h_f is the fracture height, μ is the fracture fluid viscosity, E' is the plain strain modulus (depends on Young's modulus and Poisson's ratio).

This model assumes an infinite fracture length and constant fracture width. Consequently fracture length cannot be calculated using this model. This model also neglects the fluid leak-off. The propagation criteria for this model is that the propagating fracture will continue to extend (even after pumping is stopped) until the net pressure declines to less than the minimum pressure for propagation (Zeng, 2002).

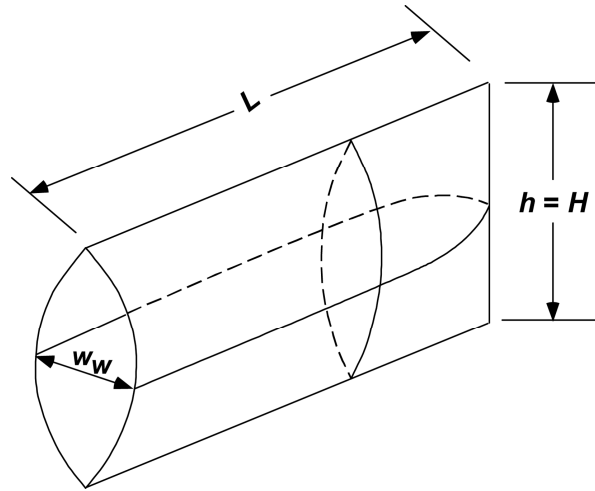


Figure 2.4: Basic notation of PKN model (Gidley, 1989)

Later, Nordgren (1972) added the leak-off effects and modified the Perkins-Kern model using the Carter's equation, which is now called the PKN model. Based on the value of dimensionless variable t_D , the PKN model is partly solved as seen below.

$$t_D = \left[\frac{64C_L^5 E' h_f}{\pi^3 \mu q_i^2} \right]^{\frac{2}{3}} t$$

Case 1: $t_D < 0.01$

$$L(t) = 0.39 \left[\frac{E' q_i^3}{\mu h_f} \right]^{\frac{1}{5}} t^{\frac{4}{5}} \quad (8)$$

$$w(t) = 2.18 \left[\frac{\mu q_i^2}{E' h_f} \right]^{\frac{1}{5}} t^{\frac{1}{5}} \quad (9)$$

Case 2: $t_D > 1.0$

$$L(t) = \frac{q_i t^{\frac{1}{2}}}{2\pi C_L h_f} \quad (10)$$

$$w(t) = 4 \left[\frac{\mu q_i^2}{\pi^3 E' C_L h_f} \right]^{\frac{1}{4}} t^{\frac{1}{8}} \quad (11)$$

2.3.3.2 KGD model

This model was developed by Geertsma and de Klerk (1969) based on Khristianovich and Zheltov's (1955) solution on fracture propagation and Barenblatt's (1962) fracture tip model. In this model, the state of plane strain is assumed to be in the horizontal plane. This implies that the fracture width at any distance from the wellbore is independent of vertical position (rectangular fracture cross-section) as shown in **Figure 2.5**. This model combines both the assumptions of constant pressure in the fracture, and zero stress intensity factors at the fracture tip. The KGD model was derived for fracture length and fracture width at the wellbore after neglecting the fluid leak-off effects as the following (Zeng, 2002):

$$L(t) = 0.38 \left[\frac{E' q_i^3}{\mu h_h^3} \right]^{\frac{1}{6}} t^{\frac{2}{3}} \quad (12)$$

$$w_w = \left[\frac{84 \mu q_i^3 L^2}{\pi E' h_f} \right]^{\frac{1}{4}} \quad (13)$$

This model was further modified by considering the fluid leak-off effects from Carter's equation by Geertsma and de Klerk (1969) to obtain the fracture length as:

$$L(t) = \frac{q_i w_w}{64 C_L^2 h_f} \left(e^{S^2} \operatorname{erfc}(S) + \frac{2}{\sqrt{\pi}} S - 1 \right) \quad (14)$$

$$\text{Where, } S = \frac{8 C_L \sqrt{\pi t}}{w_w}$$

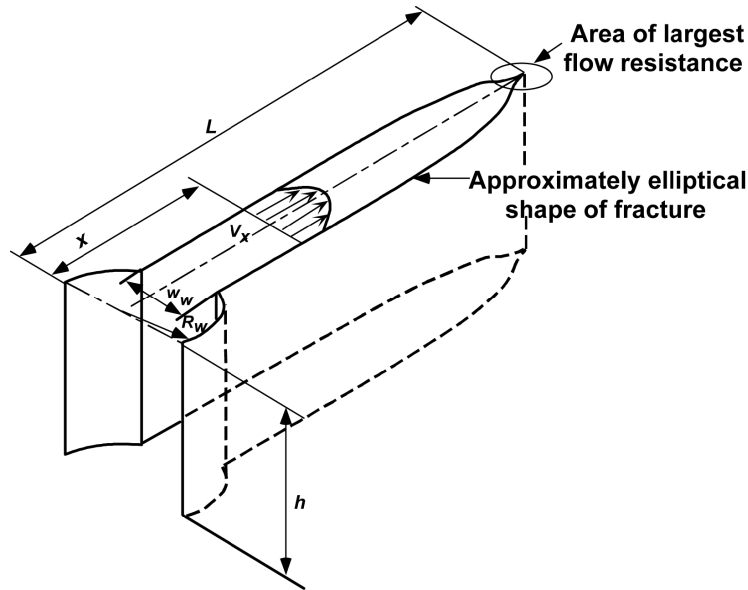


Figure 2.5: Basic notation of KGD model (Gidley, 1989)

2.3.3.3 Radial model

Radial fractures occur when the fracture initiates and grows from an unconfined point source (horizontal fractures in a vertical well or transversely vertical fractures in a horizontal well). In either case the minimum principal stress is perpendicular to the fracture (Zeng, 2002). The radial

length (radius of the fracture), R , and the width, w_w , of the KGD radial fracture can be seen below.

$$R = \sqrt{\frac{q_i (4w_w + 15S_p)}{30\pi^2 C_L^2} \left(e^{S^3} \operatorname{erfc}(S) + \frac{2}{\sqrt{\pi}} S - 1 \right)}$$

$$w_w = 2.56 \left(\frac{\mu q_i R}{E'} \right)^{\frac{1}{4}}$$

$$\text{Where, } S = \frac{15C_L \sqrt{\pi t}}{4w_w + 15S_p}$$

For the case with no fluid leak-off, the above equation can be approximated as

$$R = 0.52 \left(\frac{E' q_i^3}{\mu} \right)^{\frac{1}{9}} t^{\frac{4}{9}} \quad (15)$$

$$w_w = 2.17 \left(\frac{\mu^2 q_i^3}{E'^2} \right)^{\frac{1}{9}} t^{\frac{1}{9}} \quad (16)$$

After considering fluid leak-off, approximation for the radial model is

$$R = \frac{1}{\pi} \left(\frac{q_i^2 t}{C_L^2} \right)^{\frac{1}{4}} \quad (17)$$

$$w_w = 2.56 \left(\frac{\mu q_i R}{E'} \right)^{\frac{1}{4}} \quad (18)$$

All 2D fracture propagation models assume a planar fracture. In non-radial models, the fracture is assumed to extend vertically to the full height of the pay zone, and remain within the pay zone.

In the radial fracture models, the fractures are assumed to initiate from a point source and propagated without restrictions. While these assumptions greatly simplify the solution for fracture geometry, they do not always represent the reality. For instance, the pay zone thickness can be changed at different positions from the well to the tip. In addition, the containment by the neighboring layers cannot be satisfied all the time. So a varied fracture height is more close to reality. This leads to the development and application of 3D models (Zeng, 2002).

2.3.3.4 3D models

There are no analytical solutions for 3D models that can be simple and explicitly expressed. All 3D fracture simulation solutions need the application of numerical modeling. There are three types of 3D hydraulic fracturing models: pseudo 3D models, planar 3D models and general 3D models. Different models have different assumptions and require different computational resources. A pseudo 3D simulator was used in this study.

2.3.3.4.1 Pseudo 3D models

Pseudo 3D (P3D) models are similar to 2D models, except that the fracture height is not constrained to the payzone thickness. There are two main types of P3D models. The lumped P3D model assumes an elliptical geometry in the direction of fracture length and the fracture is symmetrical at either side of the wellbore. The fracturing fluid is assumed to flow in one dimension, from the perforations to the fracture tips. The cell-based P3D model assumes that the fracture can be treated as a series of connected but independent cells. The unrestrained fracture height improves the prediction of fracture geometry. But the assumption of one-dimensional fluid flow in both cell-based and lumped pseudo 3D models limits the ability to predict the fracture geometry (Zeng, 2002).

2.3.3.4.2 Planar 3D models

Planar 3D models assume that the fracture is planar and oriented perpendicular to the minimum principal stress. The fracture length and fracture height grows within a narrow channel. This growth is controlled by Linear Elastic Fracture Mechanics. The width of the fracture is controlled by the net pressure distribution in the fracture, determined by the fracturing fluid flow

rate in the fracture. The fluid flows in two dimensions, length and height directions. This 2D fluid flow in turn is controlled by the fracture geometry. Therefore, this is a coupled problem between the fluid flow and the fracture growth in a linear elastic solid. Due to the coupling nature between the fluid flow and the fracture initiation and propagation, simulators based on these models require high computational time. They are usually used in situations where the fracture is expected to extend to the boundary layers (Zeng, 2002).

2.3.3.4.3 General 3-D models

General 3D models have no assumptions about the orientation of the fracture. They use the local stress field and fracture mechanics criteria to estimate the fracture propagation. Factors such as wellbore orientation and perforation pattern may cause the fracture to initiate in a different direction than the minimum principal stress. Simulators based on these models require high computational time and expert personnel to use them. Due to these reasons, these models are mainly used as a research tool. With recent developments in computers the simulation time can be reduced from a day to few hours. Consequently general 3D models may become a crucial tool for fracture simulation in the near future (Zeng, 2002).

2.4 Special concerns for fracturing design in shale reservoirs

2.4.1 Reservoir characterization

A careful study of the reservoir is necessary in order to understand the complexities in shale reservoirs and evaluate the possible candidate wells. Reservoir characterization will help us in determining the increase in production, water inflow, cross flow between formation layers, and availability of sufficient pressure support (Crabtree, 1996). The geologic properties like size of reservoir, type of reservoir and the drainage area are needed to decide the well spacing and the optimum length of horizontal well. The formation lithology affects the fracture height containment and fracturing fluid selection. Clay content and its distribution affect the permeability of the rock, and are necessary to design fracturing fluid additives (Nolte and Economides, 1989). Fracture orientation depends on the fault pattern in the formation and in-situ stress field.

2.4.2 Presence and interaction of natural fractures

The presence of natural fractures and the interaction of the induced fractures with these preexisting natural fractures can create a complex fracture network, which can improve the production in shale reservoirs. There are generally two scenarios for hydraulic and natural fracture interaction. In the crossing scenario, the induced fracture crosses the natural fracture without any significant deviation in direction (**Figure 2.6**). In the opening scenario, the induced fracture interacts with the natural fracture, completely deviates into the natural fracture, and reactivates and extends it (**Figure 2.7**; Keshavarzi et al., 2012).

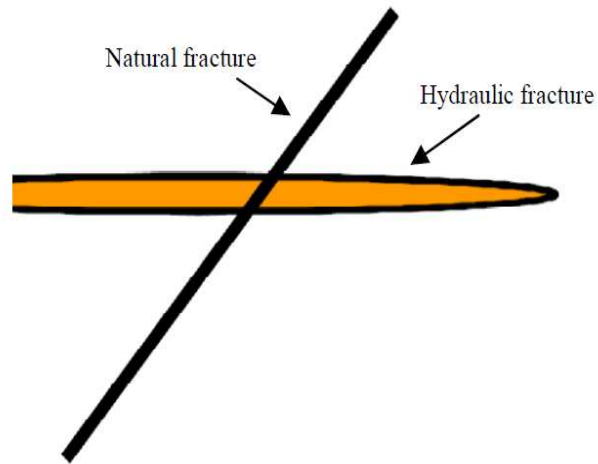


Figure 2.6: Crossing scenario for natural fracture interaction (Keshavarzi et al., 2012). Hydraulic fracture shown in orange.

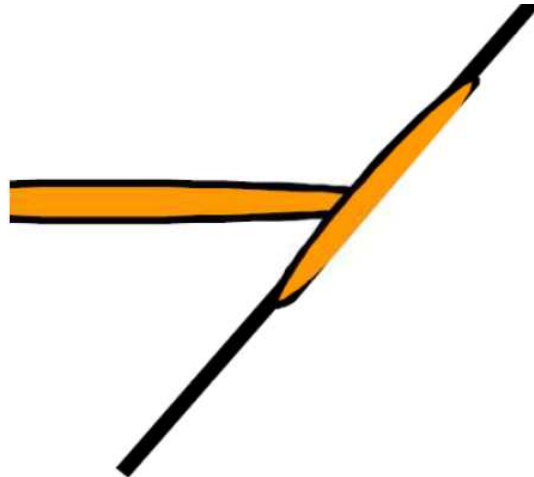


Figure 2.7: Opening scenario for natural fracture interaction (Keshavarzi et al., 2012). Hydraulic fracture shown in orange.

2.4.3 Multi-stage hydraulic fracturing

Multi-stage hydraulic fracturing is highly efficient in shale reservoirs due to maximized reservoir contact with the wellbore. The orientation and length of the well, the vertical placement of horizontal well in the formation, and the completion methodology all affect the performance of a fracturing stimulation in shales.

2.4.3.1 Horizontal well design

The reservoir rocks at a certain depth are subjected to an in-situ stress field. This field can be represented by three principal stress vectors (vertical and two horizontal components). The fracture always propagates in the direction perpendicular to the least principal stress (Economides et al., 2012). The horizontal well is preferred to be placed in the direction perpendicular to the maximum principal stress to achieve maximum reservoir contacted by the transverse fractures. Therefore understanding the in-situ stress orientation can help in determining the orientation of horizontal well.

Other factors such as reservoir geology, reserves to be developed per well, production rates expected per well, future well intervention requirements, surface logistics, and environmental impacts also affect the horizontal well design. The length of the horizontal well determines the reservoir contact and is dependent on factors like completion equipment, economic concerns, and environmental concerns (Pope et al., 2012). The vertical position of the horizontal leg within the formation (depth of the heel) depends on mechanical properties of the target formation and predicted fracture geometry (Beard, 2011).

2.4.3.2 Completion techniques

Completion techniques required for multi-stage fracturing generally fit under two categories. Completion techniques like plug-and-perf have the ability to fracture and isolate a single fracturing stage at once. This approach requires longer time to complete multiple stages (**Figure 2.8**). In contrast, completion techniques like ball-activated completion and coiled tubing-activated completion have the ability to fracture and isolate all the fracturing stages at once, thus reducing the treatment time (**Figure 2.9**; Kennedy et al., 2012).

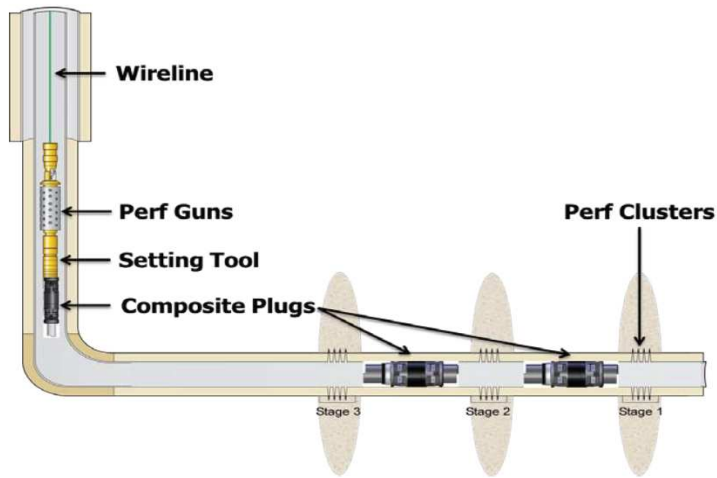


Figure 2.8: Single-stage-at-once completion system (Kennedy et al., 2012)

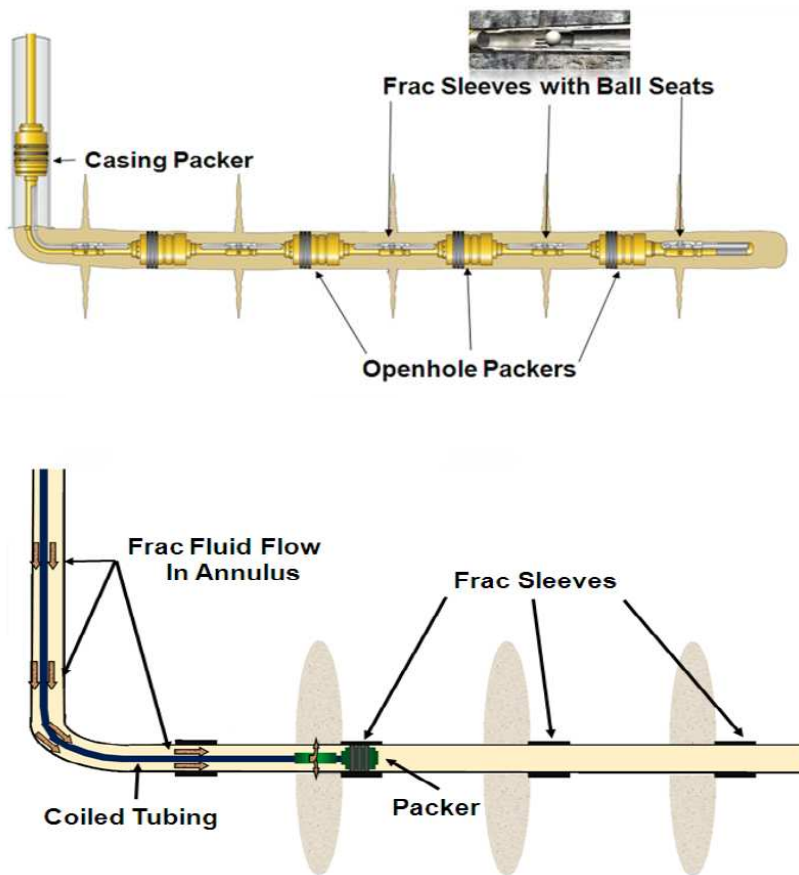


Figure 2.9: Multiple-stages-at-once completion system (Kennedy et al., 2012)

2.4.4 Fracturing fluid selection

Fracturing fluids play a vital role in reaching the designed stimulation goals. These fluids are mainly used to provide the necessary pressure to initiate and propagate the fracture. Apart from this, the fracturing fluids also transport the proppant into the fracture to prevent the fracture closure. Based on the wide range of reservoir properties like permeability, porosity, pressure, temperature, material composition and other aspects, four different types of fracturing fluids have been developed for different reservoir conditions--water-based fluids, oil-based fluids, foams and emulsions (King, 2010). Designing a fracturing fluid depends on several variables like stress anisotropy, pumping rate, and fluid-rock reactivity. Fluid and core measurements help us determine the necessary additives to prevent formation damage. The ideal fracturing fluid needs to be viscous enough so that it can carry the proppants, but also should breakdown and clean up rapidly once the treatment is over. Fracturing fluids should also exhibit low friction loss during pumping and be as economical as practical.

In shale reservoirs, massive volumes of fracturing fluid are required as large reservoir volumes are stimulated. Therefore, water-based fracturing fluids are most widely preferred for its low cost and easy availability. Even though the low viscosity of water-based fluids makes it easy to invade shales with ultralow permeabilities, they have very low proppant carrying capacity. Whenever the proppant carrying capacity is of high priority, more viscous fluids are used. An ideal fracturing fluid in shale reservoirs should have low viscosity in early stages, and the viscosity should increase whenever higher proppant concentration is needed (King, 2010).

Fracture fluid flow back (volume of fracturing fluid produced after the stimulation treatment ends and production starts) is also of main concern due to the water supply costs, disposal costs, environmental responsibilities and government regulations. Flow back recovery is mainly dependent on shale characteristics, fracture design, and type of fluid injected. Due to complex fracture network and reactivity of shale with flow back water, recovery of flow-back fluid is in the range of 10%-50% and can take several weeks (King, 2010).

2.4.5 Proppant selection

Proppants are solid particles that are flowed into the induced fractures to keep the fractures from closing. Proppant type, size and concentration determine the flow capacity of the induced fracture networks (Crabtree, 1996). Sand is the most commonly used proppant in shale reservoirs, particular smaller size ranges like 100 mesh. Resin-coated sand proppants are used when the proppants are expected to be subjected to high compressive strengths. Ceramic proppants are used when very high proppant strength and thermal resistance are required (King, 2010). Proppant selection is mainly dependent on the following parameters.

2.4.5.1 Proppant availability

The worldwide proppant utilization has increased by almost 15-fold since the development of Barnett shale in 2004. The liquid-rich Eagle Ford alone uses over 12 billion lbs of proppant a year, which is over double the global proppant consumption before the Barnett. This increase in demand for proppant has strained proppant suppliers. Due to this insufficient quantity of quality proppants, many engineers compromise with the proppant selection, which affects both the fracture conductivity and production (Palisch et al., 2012).

2.4.5.2 Conductivity requirements

Proppants mainly provide a sufficiently conductive pathway for hydrocarbons to flow. The conductivity of the fracture is represented by a dimensionless number F_{CD} , which is the ratio of hydraulic fracture permeability (k_f) times its width (w_f) to the product of formation permeability (k) by fracture half-length (x_f).

$$F_{CD} = \frac{k_f w_f}{k x_f} \quad (19)$$

Proppant conductivity mainly depends on properties like proppant particle size, proppant strength and proppant grain shape. The proppant conductivity is greatly affected by downhole conditions like fluid flow effects, fracture fluid residue, fines migration, and cyclic stresses on proppants (Palisch et al., 2012).

In multi-stage fracturing, several transverse fractures are placed along the horizontal well. When the fluids from these fractures flow and converge into the relatively small diameter horizontal wellbore, the fluid velocity near the wellbore increases rapidly. This velocity leads to an additional pressure drop that is not described by Darcy's law. The extra pressure drop caused by Non-Darcy and Multiphase flow reduces the proppant pack conductivity by over 70% (Palisch et al., 2012).

Fines are generated when proppants are crushed by in-situ stresses or proppant embedment. Fines can flow through the proppant pack and plug the pore throats, reducing the proppant conductivity. Embedment occurs when the Young's Modulus of the formation decreases. The proppants will embed into the fracture face and fines will spall into the proppant pack. Bottom hole pressure fluctuations can also induce cyclic stress on proppants, which can lead to reduced fracture conductivity (Palisch et al., 2012). All of these effects should be considered while selecting the optimum proppant.

2.5 Current methodology to select optimum hydraulic fracture design

The typical methodology for selecting the optimum fracture design can be seen in the **Figure 2.10**. This process can be divided into two phases-- pre-treatment prediction and post-treatment evaluation.

2.5.1 Pre-treatment prediction

As shown in **Figure 2.10**, reservoir properties are calculated based on geological surveys, well logs, and reservoir characterization. These reservoir properties act as inputs for a numerical fracture simulator. After evaluating various fracture designs, a fracture engineer can propose an initial fracture design. But due to the obvious heterogeneity in shale reservoirs, the calculated reservoir properties may not be accurate. Therefore, the calculated reservoir properties are usually verified by performing a minifrac test. As long as the calculated reservoir properties match the minifrac results, the proposed fracture design is considered accurate. If not, the corrected reservoir properties should be used in the numerical fracture simulator to obtain the optimum fracture design (Stegent et al., 2010).

2.5.2 Post-treatment evaluation

The treatment is performed based on the selected fracture design. The induced fracture geometry can be mapped using various techniques like impression packers, borehole televiewer, radioactive tracers, temperature logs, and micro-seismic tests (Zeng, 2002). As the fractured well produces, the production data should be analyzed by comparing it with various fractured well performance models. If the actual production does not match the production predicted by the well performance models, the entire pre-treatment prediction needs to be repeated with modified reservoir properties as seen in **Figure 2.10** (Stegent et al., 2010).

As discussed earlier, scarcity and uncertainties in reservoir data make this conventional methodology to select optimum fracture design very time-intensive. In this study we propose a new methodology for a time-efficient selection of optimum fracture design. This following section further expands on the experimental design concepts we have used in this study.

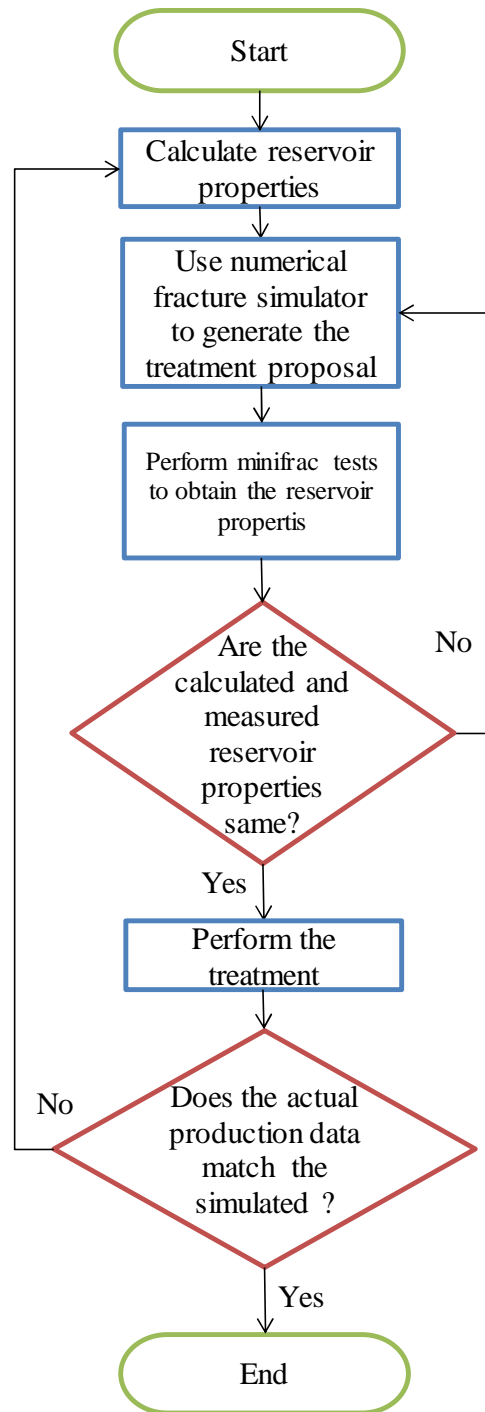


Figure 2.10: Methodology for selecting optimum fracture design (modified Stegent et al., 2010)

2.6 Experimental design and response surface concepts

Numerical models are widely used in engineering and scientific studies with the help of high performance computers. As a result, researchers have shifted to intricate mathematical models to simulate complex systems. The computer models often have multi-dimensional inputs, like scalars or functions. The output may also be multidimensional. Making a number of simulation runs at various input conditions is what we call a computer experiment. Experimental design is an efficient way to choose the input conditions which minimize the number of computer simulation runs required for data analysis, inversion problems and input uncertainty assessment. This can be achieved by building a response surface, which is an empirical fit of computed responses as a function of input variables. Experimental Design (ED) has been used in diverse areas such as aerospace, civil engineering and electronics for analysis and optimization of complex, nonlinear systems described by computer models (Parikh, 2003). Experimental designs have also been used in petroleum engineering studies (Awoleke et al., 2012; Segnini et al., 2014; Ambastha 2014; Yu and Sepehrnoori 2014).

2.6.1 Factorial design

Consider a simulation study with k input variables, with uncertainties in quantifying these input variables. Each input parameter is assigned to its maximum or minimum value based on our engineering judgment. This implies that for this study, we have k input variables in two levels (a higher value denoted by '+1', and a lower value denoted by '-1'). The factorial design considers all the possible combinations of the input variables on both levels. This implies that the total number of simulations required in a factorial design with k factors is 2^k . This design considers all the main effects and interaction effects of all the input variables. Main effect of an input parameter is the quantification of the variation in response with change in that input parameter alone. An interaction effect signifies the relative dependence of two or more input variables among themselves based on their shared effect on the response (Parikh, 2003).

2.6.2 Fractional factorial design

As the number of input variables increase, the number of simulation runs required using factorial design also increase exponentially. For such cases, fractional factorial design is utilized. This

design assumes that only main effects and few of the two/three-factor interactions of input variables have significant effect on the responses. By considering only a part of the factorial design and neglecting the less significant effect, fractional factorial drastically reduces the number of simulations required to uniquely estimate the significance all the input variables on the responses (Parikh, 2003).

2.6.3 Box-Behnken design

Box-Behnken design is a rotatable quadratic design based on 3-level fractional factorial design (Aslan and Cebeci, 2007). Each input factor is placed at one of the three equally spaced values, generally coded as -1, 0, +1 (lower, middle, and higher values of the input parameter range) as seen in **Figure 2.11**. At least three levels are required for these designs as this design fits the data into a quadratic model.

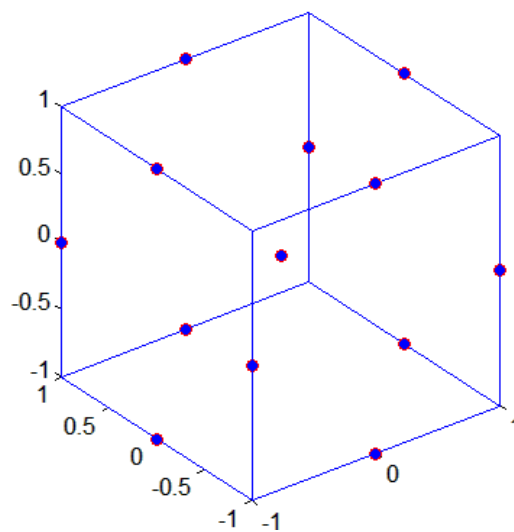


Figure 2.11: Box-Behnken design

2.6.4 Regression analysis

Regression is a method used to empirically fit the computed responses as a function of input parameters. This study used linear regression, which assumes linear relationship between the input parameters and the simulated responses. A typical regression equation is shown below.

$$y = X\hat{\beta} \quad (20)$$

Where $y = \begin{bmatrix} y_1 \\ y_2 \\ \cdot \\ y_N \end{bmatrix}$ is the response matrix computed from the simulator,

$X = \begin{bmatrix} X_{11} & X_{12} & X_{13} & \dots & X_{1M} \\ X_{21} & X_{22} & X_{23} & \dots & X_{2M} \\ \dots & \dots & \dots & \dots & \dots \\ X_{N1} & X_{N2} & X_{N3} & \dots & X_{NM} \end{bmatrix}$ is the simulation conditions determined using factorial design,

$\hat{\beta} = \begin{bmatrix} \hat{\beta}_1 \\ \hat{\beta}_2 \\ \cdot \\ \hat{\beta}_N \end{bmatrix}$ is the regression coefficient matrix calculated using $\hat{\beta} = (X^T X)^{-1} X^T y$

The regression coefficient matrix, $\hat{\beta}$, represents the statistical effect of the input parameter on the outcomes in y . The significance of individual input variable on the outcome can be estimated through the absolute magnitude of its regression coefficient.

CHAPTER 3 Using Experimental Design and Response Surface Methodology to Model Induced Fracture Geometry of Shublik Shale ¹

3.1 Methodology

The workflow procedure (**Figure 3.1**) followed in this study to model the fracture geometry using experimental design and response surface methodology is primarily divided into two stages. The first stage focuses on identifying the significant variables affecting the fracture geometry. This stage was conducted in three phases, each phase incorporating progressively more complex assumptions about geology. The second stage of the study uses the three most significant variables identified in the first stage to quantify a functional relationship between them and the predicted fracture geometry using Box-Behnken experimental design and response surface methodology. The workflow used in this study is as follows:

- Determine the output response fracture geometry variables (**Figure 3.2; Table 3.1**) to be modeled.
- Stage 1: Significant variable identification
 - Choose the publically available input variables to be investigated
 - Based on the literature review, choose a range (minimum, maximum) for the investigated input variables.
 - Use fractional factorial design to plan the number of simulations and estimate the fracture geometry parameters using the pseudo-3D numerical simulator.
 - Develop a linear model and generate the response surface for the 2-level linear model.
 - Based on the response surface, determine new variables, if any, to be added.

¹ This chapter along with an abbreviated Abstract and CHAPTER 1 is to be submitted as Poludasu, S. Awoleke, O., Ahmadi, M. and Hanks, C., 2015, “Using Experimental Design and Response Surface Methodology to Model Induced Fracture Geometry of Shublik Shale” to Hydraulic Fracturing Journal

- Add the new variables and repeat the above process.
- Stage 2: Proxy model development
 - Based on the linear model, determine the statistical significance of the input variables evaluated in Stage
 - Select the top three statistically significant variables for all of the 9 fracture geometry variables (**Table 3.1**).
 - Using these significant variables, plan a 3-level Box-Behnken design
 - Perform the planned simulations using pseudo 3D numerical simulator and generate the non-linear response surface
 - The equation governing the shape of response surface is the proxy model, a simple polynomial equation that can be used in lieu of the full numerical simulator
 - Estimate the prediction accuracy of the developed proxy models

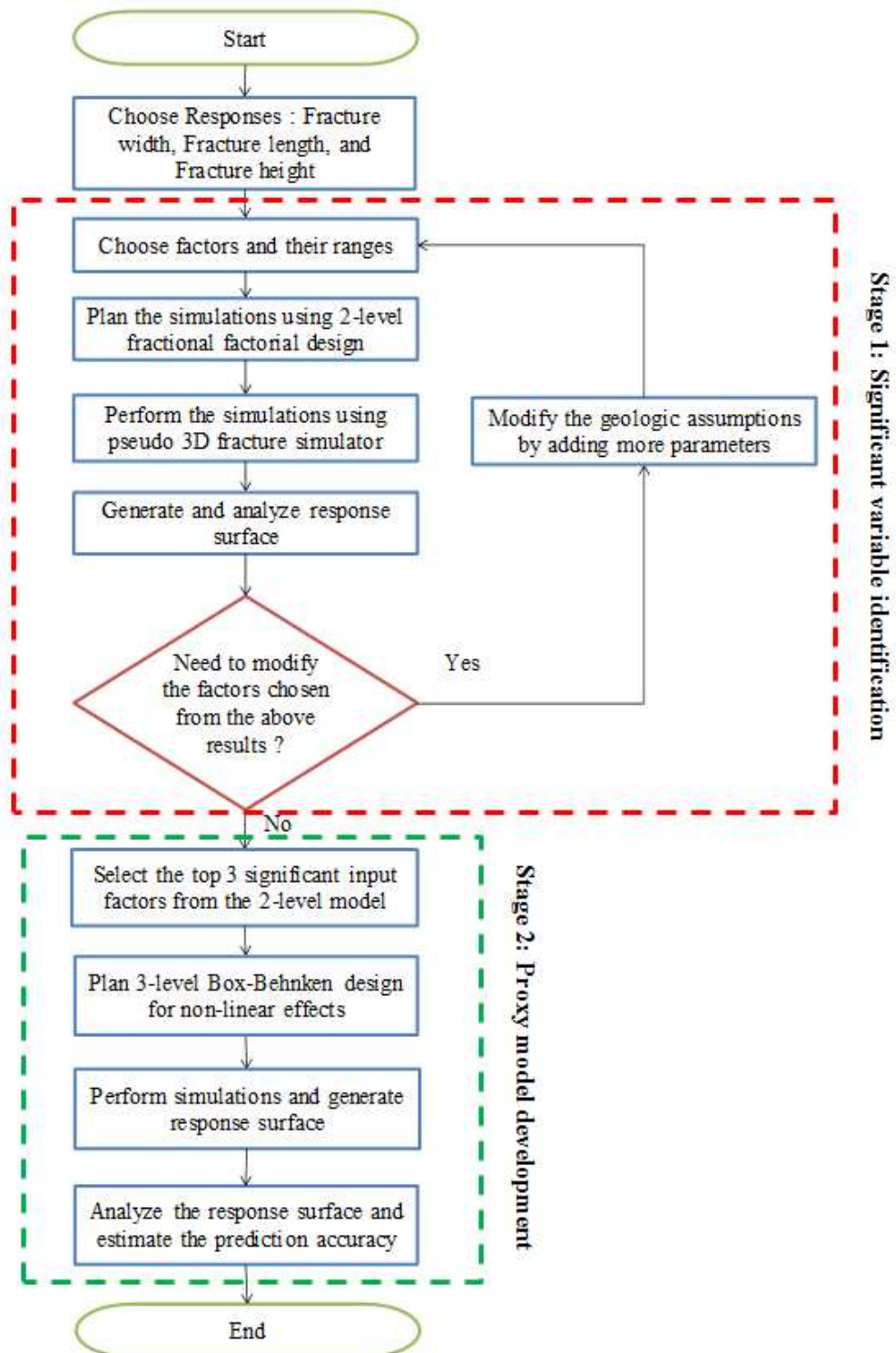
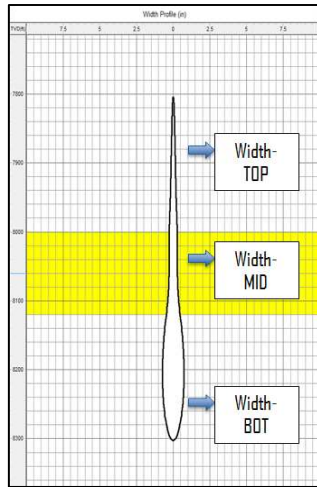
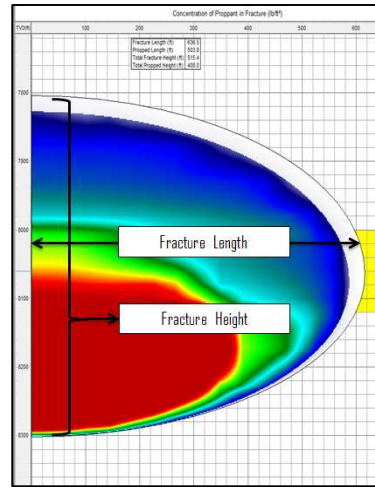


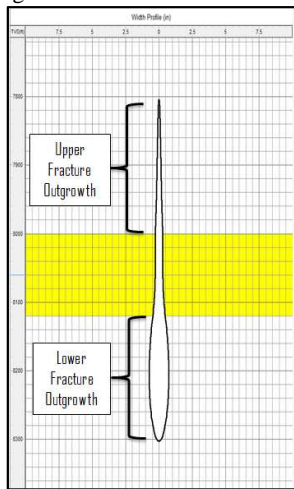
Figure 3.1: Flowchart describing the workflow used in this study



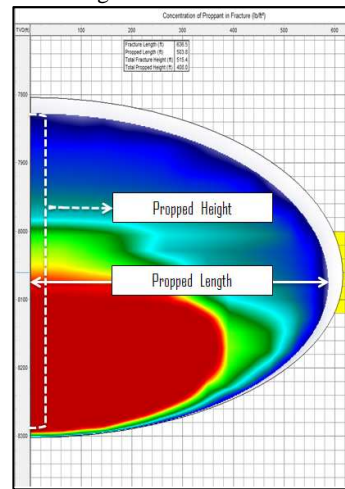
Typical width profile from the simulator showing the fracture width at three sections



Typical fracture profile from the simulator showing the fracture dimensions



Typical width profile from the simulator showing the fracture outgrowth



Typical fracture profile from the simulator showing the propped dimensions

Figure 3.2: Output variables estimation from the simulator generated fracture profile

Table 3.1: Nine fracture geometry variables modeled in this study

Dependent Parameter	Symbol
Width at the top of the fracture, in	<i>width_top</i>
Width at the middle of the fracture, in	<i>width_mid</i>
Width at the bottom of the fracture, in	<i>width_bot</i>
Fracture length, ft	<i>fracture_length</i>
Propped length, ft	<i>propped_length</i>
Fracture height, ft	<i>fracture_height</i>
Propped height, ft	<i>propped_height</i>
Upper fracture outgrowth, ft	<i>upper_outgrowth</i>
Lower fracture outgrowth, ft	<i>lower_outgrowth</i>

3.2 Stage 1: Significant parameter identification

Fracpro PT, a pseudo 3D fracture propagation model was used in this study. This simulator effectively determines the fracture treatment schedule for a known desired fracture length. After inputting the reservoir geology, mechanical properties, proppant type/size, fracturing fluid type, and the desired fracture length, Fracpro PT generates several treatment schedules and selects the treatment schedule with the predicted fracture length as close as possible to the desired estimate. As discussed earlier, pseudo 3D models have improved accuracy when compared to 2D models and they require less computational time/input data as compared to full 3D models. The Fracpro PT predictions can overestimate the fracture geometry in shales as it neglects stress shadowing, stress anisotropy and natural fractures. Regression analysis was performed Fracpro PT predictions to quantify the statistical significance using the MATLAB 8.0 software package.

3.2.1 Phase I

The Phase I of this study assumes a simple geological model as shown in **Figure 3.3**. This model treats the Shublik as homogenous shale layer bounded by sandstones. It was also assumed that the fracturing fluid is not allowed to leak-off into the boundary layers during the fracturing treatment (zero boundary layer permeability) and the horizontal well is always placed at the center of the shale formation.

From literature review, 16 variables and their parameter ranges were chosen and investigated in this phase. **Table 3.2** lists the variables, their ranges and their sources for this phase. Fractional factorial design was used to generate a planning matrix containing the 32 simulations. The planning table (**Table A.1**) and the design table (**Table A.2**) generated using the fractional factorial design for Phase I can be seen in the **Appendix A**. The fracture geometry variables predicted by the simulator were used for regression analysis. Even though all the 16 variables chosen have an impact on the fracture geometry, regression analysis captures the relative significance (variation in the response variables with a change in single input parameter) of each input variable. **Table 3.3** shows the p-values for the 16 variables evaluated in this study. In statistical significance testing, variables with p-values less than 0.05 imply a high relative impact on the predicted outcome. **Table 3.3** highlights the variables with p-value less than 0.05.

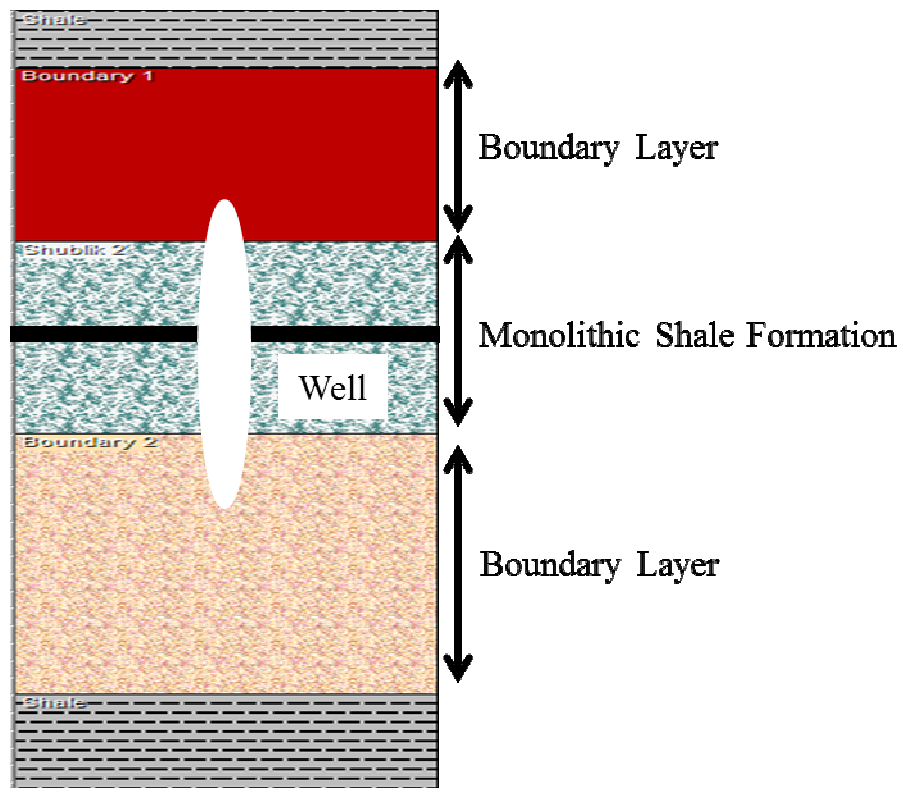


Figure 3.3: Geological assumptions made in Phase I

Table 3.2: Variables investigated by this study in Phase I

Input parameter	Symbol	Minimum anticipated value (-1)	Maximum anticipated value (+1)	Sources of parameter ranges
Desired fracture length, ft	f_l	150	450	For the analog Eagle Ford from Manchanda et al., 2012
Reservoir permeability, nD	k_r	1	800	For the analog Eagle Ford from Stegent et al., 2010
Young's modulus of the reservoir, MMpsia	E_r	1.5	6	For the analog Eagle Ford from Manchanda et al., 2012
Poisson's ratio	ν_r	0.22	0.26	Shublik thickness ranges identified by Parrish and Hulm, 2001
Reservoir thickness, ft	h_r	120	550	For the analog Eagle Ford from Centurion, 2011
Reservoir depth, ft	D	8000	13,500	
Upper layer Poisson's ratio	ν_u	0.21	0.38	The mechanical properties of typical sandstones
Upper layer Young's modulus, MMpsia	E_u	1.5	2.9	Upper layer thickness at 2 outcrop sections by Kelly et al., 2007
Upper layer thickness, ft	h_u	20	1000	
Lower layer Poisson's ratio	ν_l	0.21	0.38	The mechanical properties of typical sandstones
Lower layer Young's modulus, MMpsia	E_l	1.5	2.9	Lower layer thickness at 2 outcrop sections by Kelly et al., 2007
Lower layer thickness, ft	h_l	100	750	
Proppant type	P_t	Sand	Ceramic	
Proppant size	P_s	40/70	16/30	From that data library of Fracpro PT, numerical fracture simulator used in this study
Injection rate, bpm	q	45	100	
Fracturing fluid type	t	Slickwater	Cross-linked	

Table 3.3: p-values of the variables evaluated in Phase I (significant variables (p-values < 0.05) are highlighted). Symbols defined in Table 3.2

Input variables	width_top	width_mid	width_bot	fracture length	propped length	fracture height	propped height	upper outgrowth	lower outgrowth
<i>fl</i>	0.077	0.009	0.010	0.000	0.000	0.000	0.010	0.000	0.000
<i>kr</i>	0.912	0.721	0.811	0.748	0.962	0.838	0.543	0.666	0.635
<i>Er</i>	0.244	0.059	0.960	0.009	0.574	0.635	0.562	0.610	0.360
<i>vr</i>	0.263	0.413	0.831	0.317	0.691	0.759	0.640	0.459	0.286
<i>hr</i>	0.542	0.000	0.000	0.000	0.000	0.000	0.003	0.000	0.000
<i>D</i>	0.074	0.115	0.234	0.078	0.341	0.584	0.722	0.985	0.568
<i>vu</i>	0.035	0.757	0.471	0.886	0.568	0.879	0.543	0.667	0.952
<i>Eu</i>	0.355	0.598	0.426	0.711	0.967	0.814	0.796	0.447	0.680
<i>hu</i>	0.000	0.004	0.426	0.018	0.007	0.680	0.344	0.000	0.693
<i>vl</i>	0.434	0.384	0.384	0.904	0.571	0.376	0.625	0.785	0.194
<i>El</i>	0.315	0.997	0.743	0.467	0.303	0.388	0.660	0.282	0.092
<i>hl</i>	0.728	0.728	0.606	0.758	0.918	0.495	0.677	0.683	0.638
<i>Pt</i>	0.793	0.540	0.728	0.902	0.732	0.623	0.246	0.384	0.417
<i>Ps</i>	0.470	0.627	0.267	0.253	0.995	0.313	0.534	0.443	0.201
<i>q</i>	0.492	0.681	0.575	0.076	0.249	0.682	0.357	0.435	0.467
<i>t</i>	0.832	0.486	0.462	0.011	0.004	0.099	0.030	0.006	0.349

3.2.2 Phase II

The Phase II of this study has the same assumptions as in Phase I, except that the fracturing fluid was allowed to leak-off into the boundary layers during the fracturing treatment (non-zero boundary layer permeability; **Figure 3.4**). This phase consists of 18 variables including all the 16 variables in Phase I with addition of upper and lower layer permeabilities (**Table 3.4**). The factorial design (**Table A.3**) and planning (**Table A.4**) tables consisting of the 32 simulations required and parameter setting to evaluate the 18 variables for phase II can be seen in **Appendix A**. Following the same methodology used in Phase I, the p-values for the 18 variables are estimated and shown in **Table 3.5**, also the significant variables ($p\text{-value} < 0.05$) are highlighted.

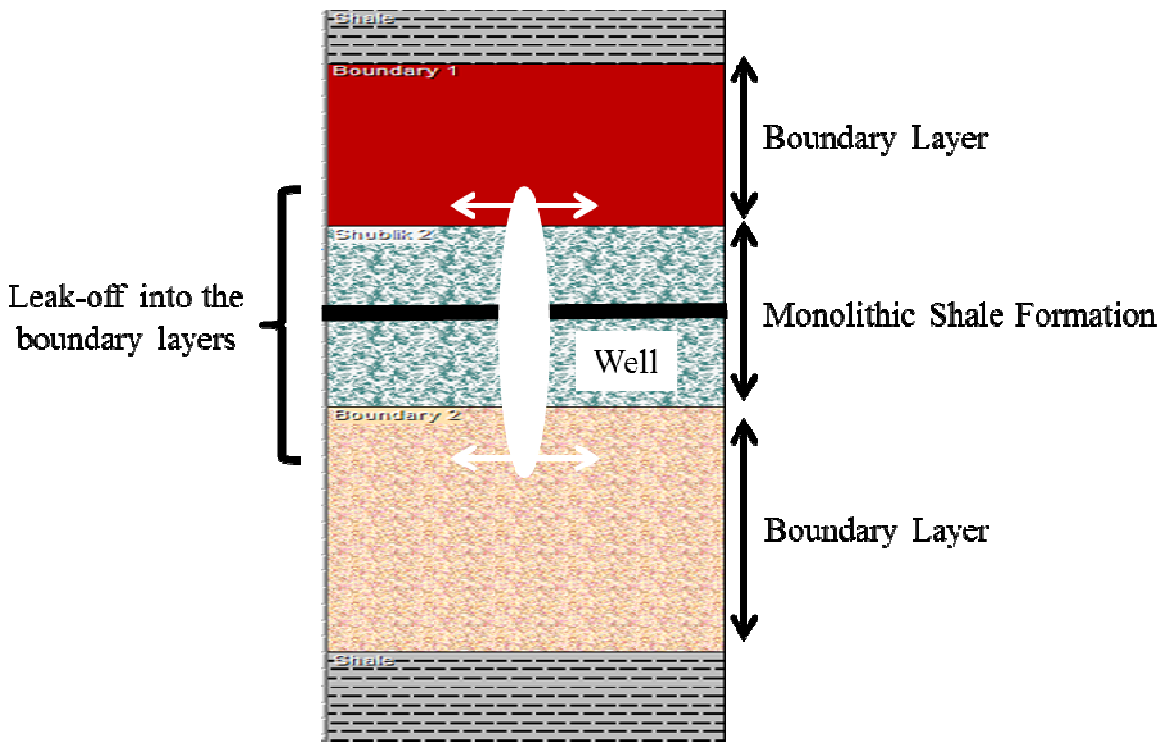


Figure 3.4: Geological assumptions made in Phase II

Table 3.4: Variables investigated by this study in Phase II (new variables added in this phase are highlighted)

Input parameter	Symbol	Minimum anticipated value (-1)	Maximum anticipated value (+1)	Sources of parameter ranges
Desired fracture length, ft	f_l	150	450	For the analog Eagle Ford from Manchanda et al., 2012
Reservoir permeability, nD	k_r	1	800	For the analog Eagle Ford from Stegent et al., 2010
Young's modulus of the reservoir, MMpsia	E_r	1.5	6	For the analog Eagle Ford from Manchanda et al., 2012
Poisson's ratio	ν_r	0.22	0.26	
Reservoir thickness, ft	h_r	120	550	Shublik thickness ranges identified by Parrish and Hulm, 2001
Reservoir depth, ft	D	8000	13,500	For the analog Eagle Ford from Centurion, 2011
Upper layer Poisson's ratio	ν_u	0.21	0.38	The mechanical properties of typical sandstones
Upper layer Young's modulus, MMpsia	E_u	1.5	2.9	
Upper layer thickness, ft	h_u	20	1000	Upper layer thickness at 2 outcrop sections by Kelly et al., 2007
Upper layer permeability, mD	k_u	1.8	21	Permeability of the Ivishak sandstone from Miller et al., 2002
Lower layer Poisson's ratio	ν_l	0.21	0.38	The mechanical properties of typical sandstones
Lower layer Young's modulus, MMpsia	E_l	1.5	2.9	
Lower layer thickness, ft	h_l	100	750	Lower layer thickness at 2 outcrop sections by Kelly et al., 2007
Lower layer permeability, mD	k_l	2.9	23	Permeability of the Sag River sandstone from Johnston and Christenson, 1998
Proppant type	P_t	Sand	Ceramic	
Proppant size	P_s	40/70	16/30	From that data library of Fracpro PT, numerical fracture simulator used in this study
Injection rate, bpm	q	45	100	
Fracturing fluid type	t	Slickwater	Cross-linked	

Table 3.5: p-values of the variables evaluated in Phase II (significant variables (p-values < 0.05) are highlighted)

Input variables	width_top	width_mid	width_bot	fracture length	propped length	fracture height	propped height	upper outgrowth	lower outgrowth
f_i	0.071	0.003	0.000	0.000	0.000	0.002	0.008	0.000	0.000
k_r	0.926	0.612	0.476	0.864	0.132	0.623	0.113	0.921	0.495
E_r	0.457	0.005	0.031	0.002	0.322	0.805	0.435	0.885	0.735
v_r	0.509	0.674	0.269	0.639	0.774	0.944	0.471	0.671	0.772
h_r	0.918	0.000	0.000	0.000	0.000	0.012	0.083	0.000	0.000
D	0.888	0.657	0.194	0.005	0.040	0.232	0.190	0.202	0.541
v_u	0.279	0.257	0.385	0.167	0.269	0.200	0.919	0.484	0.432
E_u	0.476	0.132	0.386	0.038	0.039	0.623	0.486	0.283	0.392
h_u	0.000	0.003	0.768	0.000	0.023	0.950	0.591	0.101	0.298
k_u	0.941	0.300	0.935	0.975	0.442	0.722	0.904	0.988	0.785
v_l	0.875	0.544	0.554	0.881	0.366	0.480	0.429	0.399	0.700
E_l	0.699	0.276	0.576	0.923	0.453	0.583	0.591	0.683	0.770
h_l	0.182	0.380	0.741	0.607	0.394	0.758	0.442	0.462	0.806
k_l	0.994	0.926	0.836	0.363	0.571	0.680	0.254	0.441	0.753
P_l	0.904	0.949	0.236	0.859	0.477	0.589	0.807	0.779	0.790
P_s	0.834	0.071	0.424	0.629	0.254	0.918	0.538	0.629	0.877
q	0.281	0.752	0.475	0.030	0.916	0.471	0.577	0.652	0.352
t	0.979	0.134	0.742	0.027	0.015	0.892	0.240	0.194	0.372

3.2.3 Phase III

From the results in Phases I and II, we can see that the reservoir thickness is a critical parameter with high relative impact on most of the predicted fracture geometry. The Phase III model assumes that the shale (payzone) thickness is equally divided into four sub layers with varying mechanical and reservoir properties (**Figure 3.5**). These four layers are: A (organic-rich shale), B (carbonate), C (organic-rich shale), and D (sandstone) which is the stratigraphy observed in the Shublik (**Figure 2.1**). The mechanical and reservoir properties of Shublik or Eagle Ford used in Phase I/II are used only for the organic-rich sub layers, and the other two sub layers are assumed to have the Fracpro PT software library values for carbonates and sandstones. This study also investigates the implications of placing the horizontal leg in the shale layer A or shale layer C for stimulation treatment. This phase evaluated 26 variables (**Table 3.6**). The factorial design (**Table A.5**) and planning (**Table A.6**) tables consisting of the 32 simulations required and parameter setting to evaluate the 26 variables for phase III can be seen in **Appendix A**. Following the same methodology used in Phases I and II, 26 variables were evaluated and the corresponding p-value matrix can be seen in **Table 3.7**.

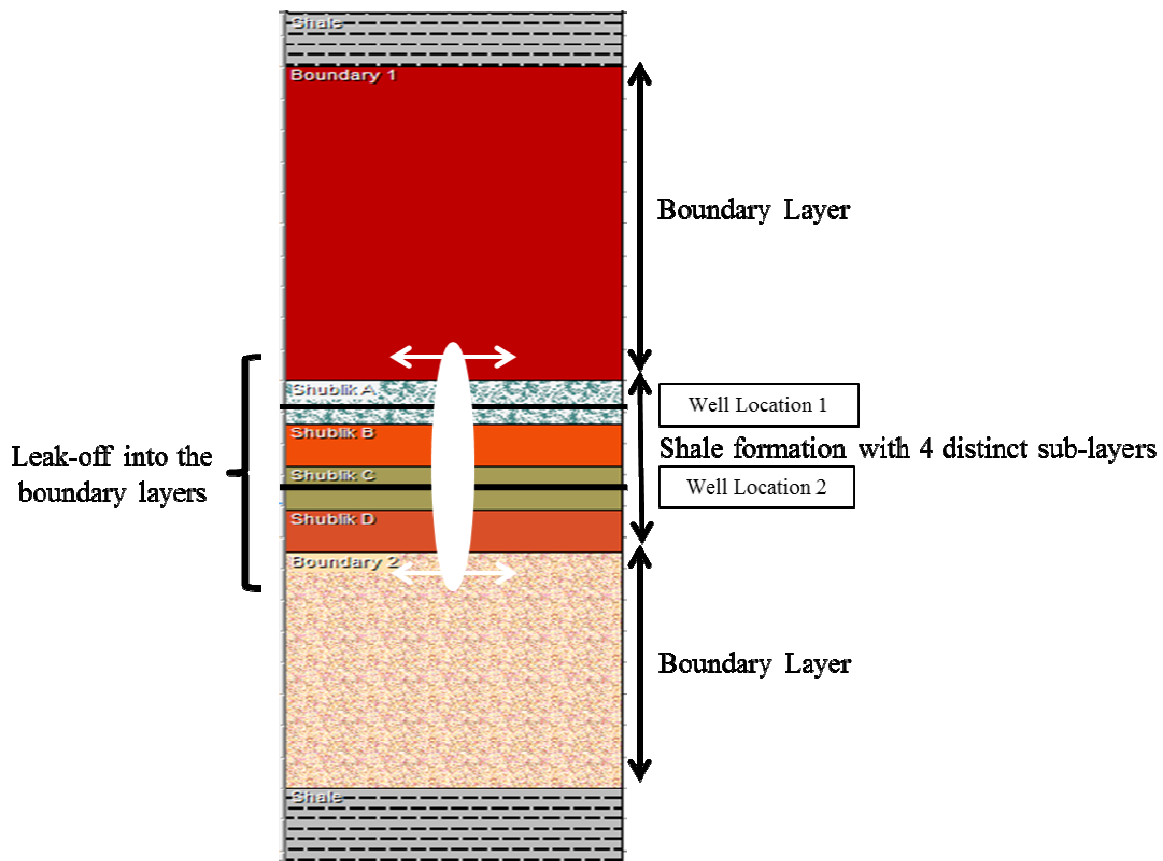


Figure 3.5: Geological assumptions made in Phase III

Table 3.6: Variables investigated by this study in Phase III (new variables added in this study are highlighted)

Input parameter	Symbol	Minimum anticipated value (-1)	Maximum anticipated value (+1)	Sources of parameter ranges
Shublik A Young's modulus	E_{rA}	1.5	6	For the analog Eagle Ford from Manchanda et al., 2012
Shublik A Poisson's ratio	ν_{rA}	0.22	0.26	
Shublik B Young's modulus	E_{rB}	3	3.6	The mechanical properties of typical carbonates
Shublik B Poisson's ratio	ν_{rB}	0.18	0.23	
Shublik C Young's modulus	E_{rC}	1.5	6	For the analog Eagle Ford from Manchanda et al., 2012
Shublik C Poisson's ratio	ν_{rC}	0.22	0.26	
Shublik D Young's modulus	E_{rD}	1.5	2.95	The mechanical properties of typical sandstones
Shublik D Poisson's ratio	ν_{rD}	0.21	0.38	
Permeability in Shublik A, nD	k_{rA}	1	800	For the analog Eagle Ford from Stegent et al., 2010
Well placement	W_p	A	C	Chosen from the 2 organic-rich shales from Hulm 1999
Permeability in Shublik C, nD	k_{rC}	1	800	For the analog Eagle Ford from Stegent et al., 2010
Permeability in Shublik B & D, mD	k_{rBD}	10	100	Permeability range of 10-100 mD was chosen
Reservoir depth, ft	D	8000	13,500	For the analog Eagle Ford from Centurion, 2011
Upper layer Poisson's ratio	ν_u	0.21	0.38	The mechanical properties of typical sandstones
Upper layer Young's modulus, MMpsi	E_u	2.38	3.55	
Upper layer thickness, ft	h_u	20	1000	Upper layer thickness at 2 outcrops by Kelly et al., 2007
Upper Layer permeability, mD	k_u	1.8	21	Permeability of the Ivishak sandstone from Miller et al., 2002
Lower layer Poisson's ratio	ν_l	0.21	0.38	The mechanical properties of typical sandstones
Lower layer Young's modulus, MMpsi	E_l	2.38	3.55	
Lower layer thickness, ft	h_l	100	750	Lower layer thickness at 2 outcrops by Kelly et al., 2007
Lower layer permeability, mD	k_l	2.9	23	Permeability of the Sag River sandstone from Johnston and Christenson, 1998
Proppant type	P_t	Sand	Ceramic	
Proppant size	P_s	40/70	16/30	
Injection rate, bpm	q	45	100	From that data library of Fracpro PT, numerical fracture simulator used in this study
Fracturing fluid type	t	Slickwater	Cross-linked	
Reservoir thickness, ft	h_r	120	550	

Table 3.7: p-values of the variables evaluated in Phase III (significant variables (p-values < 0.05) are highlighted)

Input variables	width_top	width_mid	width_bot	fracture length	propped length	fracture height	propped height	upper outgrowth	lower outgrowth
E_{rA}	0.626	0.190	0.090	0.997	0.885	0.035	0.034	0.033	0.000
v_{rA}	0.106	0.759	0.366	0.363	0.471	0.783	0.741	0.320	0.124
E_{rB}	0.050	0.386	0.821	0.580	0.599	0.718	0.648	0.299	0.714
v_{rB}	0.156	0.902	0.691	0.212	0.346	0.584	0.821	0.744	0.471
E_{rC}	0.829	0.146	0.137	0.359	0.358	0.980	0.515	0.942	0.005
v_{rC}	0.022	0.619	0.860	0.652	0.490	0.777	0.300	0.949	0.010
E_{rD}	0.940	0.978	0.489	0.901	0.930	0.268	0.528	0.320	0.012
v_{rD}	0.149	0.972	0.806	0.890	0.845	0.848	0.740	0.153	0.005
k_{rA}	0.297	0.682	0.731	0.737	0.694	0.519	0.907	0.791	0.050
D	0.035	0.495	0.272	0.726	0.798	0.081	0.484	0.095	0.044
v_u	0.033	0.758	0.495	0.724	0.675	0.632	0.824	0.823	0.851
E_u	0.100	0.133	0.282	0.838	0.885	0.456	0.333	0.977	0.787
h_u	0.000	0.383	0.529	0.183	0.228	0.227	0.981	0.567	0.275
k_u	0.876	0.952	0.375	0.960	0.865	0.389	0.498	0.641	0.851
v_l	0.038	0.310	0.114	0.724	0.805	0.162	0.683	0.877	0.044
E_l	0.018	0.765	0.769	0.245	0.268	0.244	0.828	0.347	0.275
h_l	0.003	0.302	0.916	0.785	0.948	0.284	0.229	0.459	0.787
k_l	0.794	0.915	0.932	0.571	0.657	0.550	0.849	0.382	0.012
P_t	0.010	0.163	0.041	0.794	0.596	0.647	0.459	0.737	0.010
P_s	0.079	0.655	0.782	0.453	0.455	0.416	0.946	0.299	0.050
q	0.354	0.438	0.493	0.342	0.411	0.483	0.523	0.173	0.124
t	0.195	0.220	0.326	0.510	0.503	0.474	0.362	0.629	0.353
h_r	0.013	0.028	0.647	0.017	0.014	0.002	0.000	0.008	0.000
W_p	0.407	0.939	0.141	0.477	0.579	0.907	0.864	0.002	0.000
k_{rC}	0.006	0.091	0.187	0.108	0.088	0.170	0.178	0.336	0.714
k_{rBD}	0.204	0.520	0.553	0.867	0.904	0.949	0.352	0.669	0.141

3.3 Stage 2: Proxy model development

In this stage, a quantitative relationship (proxy models) between input variables (26 variables from Phase III) and fracture geometry predicted by Fracpro PT were developed using the Box-Behnken design and response surface methodology (regression analysis). Out of the 26 variables evaluated in Phase III, the top three significant variables were chosen based on the magnitude of the p-values from the Stage 1 (as seen in **Table 3.8**) to develop non-linear proxy models. These proxy models are a simplified version of Fracpro PT (polynomial equation) with the capacity to predict the fracture geometry. These proxy models can be used as a substitute for Fracpro PT in predicting fracture geometry with relative ease.

Table 3.8: Three most important input variables affecting the modeled fracture geometry identified in Stage 1 of study

Modeled Fracture Geometry	Most significant input variables
Width at the top of the fracture	Upper layer thickness (h_u) Lower layer thickness (h_l) Permeability in Shublik C (k_{rC})
Width at the middle of the fracture	Reservoir thickness (h_r) Permeability in Shublik C (k_{rC}) Upper layer Young's modulus (E_u)
Width at the bottom of the fracture	Proppant type (P_t) Shublik A Young's modulus (E_{rA}) Lower layer Poisson's ratio (ν_l)
Fracture length	Reservoir thickness (h_r) Permeability in Shublik C (k_{rC}) Upper layer thickness (h_u)
Propped length	Reservoir thickness (h_r) Permeability in Shublik C (k_{rC}) Upper layer thickness (h_u)
Fracture height	Reservoir thickness (h_r) Shublik A Young's modulus (E_{rA}) Reservoir depth (D)
Propped height	Reservoir thickness (h_r) Shublik A Young's modulus (E_{rA}) Permeability in Shublik C (k_{rC})
Upper fracture outgrowth	Well placement (W_p) Reservoir thickness (h_r) Shublik A Young's modulus (E_{rA})
Lower fracture outgrowth	Reservoir thickness (h_r) Shublik A Young's modulus (E_{rA}) Well placement (W_p)

3.3.1 Box-Behnken design

In this study, was used to determine the relationship between the top three significant variables (**Table 3.9**) and the fracture geometry variables. Each input factor is sampled at three values, generally coded as -1, 0, +1 (minimum, median (arithmetic average), and maximum anticipated input variable).

For the 3 screened variables in **Table 3.8**, Box-Behnken design would require a total of 15 runs (as seen in **Table 3.9**). When the fracture geometry (responses) predicted by the numerical simulator for these 15 runs are plotted on 3D surface graph (versus any two input variables), a response surface is generated. A mathematical equation governing these response surfaces can be effectively used as a proxy model to predict the fracture geometry without using the actual simulator. The resultant mathematical model for a response surface with three variables after regression analysis using MATLAB 8.0 would look in the following form:

$$y = \beta_0 + \beta_1x_1 + \beta_2x_2 + \beta_3x_3 + \beta_{11}x_1^2 + \beta_{22}x_2^2 + \beta_{33}x_3^2 + \beta_{12}x_1x_2 + \beta_{13}x_1x_3 + \beta_{23}x_2x_3 \quad (21)$$

Where y is predicted response, β_0 is the intercept of the model, $\beta_1, \beta_2, \beta_3$ are the regression coefficients of the input variables x_1, x_2, x_3 , $\beta_{12}, \beta_{13}, \beta_{23}$ are the regression coefficients of two factor interaction terms, and $\beta_{11}, \beta_{22}, \beta_{33}$ are the second-order regression coefficients.

Table 3.9: Box-Behnken design for three variables coded as -1 (minimum), 0 (median), +1 (maximum)

Run#	Input Parameter 1	Input Parameter 2	Input Parameter 3
1	0	1	1
2	0	1	-1
3	1	0	1
4	1	1	0
5	-1	1	0
6	-1	0	1
7	0	0	0
8	0	-1	1
9	-1	0	-1
10	0	0	0
11	1	0	-1
12	0	0	0
13	0	-1	-1
14	1	-1	0
15	-1	-1	0

3.3.2 Stage 2: Results

A three parameter coded 3-level Box Behnken design (**Table 3.9**) was used to determine the relationships between the significant variables (**Table 3.8**) and nine fracture geometry variables. The non-linear mathematical models developed for nine fracture geometry variables are discussed in the following sections. 3D response surfaces, a graphic illustration of the relationship between any three variables, were also generated.

3.3.2.1 Fracture width at the top of the fracture

Fracture width at the top of the fracture (*width_top*) has three significant variables (1) Upper layer thickness (h_u), (2) Lower layer thickness (h_l), and (3) Permeability in Shublik C (k_{rC}). These three parameters are evaluated using Box-Behnken design. By plotting the predicted *width_top* for the 15 simulation runs (**Table 3.9**) on a 3D surface graph, response surfaces can be generated (**Figures 3.6** through **3.8**). **Figure 3.6** is the response surface plot showing the effect of k_{rC} and h_u on *width_top*. **Figure 3.7** is the response surface plot showing the effect of k_{rC} and h_l on *width_top*. **Figure 3.8** is the response surface plot showing the effect of h_l and h_u on *width_top*.

These surface plots can be used to understand the interdependence of the three input variables based on the variation in predicted *width_top*. From **Figure 3.7**, it can be observed that as the k_{rC} increases in between minimum and maximum anticipated value, the continuously increases when the h_u is at minimum anticipated value. Whereas when h_u is at maximum anticipated value, the fracture geometry initially decreases and then starts to increase again, as k_{rC} is varied between minimum and maximum. Also, the mathematical equation governing these response surfaces can be ultimately used to predict *width_top* with the knowledge of just three parameters h_u , h_l , and k_{rC} . The non-linear response surface model developed for *width_top* can be seen below.

$$\begin{aligned} \ln(\text{width_top}) = & 0.141 - 0.0219h_u + 0.0798h_l - 0.036k_{rC} + 0.0437(h_u)(h_l) + 0.0614(h_u)(k_{rC}) \\ & - 0.0192(h_l)(k_{rC}) - 0.0086h_u^2 - 0.0506h_l^2 + 0.0601k_{rC}^2 \end{aligned} \quad (22)$$

Figure 3.9 shows the relationship between *width_top* predicted by the simulator and the non-linear model from this study with the R^2 value of 0.82 (higher the R^2 value, higher is the prediction accuracy).

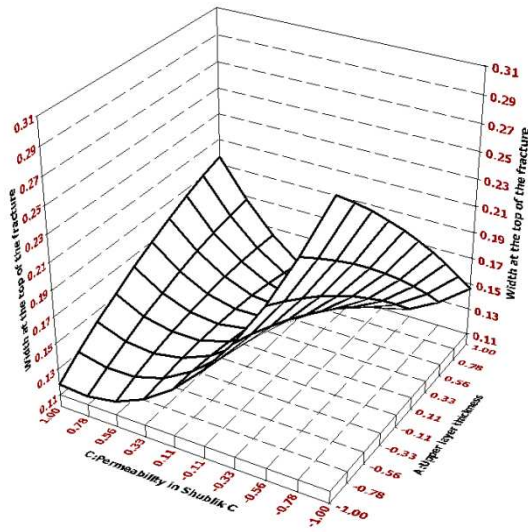


Figure 3.6: 3D response surface plot showing the effect of k_{rC} and h_u on $width_top$

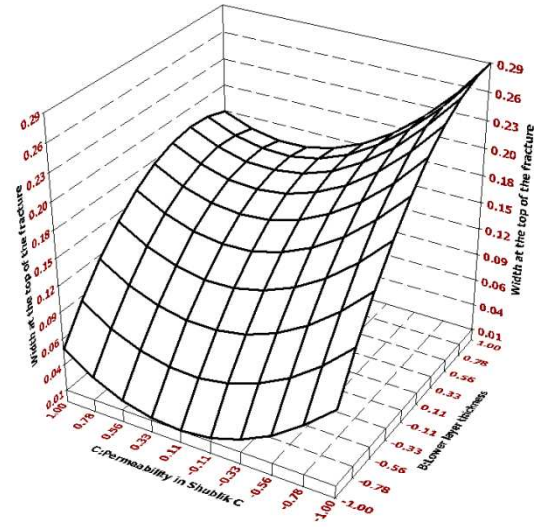


Figure 3.7: 3D response surface plot showing the effect of k_{rC} and h_l on $width_top$

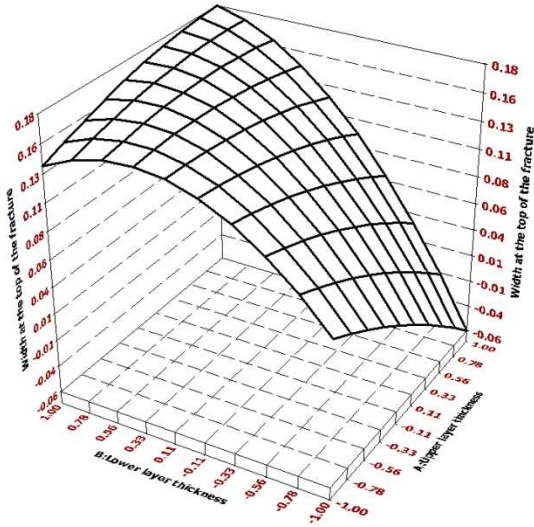


Figure 3.8: 3D response surface plot showing the effect of h_l and h_u on $width_top$

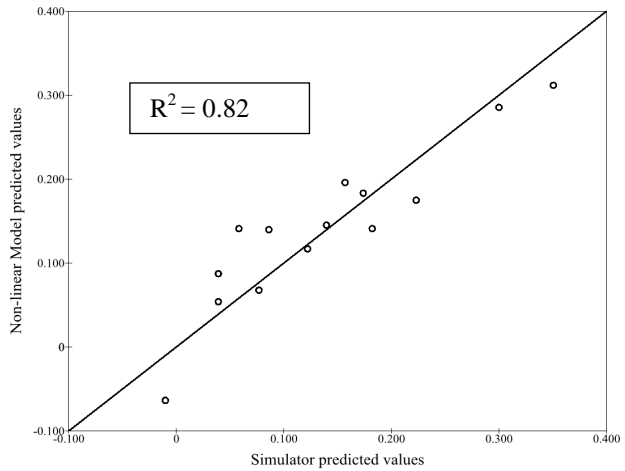


Figure 3.9: Relationship between $width_top$ predicted by the simulator and the non-linear model from this study

3.3.2.2 Fracture width at the middle of the fracture

Fracture width at the middle of the fracture ($width_mid$) has three significant variables (1) Reservoir thickness (h_r), (2) Permeability in Shublik C (k_{rC}), and (3) Upper layer Young's Modulus (E_u). By plotting the predicted $width_top$ for the 15 simulation runs (**Table 3.9**) on a 3D

surface graph we can generate the response surfaces (Figures 3.10 through 3.12). Figure 3.10 is the response surface plot showing the effect of k_{rC} and E_u on $width_mid$. Figure 3.11 is the response surface plot showing the effect of h_r and E_u on $width_mid$. Figure 3.12 is the response surface plot showing the effect of k_{rC} and h_r on $width_mid$. The non-linear response surface model for $width_mid$ developed using similar methodology can be seen below:

$$\ln(width_mid) = 0.5008 + 0.6293h_r + 0.0068k_{rC} + 0.0319E_u - 0.1181(h_r)(k_{rC}) - 0.0026(h_r)(E_u) + 0.0834(E_u)(k_{rC}) - 0.2711h_r^2 + 0.0358E_u^2 - 0.0557k_{rC}^2 \quad (23)$$

Figure 3.13 shows the relationship between $width_mid$ predicted by the simulator and the non-linear model from this study with the R^2 value of 0.97.

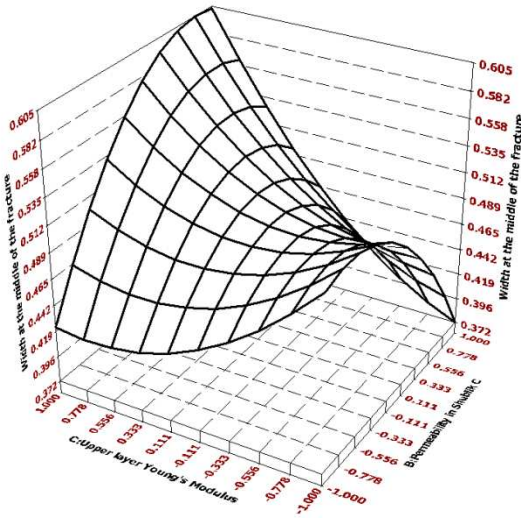


Figure 3.10: 3D response surface plot showing the effect of k_{rC} and E_u on $width_mid$

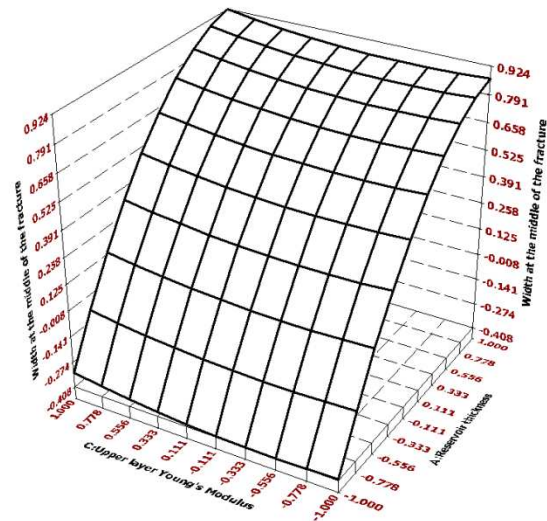


Figure 3.11: 3D response surface plot showing the effect of h_r and E_u on $width_mid$

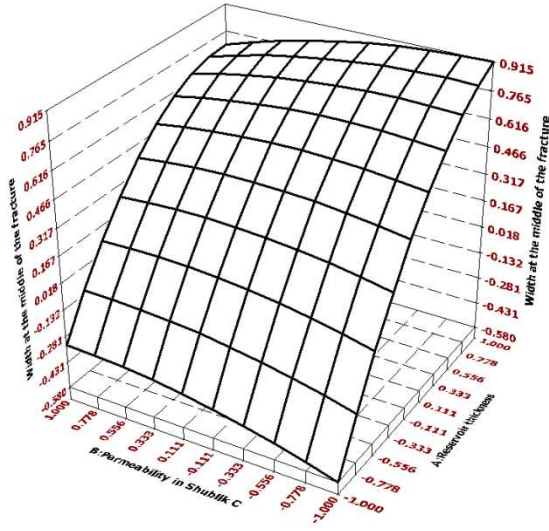


Figure 3.12: 3D response surface plot showing the effect of k_{rC} and h_r on $width_mid$

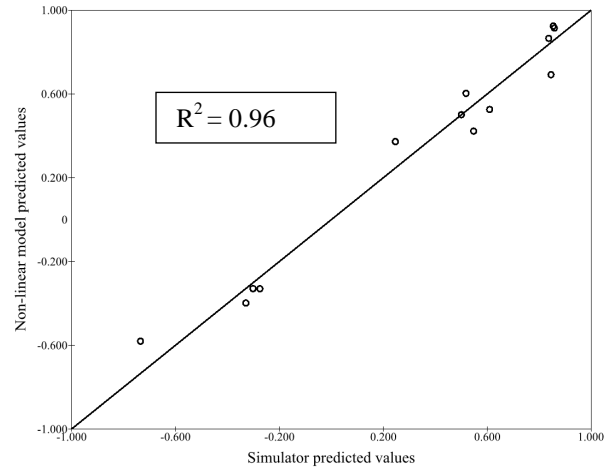


Figure 3.13: Relationship between $width_mid$ predicted by the simulator and the non-linear model from this study

3.3.2.3 Fracture width at the bottom of the fracture

Fracture width at the bottom of the fracture ($width_bot$) has three significant variables (1) Proppant type (P_t), (2) Shublik A Young's modulus (E_{rA}), and (3) Lower layer Poisson's Ratio (ν_l). **Figures 3.14** through **3.16** shows the 3D response surface plot for $width_bot$. **Figure 3.14** shows the effect of ν_l and E_{rA} on $width_bot$. **Figure 3.15** shows the effect of E_{rA} and P_t on $width_bot$. **Figure 3.16** shows the effect of P_t and ν_l on $width_bot$. The non-linear model developed can be seen below.

$$\ln(width_bot) = 0.2852 - 0.1947 P_t + 0.1664 E_{rA} + 0.1576 \nu_l - 0.1676 (P_t)(E_{rA}) - 0.0148 (P_t)(\nu_l) - 0.0323 (E_{rA})(\nu_l) - 0.3983 P_t^2 + 0.2705 E_{rA}^2 + 0.1112 \nu_l^2 \quad (24)$$

Figure 3.17 shows the relationship between $width_bot$ predicted by the simulator and the non-linear model from this study with the R^2 value of 0.68.

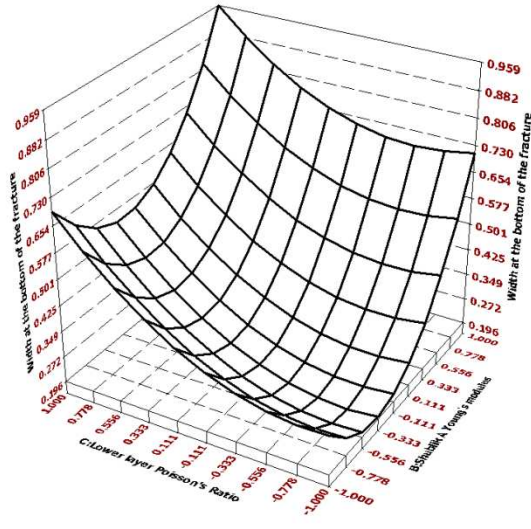


Figure 3.14: 3D response surface plot showing the effect of v_l and E_{rA} on $width_{bot}$

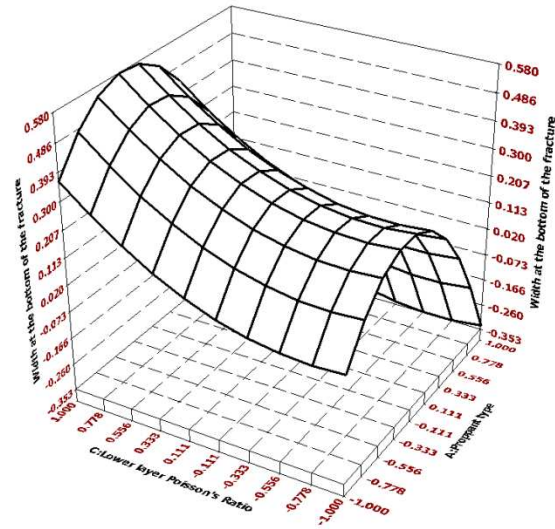


Figure 3.15: 3D response surface plot showing the effect of E_{rA} and P_l on $width_{bot}$

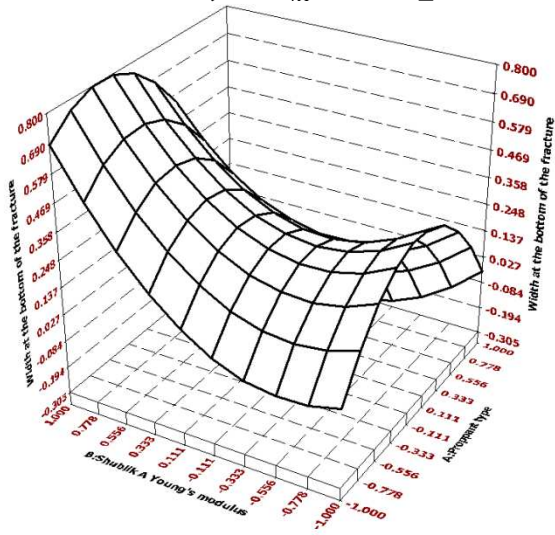


Figure 3.16: 3D response surface plot showing the effect of P_l and v_l on $width_{bot}$

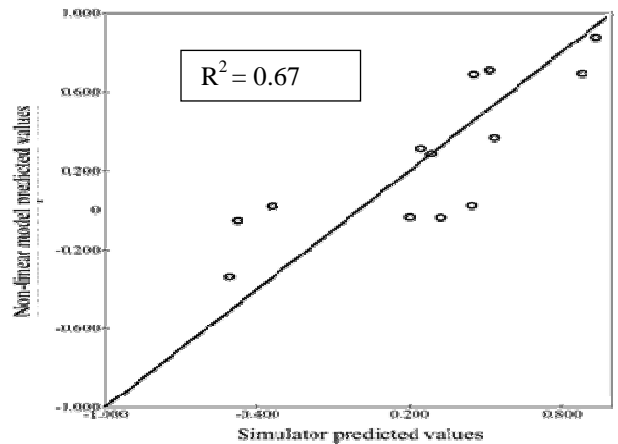


Figure 3.17: Relationship between $width_{bot}$ predicted by the simulator and the non-linear model

3.3.2.4 Fracture length

Fracture length (*fracture_length*) has three significant variables (1) Reservoir thickness (h_r), (2) Permeability in Shublik C (k_{rC}), and (3) Upper layer thickness (h_u). **Figures 3.18** through **3.20** shows the 3D response surface plot for *fracture_length*. **Figure 3.18** shows the effect of k_{rC} and h_u on *fracture_length*. **Figure 3.19** shows the effect of h_r and h_u on *fracture_length*. **Figure 3.20** shows the effect of k_{rC} and h_r on *fracture_length*. The non-linear model developed can be seen below.

$$\ln(\text{fracture_length}) = 5.507 + 0.363h_r - 0.0023k_{rC} - 0.112h_l + 0.0095(h_l)(k_{rC}) + 0.0017(h_r)(h_l) + 0.0071(k_{rC})(h_l) + 0.2509h_r^2 + 0.0062k_{rC}^2 + 0.0057h_l^2 \quad (25)$$

Figure 3.21 shows the relationship between *fracture_length* predicted by the simulator and the non-linear model from this study with the R² value of 0.99.

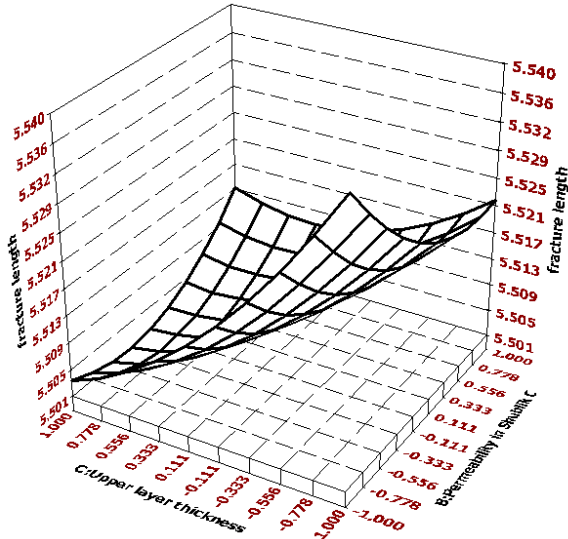


Figure 3.18: 3D response surface plot showing the effect of k_{rC} and h_u on *fracture_length*

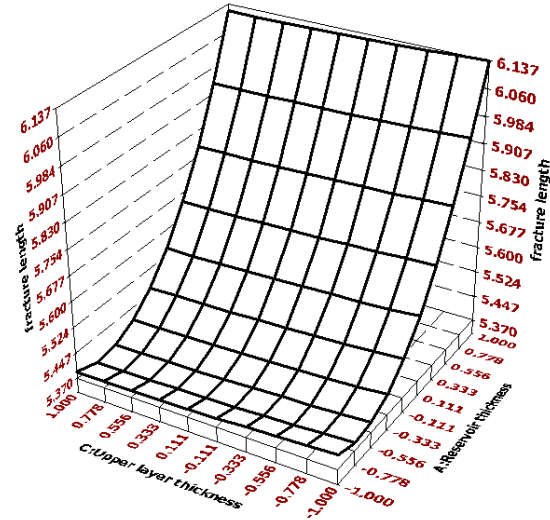


Figure 3.19: 3D response surface plot showing the effect of h_r and h_u on *fracture_length*

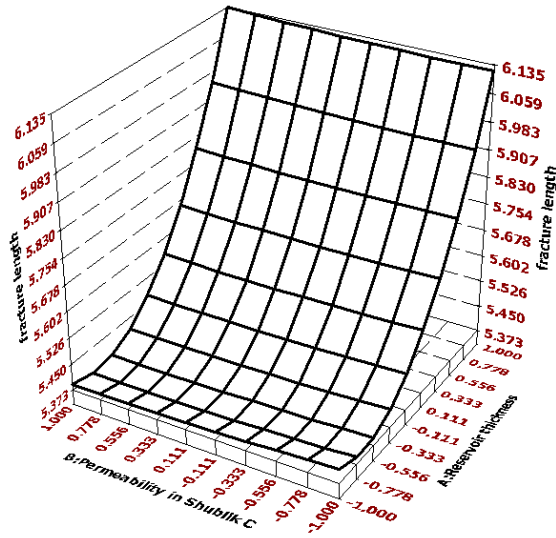


Figure 3.20: 3D response surface plot showing the effect of k_{rC} and h_r on *fracture_length*

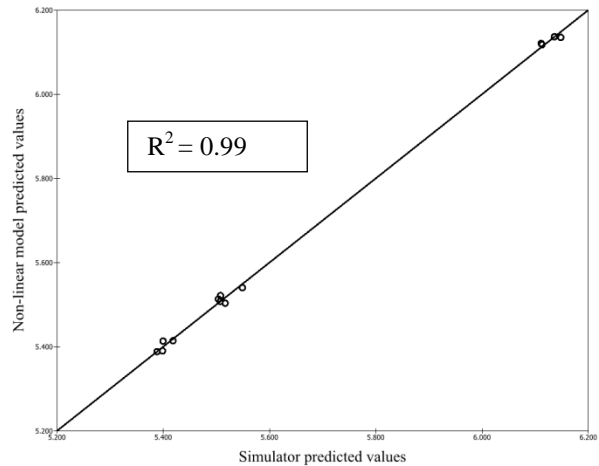


Figure 3.21: Relationship between *fracture_length* predicted by the simulator and the non-linear model

3.3.2.5 Propped length

Propped length (*propped_length*) has three significant variables (1) Reservoir thickness (h_r), (2) Permeability in Shublik C (k_{rC}), and (3) Upper layer thickness (h_u). **Figures 3.22 through 24** shows the 3D response surface plot for *propped_length*. **Figure 3.22** shows the effect of k_{rC} and h_u on *propped_length*. **Figure 3.23** shows the effect of h_r and h_u on *propped_length*. **Figure 3.24** shows the effect of k_{rC} and h_r on *propped_length*. The non-linear model developed can be seen below.

$$\ln(\text{propped_length}) = 5.507 + 0.393h_r - 0.0023k_{rC} - 0.0146h_u + 0.0079(h_u)(k_{rC}) + 0.0048(h_r)(h_u) + 0.0048(k_{rC})(h_u) + 0.2142h_r^2 + 0.0033k_{rC}^2 + 0.0027h_u^2 \quad (26)$$

Figure 3.25 shows the relationship between *propped_length* predicted by the simulator and the non-linear model from this study with the R^2 value of 0.99.

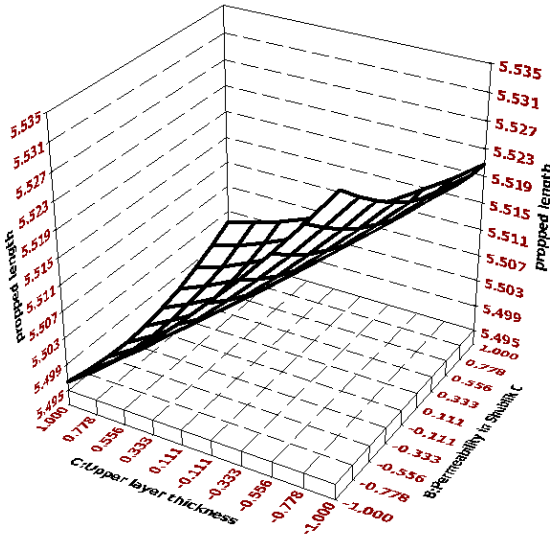


Figure 3.22: 3D response surface plot showing the effect of k_{rC} and h_u on *propped_length*

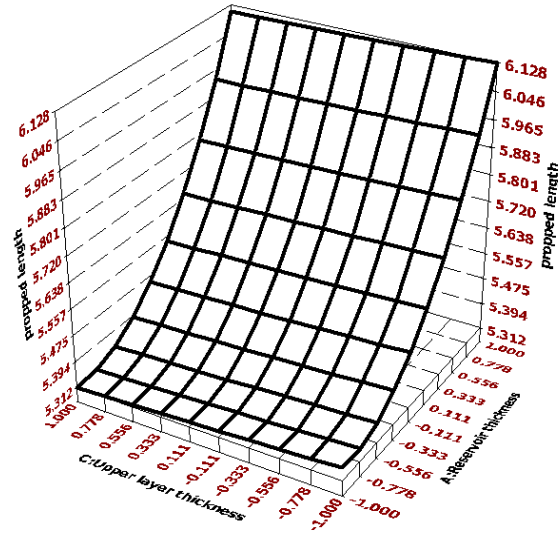


Figure 3.23: 3D response surface plot showing the effect of h_r and h_u on *propped_length*

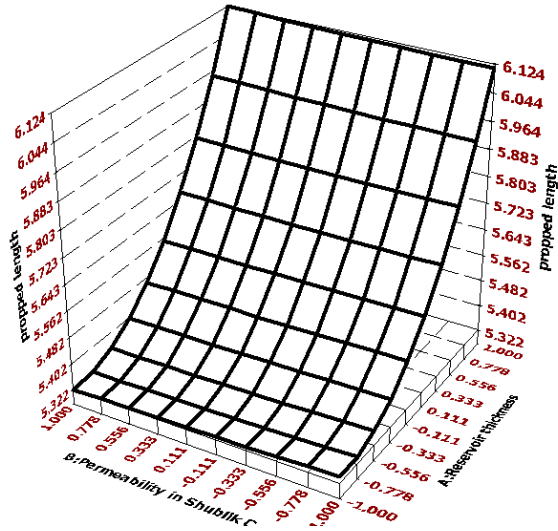


Figure 3.24: 3D response surface plot showing the effect of k_{rC} and h_r on $propped_length$

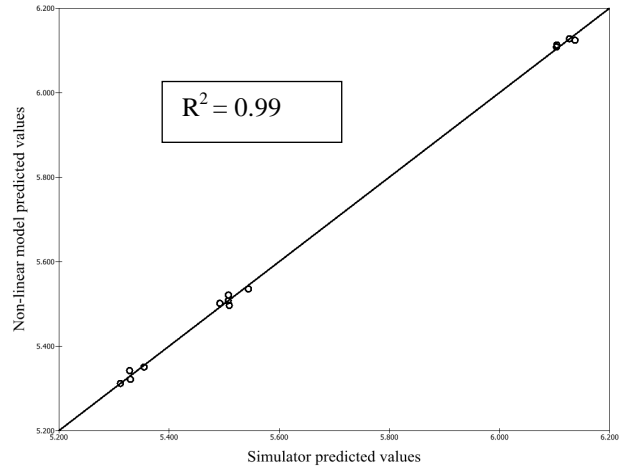


Figure 3.25: Relationship between $propped_length$ predicted by the simulator and the non-linear model from this study

3.3.2.6 Fracture height

Fracture height ($fracture_height$) has three significant variables (1) Reservoir thickness (h_r), (2) Shublik A Young's modulus (E_{rA}), (3) Reservoir depth (D). **Figures 3.26** through **3.28** shows the 3D response surface plot for $fracture_height$. **Figure 3.26** shows the effect of h_r and D on $fracture_height$. **Figure 3.27** shows the effect of h_r and D on $fracture_height$. **Figure 3.28** shows the effect of E_{rA} and D on $fracture_height$. The non-linear model developed can be seen below.

$$\ln(fracture_height) = 5.8093 + 0.6365 h_r - 0.0104 E_{rA} - 0.0104 D + 0.0208 (h_r)(E_{rA}) + 0.008 (h_r)(D) - 0.0207 (E_{rA})(D) - 0.2228 h_r^2 + 0.0243 E_{rA}^2 - 0.00468 D^2 \quad (27)$$

Figure 3.29 shows the relationship between $fracture_height$ predicted by the simulator and the non-linear model from this study with the R^2 value of 0.99.

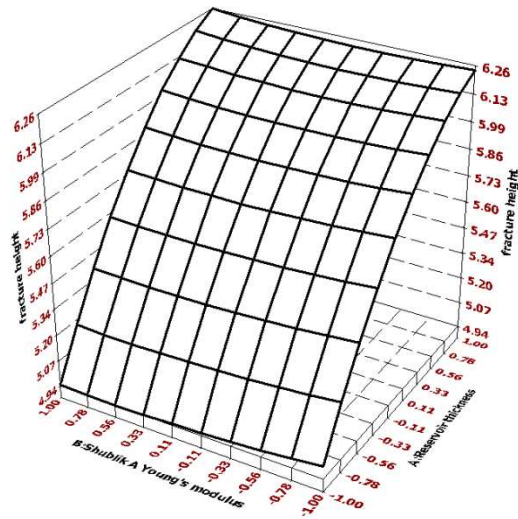


Figure 3.26: 3D response surface plot showing the effect of E_{rA} and h_r on *fracture_height*

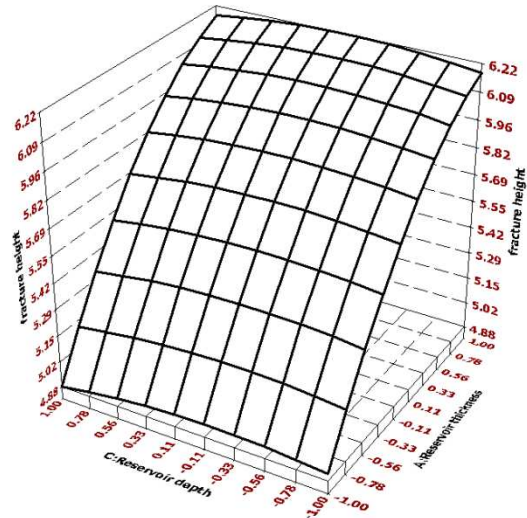


Figure 3.27: 3D response surface plot showing the effect of h_r and D on *fracture_height*

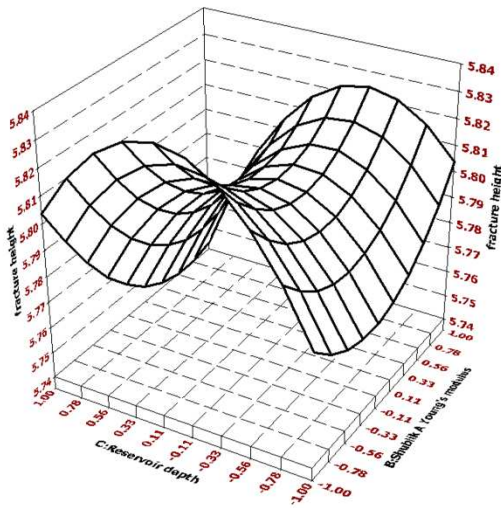


Figure 3.28: 3D response surface plot showing the effect of E_{rA} and D on *fracture_height*

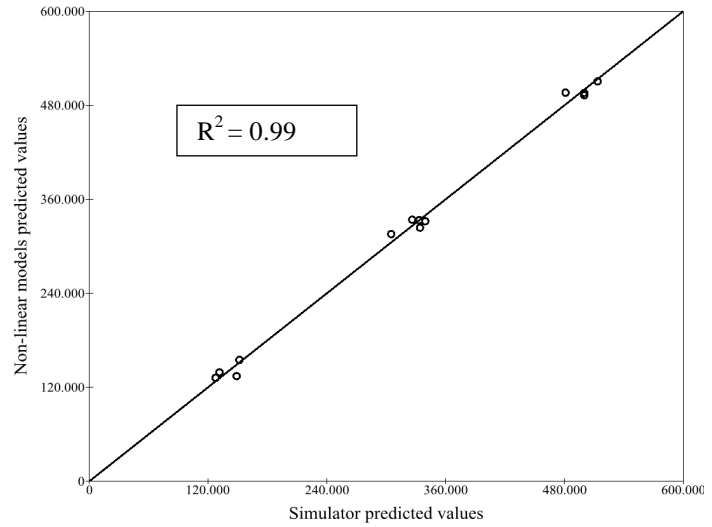


Figure 3.29: Relationship between *fracture_height* predicted by the simulator and the non-linear model from this study

3.3.2.7 Propped height

Propped height (*propped _ height*) has three significant variables (1) Reservoir thickness (h_r), (2) Shublik A Young's modulus (E_{rA}) and (3) Permeability in Shublik C (k_{rC}). **Figures 3.30** through **3.32** show the 3D response surface plot for *propped _ height*. **Figure 3.30** shows the effect of k_{rC} and E_{rA} on *propped _ height*. **Figure 3.31** shows the effect of h_r and E_{rA} on *propped _ height*. **Figure 3.32** shows the effect of k_{rC} and h_r on *propped _ height*. The non-linear model developed can be seen below.

$$\ln(\text{propped_height}) = 5.7981 + 0.647h_r + 0.009E_{rA} - 0.0017k_{rC} - 0.0019(h_r)(k_{rC}) + 0.0211(h_r)(E_{rA}) - 0.004(k_{rC})(E_{rA}) - 0.2445h_r^2 + 0.0047k_{rC}^2 + 0.0000565h_r^2 \quad (28)$$

Figure 3.33 shows the relationship between *propped _ height* predicted by the simulator and the non-linear model from this study with the R^2 value of 0.99.

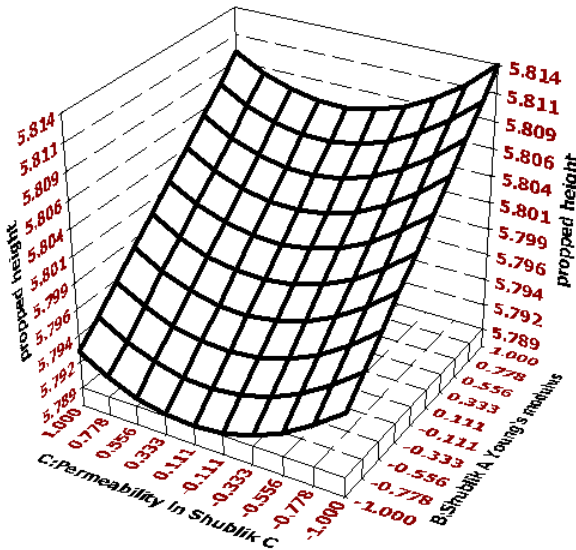


Figure 3.30: 3D response surface plot showing the effect k_{rC} and E_{rA} on *propped _ height*

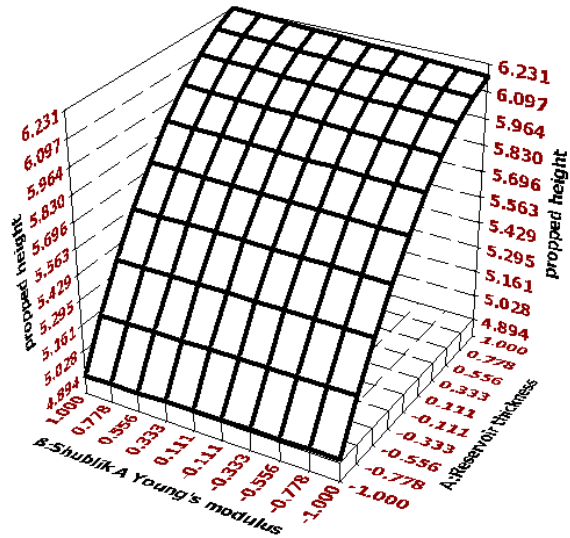


Figure 3.31: 3D response surface plot showing the effect of h_r and E_{rA} on *propped _ height*

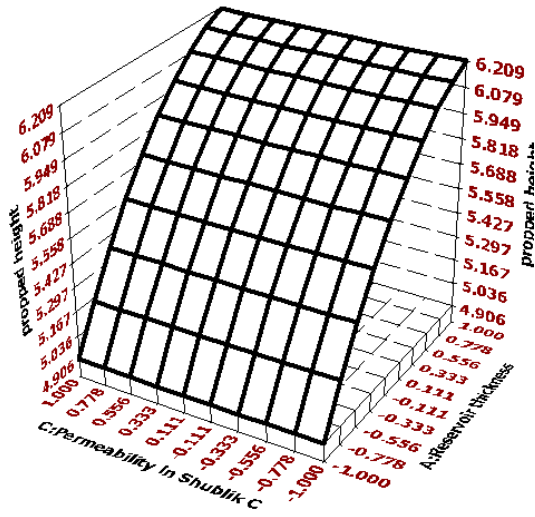


Figure 3.32: 3D response surface plot showing the effect of k_{rC} and h_r on *propped_height*

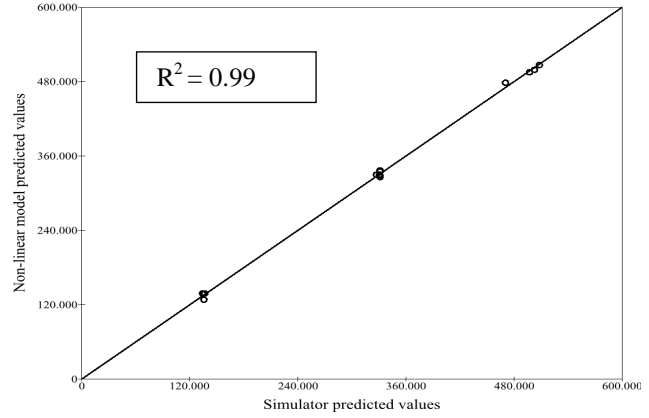


Figure 3.33: Relationship between *upper_outgrowth* predicted by the simulator and the non-linear model from this study

3.3.2.8 Upper fracture outgrowth

Upper fracture outgrowth (*upper_outgrowth*) has three significant variables (1) Well placement (W_p), (2) Reservoir thickness (h_r), and (3) Shublik A Young's modulus (E_{rA}). **Figures 3.34** through **3.36** shows the 3D response surface plot for *upper_outgrowth*. **Figure 3.34** shows the effect of h_r and W_p on *upper_outgrowth*. **Figure 3.35** shows the effect of h_r and E_{rA} on *upper_outgrowth*. **Figure 3.36** shows the effect of E_{rA} and W_p on *upper_outgrowth*. The non-linear model developed can be seen below.

$$\ln(\text{upper_outgrowth}) = 3.96 - 0.999h_r - 0.835E_{rA} - 3.060W_p - 0.725(h_r)(E_{rA}) - 0.127(h_r)(W_p) - 0.802(E_{rA})(W_p) - 1.736h_r^2 - 0.904E_{rA}^2 - 1.035W_p^2 \quad (29)$$

Figure 3.37 shows the relationship between *upper_outgrowth* predicted by the simulator and the non-linear model from this study with the R^2 value of 0.90.

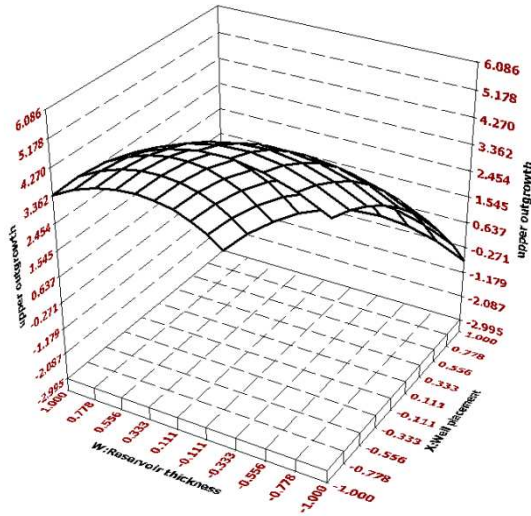


Figure 3.34: 3D response surface plot showing the effect of h_r and W_p on $upper_outgrowth$

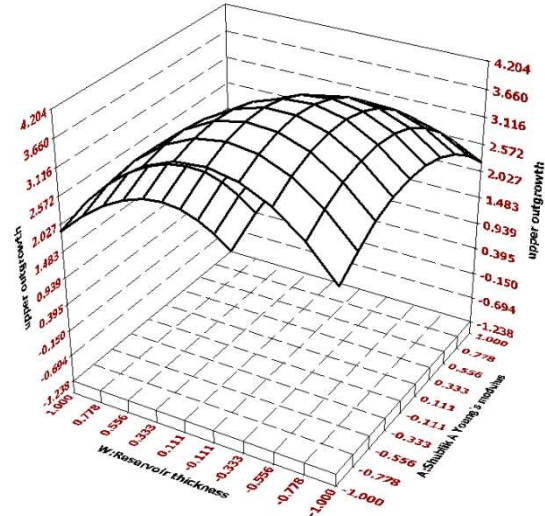


Figure 3.35: 3D response surface plot showing the effect h_r and E_{rA} on $upper_outgrowth$

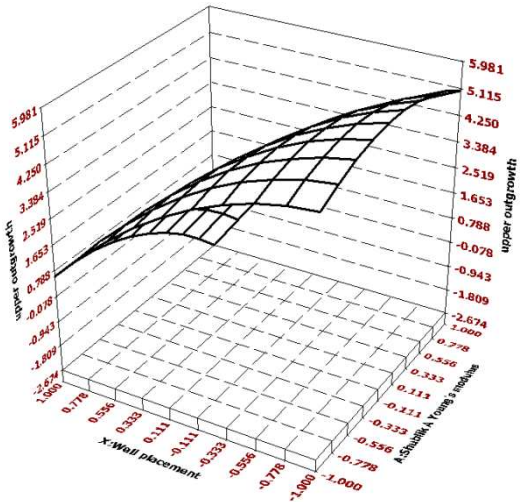


Figure 3.36: 3D response surface plot showing the effect of E_{rA} and W_p on $upper_outgrowth$

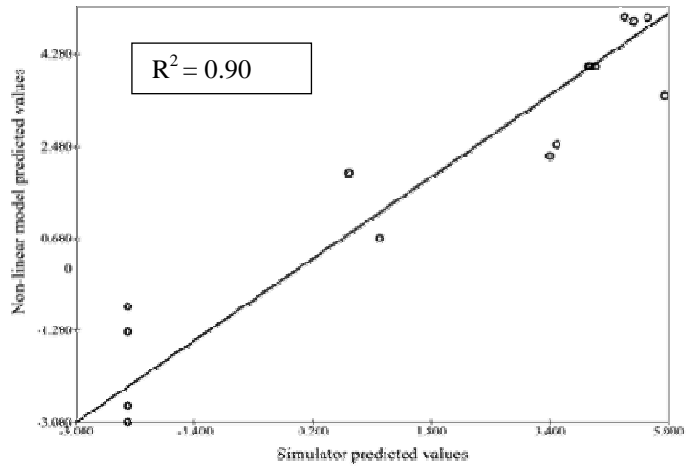


Figure 3.37: Relationship between $upper_outgrowth$ predicted by the simulator and the non-linear model from this study

3.3.2.9 Lower fracture outgrowth

Lower fracture outgrowth (*lower_outgrowth*) has three significant variables (1) Well placement (W_p), (2) Reservoir thickness (h_r), and (3) Shublik A Young's modulus (E_{rA}). **Figures 3.38** through **3.40** shows the 3D response surface plot for *lower_outgrowth*. **Figure 3.38** shows the effect of h_r and W_p on *lower_outgrowth*. **Figure 3.39** shows the effect of h_r and E_{rA} on *lower_outgrowth*. **Figure 3.40** shows the effect of E_{rA} and W_p on *lower_outgrowth*.

The non-linear model developed can be seen below.

$$\begin{aligned} \ln(\text{lower_outgrowth}) = & 1.551 - 2.251h_r + 0.310E_{rA} + 1.090W_p - 0.101(h_r)(E_{rA}) - 0.162(h_r)(W_p) \\ & + 0.519(E_{rA})(W_p) - 0.684h_r^2 - 1.223E_{rA}^2 - 0.612W_p^2 \end{aligned} \quad (30)$$

Figure 3.41 shows the relationship between *lower_outgrowth* predicted by the simulator and the non-linear model from this study with the R^2 value of 0.87.

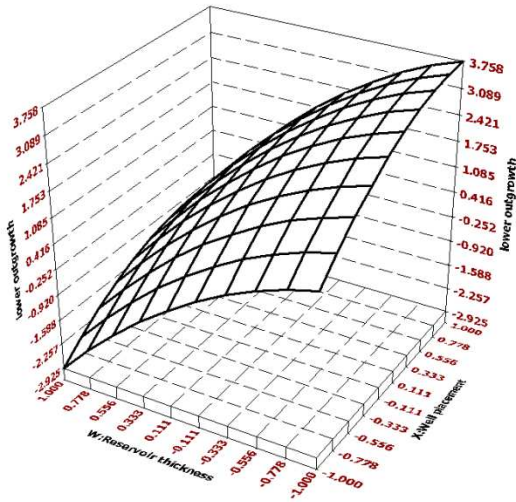


Figure 3.38: 3D response surface plot showing the effect of h_r and W_p on *lower_outgrowth*

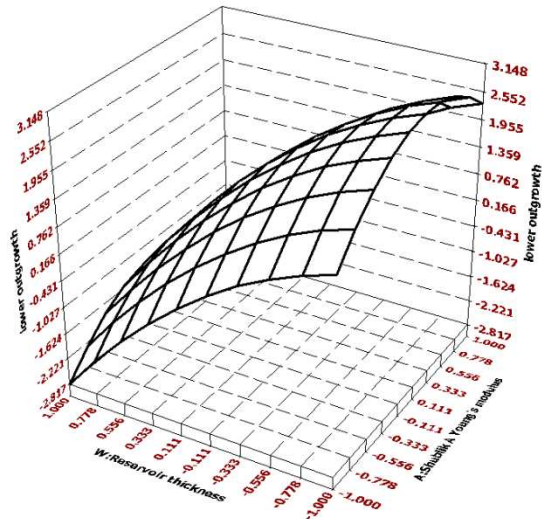


Figure 3.39: 3D response surface plot showing the effect h_r and E_{rA} on *lower_outgrowth*

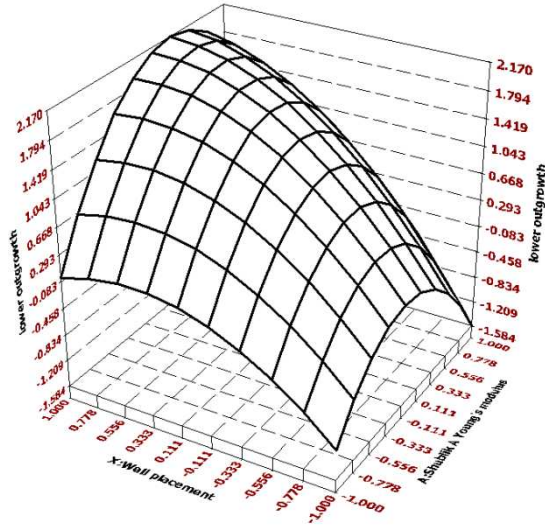


Figure 3.40: 3D response surface plot showing the effect of E_{rA} and W_p on $lower_outgrowth$

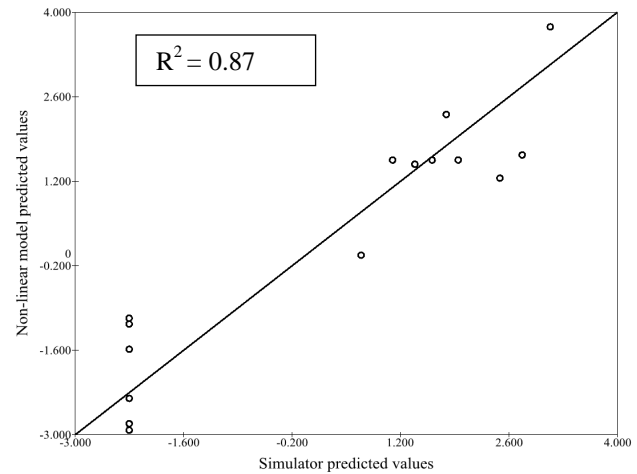


Figure 3.41: Relationship between $lower_outgrowth$ predicted by the simulator and the non-linear model from this study

3.4 Discussions

3.4.1 Stage 1

This study evaluated 16/18/26 variables (reservoir/mechanical/treatment properties) and identified the critical variables based on their statistical significance along the three phases. Although all the input variables evaluated in this study play some role on fracture initiation and propagation, based on the p-values, the critical variables affecting the induced fracture geometry can be identified. Identification of these critical variables can help focus a careful, calibrated and targeted campaign of data acquisition and development of a new shale play.

3.4.1.1 Phases I and II

The only difference between the geologic assumptions in Phase I and II is that the boundary layers have non-zero permeability and fracturing fluid is allowed to leak-off in Phase II. From **Table 3.3** and **Table 3.5**, we can observe that Phase I and II effectively have the same set of critical variables for most of the fracture geometry variables. This implies that the effect of fluid leak-off into the boundary layers on fracture geometry is negligible. Considering the ultra-low

permeabilities and the fracture containment within the shales, we can agree that boundary layers leak-off properties have negligible effects on the magnitude of fracture geometry. ‘Fracturing fluid type’ is the combined effect of the rheological properties of the fracturing fluid (viscosity, density, etc.) on fracture geometry. Therefore, it can be observed to play a vital role in quantifying fracture height, propped height and propped length.

From **Table 3.1** and **3.2**, it can be observed that fracture length is both an input and an output variable. Desired fracture length (input parameter) is the desired estimate given to the numerical simulator. The simulator designs a treatment with predicted fracture length (output variable) as close as possible to the initial desired estimate. The critical importance of this parameter observed is strictly related to computation process of the simulator rather than the physics of a fracturing treatment. Therefore, this parameter is eliminated in the next phase of the study.

Thicknesses of the reservoir and boundary layers were identified as critical variables for all the fracture geometry variables in Phases I and II. This implies that accurate identification of target lithostratigraphy is of high importance when designing a fracturing treatment. To better understand the significance of reservoir thickness, Phase III of this study evaluated the effects of reservoir thickness by dividing the reservoir interval into 4 sub layers.

3.4.1.2 Phase III

Apart from dividing the shale layer into four layers, Phase III of this study eliminates the parameter ‘desired fracture length’ and includes a parameter ‘well placement’. The parameter ‘well placement’ represents the position of the heel of the horizontal well within the formation.

Even with the adjustments in the geologic assumptions, the reservoir and boundary layer thicknesses still have significant effects on fracture geometry (**Table 3.7**). Among the four layers of the reservoir, it was assumed that the first and the third layer are organic rich shales with high probability of hydrocarbon presence (**Figure 2.1**). Therefore the results of this study indicate that the permeability and Young’s modulus of the shale layers have relatively higher impact on fracture geometry than do the mechanical properties of the other layers of the reservoir. From this study, the position of the horizontal leg (Well placement) in between shale layers (A and C)

of the reservoir has a substantial influence on the fracture outgrowth. This is due to the fact that the depth of the horizontal well is also the fracture initiation depth.

3.4.2 Stage 2

3.4.2.1 Analysis of response surfaces

The 3D response surfaces presented in this section represents the complex interdependent relationships between input variables and fracture geometry. The following observations can be made from the response surfaces.

- The width at the top of the fracture decreases with increase in permeability in Shublik layer C and upper layer thickness, and increases with increase in lower layer thickness (**Figures 3.6 through 3.8**).
- The width at the middle of the fracture decreases with increase in upper layer Young's modulus and permeability in Shublik layer, and increases with increase in reservoir thickness (**Figures 3.10 through 3.12**).
- The width at the bottom of the fracture increases with increase in lower layer Poisson's ratio and Young's modulus of Shublik layer A, and increases until the median and then starts to decrease when proppant type varies (**Figures 3.14 through 3.16**).
- The fracture length and propped length increases with increase in reservoir thickness and permeability in Shublik C, and decreases with increase in upper layer thickness(**Figures 3.18 through 3.20 and Figures 3.22 through 3.24**).
- The fracture height increases with increase in reservoir thickness and Young's modulus of Shublik layer A, initially increases and then starts to decrease at median with increase in reservoir depth (**Figures 3.26 through 3.28**).
- The propped height increases with increase in reservoir thickness and Young's modulus of Shublik layer A, initially decrease and then starts to increases at median with increase in permeability in Shublik C (**Figures 3.30 through 3.32**).

- Upper outgrowth decreases as the well location is varied, and initially increases and then starts to decrease at median with increase in reservoir thickness and Young's modulus of Shublik layer A (**Figures 3.34 through 3.36**).
- Lower outgrowth decreases as the well location is varied and increase in reservoir thickness, and initially increases and then starts to decrease at median with increase in Young's modulus of Shublik layer A (**Figures 3.38 through 3.40**).

3.4.2.2 Applications of proxy models

The proxy models developed for nine fracture geometry variables (**Equations 22 through 30**) have the following possible applications.

- These proxy models can be used to perform sensitivity analysis and understand the effect of all the input variables on the predicted fracture geometry.
- These proxy models can be used evaluate a particular treatment design by estimating fracture geometry in a time efficient manner. This quick estimation is useful in screening and ranking several available stimulation treatments.
- These proxy models can also be used to solve inversion problems (reverse calculating the input parameters based on the desired fracture geometry). This capability of the proxy models is very useful especially in the case of Shublik shale (water bearing boundary layers of Shublik creates a need to contain the fracture within the reservoir thickness). Therefore, reverse calculating the treatment properties by setting the fracture outgrowth to zero can be very helpful.

These proxy models can also be used to estimate the statistics of uncertainty. Monte Carlo simulations performed using the proxy model can estimate the P10, P50, and P90 scenarios

CHAPTER 4 CONCLUSIONS AND RECOMMENDATIONS

4.1 Conclusions

In stage 1 of this study, we proposed a methodology that can identify the most significant reservoir variables affecting the modeled fracture geometry by using a pseudo 3D fracture propagation model and fractional experiment design. This methodology was applied to the Shublik shale of the Alaskan North Slope. The study was conducted in 3 phases representing increasingly more complex assumptions about the geology. The total number of model input variables considered for Phase I, II, and III are 16, 18, and 26 respectively. Fractional factorial method and regression analysis was used to quantify the relative significance of each individual input parameter on the resulting modeled fracture geometry. An analysis of the results from this study indicates the following conclusions.

- Fracturing fluid leak-off into the boundary layers has little or no effect on fracture geometry.
- Reservoir and boundary layer thicknesses are the critical variables affecting the most fracture geometry variables.
- The mechanical properties of the shale layers (in Phase III when the reservoir is divided into 4 sub-layers) have higher significance than the rest of the sub-layers or the boundaries on the fracture geometry.
- The type of fracturing fluid has considerable impact on the fracture and propped dimensions.
- Well placement between the shale layers has a significant effect on the upper and lower fracture outgrowth.
- The top three significant variables for fracture width at the top of the fracture were upper layer thickness, lower layer thickness and permeability in Shublik C (**Table 3.8**).
- For fracture width at the middle of the fracture, the significant variables were reservoir thickness, permeability in Shublik C and upper layer Young's Modulus (**Table 3.8**).
- For fracture width at the bottom of the fracture, the significant variables were proppant type, Shublik A Young's modulus and lower layer Poisson's Ratio (**Table 3.8**).

- For fracture and propped length, the significant variables were reservoir thickness, permeability in Shublik and upper layer thickness (**Table 3.8**).
- For fracture height, the significant variables were reservoir thickness, Shublik A Young's modulus and reservoir depth (**Table 3.8**).
- For propped height, the significant variables were reservoir thickness, Shublik A Young's and permeability in Shublik C (**Table 3.8**).
- For the upper and lower fracture outgrowth, the significant variables were well placement, reservoir thickness and Shublik A Young's modulus (**Table 3.8**).

In stage 2 of this study, the Box-Behnken experimental design and response surface methodology were applied to model fracture geometry in Shublik shale of Alaskan North Slope. With a total of 137 simulation runs (32 simulations for screening and $15 \times 7 = 105$ simulations for non-linear model building), 26 variables are evaluated and non-linear proxy models are developed for all the nine fracture geometry variables.

- The non-linear model developed for fracture width (*width_top*, *width_mid*, and *width_mid*) in this study has good prediction accuracy with R^2 values of 0.82, 0.97, and 0.68 respectively.
- Similarly, the R^2 value of 0.99 was achieved for the non-linear models predicting fracture length (*fracture_length* and *propped_length*) and fracture height (*fracture_height* and *propped_height*).
- The non-linear model for fracture outgrowth (*upper_outgrowth* and *lower_outgrowth*) has good prediction accuracy with R^2 values of 0.9 and 0.87 respectively.

4.2 Recommendations

The proxy model was developed using a pseudo-3D numerical fracturing simulator. This pseudo-3D simulator neglect the effects of permeability anisotropy, stress shadowing, and natural fracture interactions. These ignored effects might play an important role in fracture initiation and propagation; therefore a better full 3D simulator should be used to further improve the proxy model.

REFERENCES

- Ambastha, A. K. (2014). Guidelines for Uncertainty Assessment Using Reservoir Simulation Models for Green- and Brown-field Situations. Society of Petroleum Engineers. . doi:10.2118/172432-MS.
- Aslan, N., and Cebeci, Y. (2007). Application of Box–Behnken Design and Response Surface Methodology for Modeling of Some Turkish Coals, Fuel, Volume 86, Issues 1–2, Pages 90-97.
- Awoleke, O. O., Romero, J. D., Zhu, D., and Hill, D. (2012). Experimental Investigation of Propped Fracture Conductivity in Tight Gas Reservoirs Using Factorial Design. Society of Petroleum Engineers.
- Barenblatt, G.I. (1962). The Mathematical Theory of Equilibrium Cracks in Brittle Fracture. Adv. Appl. Mech. 7, 55-129.
- Beard, T. (2011). Fracture Design in Horizontal Shale Wells - Data Gathering to Implementation. Chesapeake Energy Corporation. Retrieved from <http://www2.epa.gov/sites/production/files/documents/fracturedesigninhorizontalshalewells.pdf> on October 31, 2014
- Carter, R.D. (1957) Derivation of the General Equation for Estimating the Extent of the Fractured Area, Appendix to "Optimum Fluid Characteristics for Fracture Extension", by Howard, G.C. and Fast, C.R., Drilling and Production Practices, API, p. 261-270.
- Centurion, S. M. (2011). Eagle Ford Shale: A Multistage Hydraulic Fracturing, Completion Trends and Production Outcome Study Using Practical Data Mining Techniques. SPE Eastern Regional Meeting. Columbus, Ohio, USA: Society of Petroleum Engineers.
- Crabtree, C. (1996). Design of Hydraulic Fractures in the Kuparuk River Field of Alaska. Fairbanks, Alaska. University of Alaska, Fairbanks.
- Decker, P. L. (2011). Source-Reservoired Oil Resources Alaskan North Slope. Presentation for Alaska Department of Natural Resources, Division of Oil and Gas.

Economides, M., Oligney, R., and Valko, R. (2002). Unified Fracture Design: Bridging the Gap Between Theory and Practice. <http://books.google.com/books?id=nleGAAAACAAJ>.

Economides, M.J., Hill, A.D., Ehlig-Economides, C., and Zhu, D. (2012). Petroleum Production Systems. http://books.google.com/books?id=5rvM_-kxao0C.

Geertsma, J. and de Klerk, F.D. (1969). A Rapid Method of Predicting Width and Extent of Hydraulically Induced Fractures. J. Pet. Tech. 21: 1571-1581.

Gidley, J.L. (1989). Recent Advances in Hydraulic Fracturing. Society of Petroleum Engineers. <http://books.google.com/books?id=sT5jQgAACAAJ>.

Griffith, A.A. (1921). The Phenomena of Rupture and Flow in Solids. Phil. Trans. Roy. Soc. 221: 163-198.

Houseknecht, D. W., Rouse, W. A. and Garrity, C. P. (2012). Arctic Alaska Shale-Oil and Shale-Gas Resource Potential. OTC Arctic Technology Conference. Houston, Texas, USA.

Hulm, E. J. (1999). Facies and Sequence Analysis of Eileen-Sag River Interval. University of Alaska Fairbanks.

Hutton, E., Agboada, D. K., Whalen, M. T., and Hanks, C. L. (2012). Upper Triassic Shublik Formation of North Alaska - An Eagle Ford Type Shale Reservoir? AAPG.

Jiang, M. (1989). Biostratigraphy and Geochronology of the Eagle Ford Shale, Austin chalk, and Lower Taylor Marl in Texas Based on Calcareous Nannofossils. Texas A & M University.

Johnston, D. W. and Christenson, R. N., (1998). The Application of BP Exploration (Alaska) Inc. to Present Testimony for Classification of a New Pool and the Establishment of Pool Rules for Development of the Sag River Oil Pool in the Milne Point Unit. http://doa.alaska.gov/ogc/orders/co/co400_499/co423.htm

Kelly, L. N. (2004). High Resolution Sequence Stratigraphy and Geochemistry of Middle and Upper Triassic Sedimentary Rocks, Northeast and Central Brooks Range, Alaska. MS thesis, University of Alaska Fairbanks.

Kelly, L. N., Whalen, M. T., McRoberts, C. A., Hopkin, E. and Tomsich, C. S., (2007), Sequence Stratigraphy and Geochemistry of the Upper Lower Through Upper Triassic of Northern Alaska: Implications for Paleoredox history, Source Rock Accumulation and Paleooceanography: Division of Geological and Geophysical Surveys, Alaska, Report of Investigations, 2007-1.

Kennedy, R. L., Gupta, R., Kotov, S. V., Burton, W. A., Knecht, W. N. and Ahmed, U. (2012). Optimized Shale Resource Development: Proper Placement of Wells and Hydraulic Fracture Stages. Abu Dhabi International Petroleum Conference and Exhibition. Abu Dhabi, UAE: Society of Petroleum Engineers.

Keshavarzi, R., Mohammadi, S. and Bayesteh, H. (2012). Hydraulic Fracture Propagation in Unconventional Reservoirs: The Role of Natural Fractures. American Rock Mechanics Association.

Khristianovitch, S.A. and Zheltov, Y.P. (1955). Formation of Vertical Fractures by Means of Highly Viscous Fluids. Proc., 4th World Petroleum Congress, Rome, 2:579-586.

King, G. E. (2010). Thirty Years of Gas Shale Fracturing: What Have We Learned? SPE Annual Technical Conference and Exhibition. Florence, Italy: Society of Petroleum Engineers.

King, G. E. (2012, January 1). Hydraulic Fracturing 101: What Every Representative, Environmentalist, Regulator, Reporter, Investor, University Researcher, Neighbor and Engineer Should Know About Estimating Frac Risk and Improving Frac Performance in Unconventional Gas and Oil Wells. Society of Petroleum Engineers.

Kupez, J. A. (1995). Depositional Setting, Sequence Stratigraphy, Diagenesis, and Reservoir Potential of a Mixed Lithology, Upwelling Deposit: The Upper Triassic Shublik Formation, Prudhoe Bay, Alaska. American Association of Petroleum Geologists Bulletin, v. 79, p. 1301-1319.

Manchanda, R., Roussel, N. P. and Sharma, M. M. (2012). Factors Influencing Fracture Trajectories and Fracturing Pressure Data in a Horizontal Completion. American Rock Mechanics Association.

- Martinez, D. (2012). Fundamental Hydraulic fracturing concepts for poorly consolidated formations. Mewbourne School of Petroleum and Geological Engineering. Norman: University of Oklahoma.
- Masters, J.A. (1979). Deep Basin Gas Trap, Western Canada. AAPG Bulletin 63, No. 2, 152.
- Miller, E. L., Grantz, A., and Klemperer, S. (2002). Tectonic Evolution of the Bering Shelf-Chukchi Sea-Arctic Margin and Adjacent Landmasses. Geological Society of America.
- Nolte, K.G. and Economides, M.J. (1989). Fracturing Diagnosis Using Pressure Analysis. In Reservoir Stimulation, ed. M.J. Economides and K.G. Nolte, Chap. 7, Englewood Cliffs, NJ.: Prentice Hall, Inc.
- Nordgren, R.P. (1972). Propagation of a Vertical Hydraulic Fracture. SPE J. 12 (4): 306–314. SPE-3009-PA. <http://dx.doi.org/10.2118/3009-PA>.
- Palisch, T. T., Chapman, M. A. and Godwin, J. W. (2012). Hydraulic Fracture Design Optimization in Unconventional Reservoirs - A Case History. SPE Annual Technical Conference and Exhibition. San Antonio, Texas, USA: Society of Petroleum Engineers.
- Parikh, H. (2003). Reservoir Characterization Using Experimental Design and Response Surface Methodology. M.S. Thesis. Texas A&M University.
- Parrish, J. T., and Hulm, E. J. (2001). Shublik formation lithofacies, Environments, and Sequence stratigraphy, Arctic Alaska, U.S.A.
- Perkins, T.K. and Kern, L.R. (1961). Widths of Hydraulic Fractures. J. Pet. Tech. 13: 937-949.
- Pope, C. D., Palisch, T. and Saldungaray, P. (2012). Improving Completion and Stimulation Effectiveness in Unconventional Reservoirs- Field Results in the Eagle Ford Shale of North America. SPE/EAGE European Unconventional Resources Conference and Exhibition. Vienna, Austria: Society of Petroleum Engineers.
- Rahim Z., Al-Anazi H., and Al-Kanaan A. (2012). IMPROVED GAS RECOVERY—1: Maximizing Postfrac Gas Flow Rates From Conventional, Tight Reservoirs. Oil and Gas Journal

vol. 110 issue: 3. <http://www.ogj.com/articles/print/vol-110/issue-3/drilling-production/special-report-drilling/maximizing-postfrac.html>.

Segnini, C. J., Rashwan, M., Hernandez, M. J., Rojas, J. A., and Infante, M. A. (2014). Probabilistic Analysis by Applying Uncertainty Workflows: A Case Study of the Teak Field, East Coast Trinidad. Society of Petroleum Engineers.

Sneddon, I. (1973). Integral Transform Methods. In: Methods of Analysis and Solutions of Crack Problems. Leyden: Nordhoff International.

Stegent, N. A., Wagner, A. L., Mullen, J. and Borstmayer, R. E. (2010). Engineering a Successful Fracture-Stimulation Treatment in the Eagle Ford Shale. Tight Gas Completions Conference. San Antonio, Texas, USA: Society of Petroleum Engineers.

U.S. Energy Information Administration, July 2011. Review of Emerging Resources: U.S. Shale Gas and Shale Oil Plays, Washington, DC. <http://www.eia.gov/analysis/studies/usshalegas/> accessed on October 31, 2014.

U.S. Energy Information Administration's Annual Energy Outlook (2013). http://www.eia.gov/pressroom/presentations/sieminski_12162013.pdf accessed on October 31, 2014.

Yu, W., and Sepehrnoori, K. (2014). Sensitivity Study and History Matching and Economic Optimization for Marcellus Shale. URTeC 2014, Denver, Colorado, USA: Society of Petroleum Engineers.

Zeng, Z. (2002). Laboratory Imaging of Hydraulic Fractures Using Microseismicity. University of Oklahoma, Norman, Oklahoma, US

Appendix A Design and Planning tables for all the three phases in Stage 1

Table A.1: Factorial planning table for the 16 variables chosen in Phase I

<i>fl</i>	<i>kr</i>	<i>Er</i>	<i>vr</i>	<i>hr</i>	<i>D</i>	<i>vu</i>	<i>Eu</i>	<i>hu</i>	<i>vl</i>	<i>El</i>	<i>hl</i>	<i>Pt</i>	<i>Ps</i>	<i>q</i>	<i>t</i>
450	800	6	0.26	550	13500	0.38	3.55	1000	0.38	3.55	750	Ceramic	16/30	100	X-linked
150	800	6	0.26	550	8000	0.21	2.38	1000	0.21	2.38	750	Sand	16/30	100	Slickwater
450	1	6	0.26	550	8000	0.21	3.55	20	0.21	3.55	100	Ceramic	40/70	100	Slickwater
450	800	1.5	0.26	550	8000	0.38	2.38	20	0.38	2.38	100	Ceramic	16/30	45	Slickwater
450	800	6	0.22	550	13500	0.21	2.38	20	0.38	3.55	750	Sand	40/70	45	Slickwater
450	800	6	0.26	120	13500	0.38	3.55	1000	0.21	2.38	100	Sand	40/70	45	Slickwater
150	1	6	0.26	550	13500	0.38	2.38	20	0.38	2.38	100	Sand	40/70	100	X-linked
150	800	1.5	0.26	550	13500	0.21	3.55	20	0.21	3.55	100	Sand	16/30	45	X-linked
150	800	6	0.22	550	8000	0.38	3.55	20	0.21	2.38	750	Ceramic	40/70	45	X-linked
150	800	6	0.26	120	8000	0.21	2.38	1000	0.38	3.55	100	Ceramic	40/70	45	X-linked
450	1	1.5	0.26	550	13500	0.21	2.38	1000	0.21	2.38	750	Ceramic	40/70	45	X-linked
450	1	6	0.22	550	8000	0.38	2.38	1000	0.21	3.55	100	Sand	16/30	45	X-linked
450	1	6	0.26	120	8000	0.21	3.55	20	0.38	2.38	750	Sand	16/30	45	X-linked
450	800	1.5	0.22	550	8000	0.21	3.55	1000	0.38	2.38	100	Sand	40/70	100	X-linked
450	800	1.5	0.26	120	8000	0.38	2.38	20	0.21	3.55	750	Sand	40/70	100	X-linked
450	800	6	0.22	120	13500	0.21	2.38	20	0.21	2.38	100	Ceramic	16/30	100	X-linked
150	1	1.5	0.26	550	8000	0.38	3.55	1000	0.38	3.55	750	Sand	40/70	45	Slickwater
150	1	6	0.22	550	13500	0.21	3.55	1000	0.38	2.38	100	Ceramic	16/30	45	Slickwater
150	1	6	0.26	120	13500	0.38	2.38	20	0.21	3.55	750	Ceramic	16/30	45	Slickwater
450	1	1.5	0.22	550	13500	0.38	3.55	20	0.21	2.38	750	Sand	16/30	100	Slickwater
450	1	1.5	0.26	120	13500	0.21	2.38	1000	0.38	3.55	100	Sand	16/30	100	Slickwater
450	800	1.5	0.22	120	8000	0.21	3.55	1000	0.21	3.55	750	Ceramic	16/30	45	Slickwater
150	800	1.5	0.22	550	13500	0.38	2.38	1000	0.21	3.55	100	Ceramic	40/70	100	Slickwater
150	800	1.5	0.26	120	13500	0.21	3.55	20	0.38	2.38	750	Ceramic	40/70	100	Slickwater
150	800	6	0.22	120	8000	0.38	3.55	20	0.38	3.55	100	Sand	16/30	100	Slickwater
450	1	6	0.22	550	8000	0.38	2.38	1000	0.21	3.55	100	Sand	16/30	45	X-linked
150	1	1.5	0.22	550	8000	0.21	2.38	20	0.38	3.55	750	Ceramic	16/30	100	X-linked
150	1	1.5	0.26	120	8000	0.38	3.55	1000	0.21	2.38	100	Ceramic	16/30	100	X-linked
150	1	6	0.22	120	13500	0.21	3.55	1000	0.21	3.55	750	Sand	40/70	100	X-linked
150	800	1.5	0.22	120	13500	0.38	2.38	1000	0.38	2.38	750	Sand	16/30	45	X-linked
450	1	1.5	0.22	120	13500	0.38	3.55	20	0.38	3.55	100	Ceramic	40/70	45	X-linked
150	1	1.5	0.22	120	8000	0.21	2.38	20	0.21	2.38	100	Sand	40/70	45	Slickwater

Table A.2: Factorial design table for the 16 variables chosen in Phase I (1 being the higher and -1 being the lower end of parameter range)

<i>fl</i>	<i>kr</i>	<i>Er</i>	<i>vr</i>	<i>hr</i>	<i>D</i>	<i>vu</i>	<i>Eu</i>	<i>hu</i>	<i>vl</i>	<i>El</i>	<i>hl</i>	<i>Pt</i>	<i>Ps</i>	<i>q</i>	<i>t</i>
1	1	1	1	1	1	1	1	1	1	1	1	1	1	1	1
-1	1	1	1	1	-1	-1	-1	1	-1	-1	1	-1	1	1	-1
1	-1	1	1	1	-1	-1	1	-1	-1	1	-1	1	-1	1	-1
1	1	-1	1	1	-1	1	-1	-1	1	-1	-1	1	1	-1	-1
1	1	1	-1	1	1	-1	-1	-1	1	1	1	-1	-1	-1	-1
1	1	1	1	-1	1	1	1	1	-1	-1	-1	-1	-1	-1	-1
-1	-1	1	1	1	1	1	-1	-1	1	-1	-1	-1	-1	1	1
-1	1	-1	1	1	1	-1	1	-1	-1	1	-1	-1	1	-1	1
-1	1	1	-1	1	-1	1	1	-1	-1	-1	1	1	-1	-1	1
-1	1	1	1	-1	-1	-1	-1	1	1	1	-1	1	-1	-1	1
1	-1	-1	1	1	1	-1	-1	1	-1	-1	1	1	-1	-1	1
1	-1	1	-1	1	-1	1	-1	1	-1	1	-1	-1	1	-1	1
1	-1	1	1	-1	-1	-1	-1	1	-1	-1	1	-1	1	-1	1
1	1	-1	-1	1	-1	-1	1	1	1	-1	-1	-1	-1	1	1
1	1	1	-1	-1	1	-1	-1	-1	-1	-1	-1	1	1	1	1
-1	-1	-1	1	1	-1	1	1	1	1	1	1	-1	-1	-1	-1
-1	-1	1	-1	1	1	-1	1	1	1	-1	-1	1	1	-1	-1
-1	-1	1	1	-1	1	1	-1	-1	-1	1	1	1	1	-1	-1
1	-1	-1	-1	1	1	1	1	-1	-1	-1	1	-1	1	1	-1
1	-1	-1	1	-1	1	-1	-1	1	1	1	-1	-1	1	1	-1
1	1	-1	-1	-1	-1	-1	-1	1	1	1	1	1	1	-1	-1
-1	1	-1	-1	1	1	1	-1	1	-1	1	-1	1	-1	1	-1
-1	1	-1	1	-1	1	-1	1	-1	1	-1	1	1	-1	1	-1
-1	1	1	-1	-1	-1	1	1	-1	1	1	-1	-1	1	1	-1
1	-1	1	-1	1	-1	1	-1	1	-1	1	-1	-1	1	-1	1
-1	-1	-1	-1	1	-1	-1	-1	-1	1	1	1	1	1	1	1
-1	-1	-1	1	-1	-1	1	1	1	-1	-1	-1	1	1	1	1
-1	-1	1	-1	-1	1	-1	1	1	-1	1	1	-1	-1	1	1
-1	1	-1	-1	-1	1	1	-1	1	1	-1	1	-1	1	-1	1
1	-1	-1	-1	-1	1	1	1	-1	1	1	-1	1	-1	-1	1
-1	-1	-1	-1	-1	-1	-1	-1	-1	-1	-1	-1	-1	-1	-1	-1

Table A.3: Factorial planning table for the 18 variables chosen in Phase II

	f_l	k_r	E_r	v_r	h_r	D	v_u	E_u	h_u	k_u	v_l	E_l	h_l	k_l	P_t	P_s	q	t
1	150	1	1.5	0.22	120	8000	0.38	3.55	20	21	0.21	2.38	750	23	Sand	40/70	100	Slickwater
2	150	1	1.5	0.22	550	13500	0.21	2.38	1000	1.8	0.38	3.55	100	2.9	Ceramic	16/30	45	X-linked
3	150	1	1.5	0.26	120	13500	0.21	2.38	1000	1.8	0.38	3.55	100	23	Sand	40/70	100	Slickwater
4	150	1	1.5	0.26	550	8000	0.38	3.55	20	21	0.21	2.38	750	2.9	Ceramic	16/30	45	X-linked
5	150	1	6	0.22	120	13500	0.21	2.38	1000	21	0.21	2.38	750	2.9	Ceramic	16/30	45	Slickwater
6	150	1	6	0.22	550	8000	0.38	3.55	20	1.8	0.38	3.55	100	23	Sand	40/70	100	X-linked
7	150	1	6	0.26	120	8000	0.38	3.55	20	1.8	0.38	3.55	100	2.9	Ceramic	16/30	45	Slickwater
8	150	1	6	0.26	550	13500	0.21	2.38	1000	21	0.21	2.38	750	23	Sand	40/70	100	X-linked
9	150	800	1.5	0.22	120	13500	0.21	3.55	20	1.8	0.38	2.38	750	2.9	Ceramic	40/70	100	X-linked
10	150	800	1.5	0.22	550	8000	0.38	2.38	1000	21	0.21	3.55	100	23	Sand	16/30	45	Slickwater
11	150	800	1.5	0.26	120	8000	0.38	2.38	1000	21	0.21	3.55	100	2.9	Ceramic	40/70	100	X-linked
12	150	800	1.5	0.26	550	13500	0.21	3.55	20	1.8	0.38	2.38	750	23	Sand	16/30	45	Slickwater
13	150	800	6	0.22	120	8000	0.38	2.38	1000	1.8	0.38	2.38	750	23	Sand	16/30	45	X-linked
14	150	800	6	0.22	550	13500	0.21	3.55	20	21	0.21	3.55	100	2.9	Ceramic	40/70	100	Slickwater
15	150	800	6	0.26	120	13500	0.21	3.55	20	21	0.21	3.55	100	23	Sand	16/30	45	X-linked
16	150	800	6	0.26	550	8000	0.38	2.38	1000	1.8	0.38	2.38	750	2.9	Ceramic	40/70	100	Slickwater
17	450	1	1.5	0.22	120	13500	0.38	2.38	20	1.8	0.21	3.55	750	2.9	Sand	16/30	100	X-linked
18	450	1	1.5	0.22	550	8000	0.21	3.55	1000	21	0.38	2.38	100	23	Ceramic	40/70	45	Slickwater
19	450	1	1.5	0.26	120	8000	0.21	3.55	1000	21	0.38	2.38	100	2.9	Sand	16/30	100	X-linked
20	450	1	1.5	0.26	550	13500	0.38	2.38	20	1.8	0.21	3.55	750	23	Ceramic	40/70	45	Slickwater
21	450	1	6	0.22	120	8000	0.21	3.55	1000	1.8	0.21	3.55	750	23	Ceramic	40/70	45	X-linked
22	450	1	6	0.22	550	13500	0.38	2.38	20	21	0.38	2.38	100	2.9	Sand	16/30	100	Slickwater
23	450	1	6	0.26	120	13500	0.38	2.38	20	21	0.38	2.38	100	23	Ceramic	40/70	45	X-linked
24	450	1	6	0.26	550	8000	0.21	3.55	1000	1.8	0.21	3.55	750	2.9	Sand	16/30	100	Slickwater
25	450	800	1.5	0.22	120	8000	0.21	2.38	20	21	0.38	3.55	750	23	Ceramic	16/30	100	Slickwater
26	450	800	1.5	0.22	550	13500	0.38	3.55	1000	1.8	0.21	2.38	100	2.9	Sand	40/70	45	X-linked
27	450	800	1.5	0.26	120	13500	0.38	3.55	1000	1.8	0.21	2.38	100	23	Ceramic	16/30	100	Slickwater
28	450	800	1.5	0.26	550	8000	0.21	2.38	20	21	0.38	3.55	750	2.9	Sand	40/70	45	X-linked
29	450	800	6	0.22	120	13500	0.38	3.55	1000	21	0.38	3.55	750	2.9	Sand	40/70	45	Slickwater
30	450	800	6	0.22	550	8000	0.21	2.38	20	1.8	0.21	2.38	100	23	Ceramic	16/30	100	X-linked
31	450	800	6	0.26	120	8000	0.21	2.38	20	1.8	0.21	2.38	100	2.9	Sand	40/70	45	Slickwater
32	450	800	6	0.26	550	13500	0.38	3.55	1000	21	0.38	3.55	750	23	Ceramic	16/30	100	X-linked

Table A.4: Factorial design table for the 18 variables chosen in Phase II

f_l	k_r	E_r	v_r	h_r	D	v_u	E_u	h_u	k_u	v_l	E_l	h_l	k_l	P_t	P_s	q	t
-1	-1	-1	-1	-1	-1	1	1	-1	1	-1	-1	1	1	-1	-1	1	-1
-1	-1	-1	-1	1	1	-1	-1	1	-1	1	1	-1	-1	1	1	-1	1
-1	-1	-1	1	-1	1	-1	-1	1	-1	1	1	-1	1	-1	-1	1	-1
-1	-1	-1	1	1	-1	1	1	-1	1	-1	-1	1	-1	1	1	-1	1
-1	-1	1	-1	-1	1	-1	-1	1	1	-1	-1	1	-1	1	1	-1	-1
-1	-1	1	-1	1	-1	1	1	-1	-1	1	1	-1	1	-1	-1	1	1
-1	-1	1	1	-1	-1	1	1	-1	-1	1	1	-1	-1	1	1	-1	-1
-1	-1	1	1	1	1	-1	-1	1	1	-1	-1	1	1	-1	-1	1	1
-1	1	-1	-1	-1	1	-1	1	-1	-1	1	-1	1	-1	1	-1	1	1
-1	1	-1	-1	1	-1	1	-1	1	1	-1	1	-1	1	-1	1	-1	-1
-1	1	-1	1	-1	-1	1	-1	1	1	-1	1	-1	-1	1	-1	1	1
-1	1	-1	1	1	1	-1	1	-1	-1	1	-1	1	1	-1	1	-1	-1
-1	1	1	-1	-1	-1	1	-1	1	-1	1	-1	1	1	-1	1	-1	1
-1	1	1	-1	1	1	-1	1	-1	1	-1	1	-1	1	-1	1	-1	1
-1	1	1	1	-1	1	-1	1	-1	1	-1	1	-1	1	-1	1	-1	1
-1	1	1	1	1	1	-1	1	-1	-1	1	-1	1	-1	1	-1	1	-1
1	-1	-1	-1	-1	1	1	-1	-1	-1	-1	1	1	-1	-1	1	1	1
1	-1	-1	-1	1	-1	-1	1	1	1	1	-1	-1	1	1	-1	-1	-1
1	-1	-1	1	-1	-1	-1	1	1	1	1	-1	-1	-1	-1	1	1	1
1	-1	-1	1	1	1	1	-1	-1	-1	-1	1	1	1	1	-1	-1	-1
1	-1	1	-1	-1	-1	-1	1	1	-1	-1	1	1	1	1	-1	-1	1
1	-1	1	-1	1	1	-1	-1	-1	1	1	-1	-1	-1	-1	1	-1	1
1	-1	1	1	-1	1	1	-1	-1	1	-1	1	1	-1	-1	1	1	-1
1	-1	1	1	1	1	-1	-1	-1	-1	-1	1	1	1	1	1	1	-1
1	1	-1	-1	1	1	1	1	1	-1	-1	-1	-1	-1	-1	-1	-1	1
1	1	-1	1	-1	1	1	1	1	-1	-1	-1	-1	1	1	1	1	-1
1	1	-1	1	1	-1	-1	-1	-1	1	1	1	1	-1	-1	-1	-1	1
1	1	1	-1	-1	1	1	1	1	1	1	1	1	-1	-1	-1	-1	-1
1	1	1	-1	1	-1	-1	-1	-1	-1	-1	-1	-1	1	1	1	1	1
1	1	1	1	-1	-1	-1	-1	-1	-1	-1	-1	-1	-1	-1	-1	-1	-1
1	1	1	1	1	1	1	1	1	1	1	1	1	1	1	1	1	1

Table A.5: Factorial planning table for the 26 variables chosen in Phase III

E_{rA}	v_{rA}	E_{rB}	v_{rB}	E_{rC}	v_{rC}	E_{rD}	v_{rD}	k_{rA}	D	v_u	E_u	h_u	k_u	v_l	E_l	h_l	k_l	P_l	P_s	q	t	h_r	W_p	k_{rC}	k_{rBD}
1.5	0.22	3	0.18	1.5	0.22	2.95	0.38	1	13500	0.21	2.38	1000	21	0.21	2.38	750	2.9	Ceramic	16/30	100	Slickwater	120	C	1	100
1.5	0.22	3	0.18	6	0.26	1.5	0.21	800	8000	0.38	3.55	20	1.8	0.38	3.55	100	23	Sand	40/70	100	Slickwater	120	C	1	100
1.5	0.22	3	0.23	1.5	0.26	1.5	0.21	800	8000	0.38	3.55	20	21	0.21	2.38	750	2.9	Ceramic	16/30	45	X-linked	550	A	800	10
1.5	0.22	3	0.23	6	0.22	2.95	0.38	1	13500	0.21	2.38	1000	1.8	0.38	3.55	100	23	Sand	40/70	45	X-linked	550	A	800	10
1.5	0.22	3.6	0.18	1.5	0.26	1.5	0.21	800	13500	0.21	2.38	1000	1.8	0.38	3.55	100	2.9	Ceramic	16/30	45	X-linked	550	A	1	100
1.5	0.22	3.6	0.18	6	0.22	2.95	0.38	1	8000	0.38	3.55	20	21	0.21	2.38	750	23	Sand	40/70	45	X-linked	550	A	1	100
1.5	0.22	3.6	0.23	1.5	0.22	2.95	0.38	1	8000	0.38	3.55	20	1.8	0.38	3.55	100	2.9	Ceramic	16/30	100	Slickwater	120	C	800	10
1.5	0.22	3.6	0.23	6	0.26	1.5	0.21	800	13500	0.21	2.38	1000	21	0.21	2.38	750	23	Sand	40/70	100	Slickwater	120	C	800	10
1.5	0.26	3	0.18	1.5	0.26	1.5	0.38	1	8000	0.38	2.38	1000	1.8	0.38	2.38	750	23	Sand	16/30	45	X-linked	120	C	800	10
1.5	0.26	3	0.18	6	0.22	2.95	0.21	800	13500	0.21	3.55	20	21	0.21	3.55	100	2.9	Ceramic	40/70	45	X-linked	120	C	800	10
1.5	0.26	3	0.23	1.5	0.22	2.95	0.21	800	13500	0.21	3.55	20	1.8	0.38	2.38	750	23	Sand	16/30	100	Slickwater	550	A	1	100
1.5	0.26	3	0.23	6	0.26	1.5	0.38	1	8000	0.38	2.38	1000	21	0.21	3.55	100	2.9	Ceramic	40/70	100	Slickwater	550	A	1	100
1.5	0.26	3.6	0.18	1.5	0.22	2.95	0.21	800	8000	0.38	2.38	1000	21	0.21	3.55	100	23	Sand	16/30	100	Slickwater	550	A	800	10
1.5	0.26	3.6	0.18	6	0.26	1.5	0.38	1	13500	0.21	3.55	20	1.8	0.38	2.38	750	2.9	Ceramic	40/70	100	Slickwater	550	A	800	10
1.5	0.26	3.6	0.23	1.5	0.26	1.5	0.38	1	13500	0.21	3.55	20	21	0.21	3.55	100	23	Sand	16/30	45	X-linked	120	C	1	100
1.5	0.26	3.6	0.23	6	0.22	2.95	0.21	800	8000	0.38	2.38	1000	1.8	0.38	2.38	750	2.9	Ceramic	40/70	45	X-linked	120	C	1	100
6	0.22	3	0.18	1.5	0.26	2.95	0.21	1	8000	0.21	3.55	1000	1.8	0.21	3.55	750	23	Ceramic	40/70	45	Slickwater	550	C	800	100
6	0.22	3	0.18	6	0.22	1.5	0.38	800	13500	0.38	2.38	20	21	0.38	2.38	100	2.9	Sand	16/30	45	Slickwater	550	C	800	100
6	0.22	3	0.23	1.5	0.22	1.5	0.38	800	13500	0.38	2.38	20	1.8	0.21	3.55	750	23	Ceramic	40/70	100	X-linked	120	A	1	10
6	0.22	3	0.23	6	0.26	2.95	0.21	1	8000	0.21	3.55	1000	21	0.38	2.38	100	2.9	Sand	16/30	100	X-linked	120	A	1	10
6	0.22	3.6	0.18	1.5	0.22	1.5	0.38	800	8000	0.21	3.55	1000	21	0.38	2.38	100	23	Ceramic	40/70	100	X-linked	120	A	800	100
6	0.22	3.6	0.18	6	0.26	2.95	0.21	1	13500	0.38	2.38	20	1.8	0.21	3.55	750	2.9	Sand	16/30	100	X-linked	120	A	800	100
6	0.22	3.6	0.23	1.5	0.26	2.95	0.21	1	13500	0.38	2.38	20	21	0.38	2.38	100	23	Ceramic	40/70	45	Slickwater	550	C	1	10
6	0.22	3.6	0.23	6	0.22	1.5	0.38	800	8000	0.21	3.55	1000	1.8	0.21	3.55	750	2.9	Sand	16/30	45	Slickwater	550	C	1	10
6	0.26	3	0.18	1.5	0.22	1.5	0.21	1	13500	0.38	3.55	1000	21	0.38	3.55	750	2.9	Sand	40/70	100	X-linked	550	C	1	10
6	0.26	3	0.18	6	0.26	2.95	0.38	800	8000	0.21	2.38	20	1.8	0.21	2.38	100	23	Ceramic	16/30	100	X-linked	550	C	1	10
6	0.26	3	0.23	1.5	0.26	2.95	0.38	800	8000	0.21	2.38	20	21	0.38	3.55	750	2.9	Sand	40/70	45	Slickwater	120	A	800	100
6	0.26	3	0.23	6	0.22	1.5	0.21	1	13500	0.38	3.55	1000	1.8	0.21	2.38	100	23	Ceramic	16/30	45	Slickwater	120	A	800	100
6	0.26	3.6	0.18	1.5	0.26	2.95	0.38	800	13500	0.38	3.55	1000	1.8	0.21	2.38	100	2.9	Sand	40/70	45	Slickwater	120	A	1	10
6	0.26	3.6	0.18	6	0.22	1.5	0.21	1	8000	0.21	2.38	20	21	0.38	3.55	750	23	Ceramic	16/30	45	Slickwater	120	A	1	10
6	0.26	3.6	0.23	1.5	0.22	1.5	0.21	1	8000	0.21	2.38	20	1.8	0.21	2.38	100	2.9	Sand	40/70	100	X-linked	550	C	800	100
6	0.26	3.6	0.23	6	0.26	2.95	0.38	800	13500	0.38	3.55	1000	21	0.38	3.55	750	23	Ceramic	16/30	100	X-linked	550	C	800	100

Table A.6: Factorial design table for the 26 variables chosen in Phase III

E_{rA}	v_{rA}	E_{rB}	v_{rB}	E_{rC}	v_{rC}	E_{rD}	v_{rD}	k_{rA}	D	v_u	E_u	h_u	k_u	v_l	E_l	h_l	k_l	P_t	P_s	q	t	h_r	W_p	k_{rC}	k_{rBD}	
-1	-1	-1	-1	-1	-1	1	1	-1	1	-1	-1	1	1	-1	-1	1	-1	1	1	1	-1	-1	1	-1	1	
-1	-1	-1	-1	1	1	-1	-1	1	-1	1	1	-1	-1	1	1	-1	1	-1	-1	-1	1	-1	-1	1	-1	1
-1	-1	-1	1	-1	1	-1	-1	1	-1	1	1	-1	1	-1	-1	1	-1	1	1	-1	1	1	-1	1	-1	-1
-1	-1	-1	1	1	-1	1	1	-1	1	-1	-1	1	-1	1	1	-1	1	-1	-1	-1	1	1	-1	1	-1	-1
-1	-1	1	-1	-1	1	-1	-1	1	1	-1	-1	1	-1	1	1	-1	-1	1	1	-1	1	1	-1	-1	-1	1
-1	-1	1	-1	1	-1	1	1	-1	-1	1	1	-1	1	-1	-1	1	1	-1	-1	-1	1	1	-1	-1	-1	1
-1	-1	1	1	-1	-1	1	1	-1	-1	1	1	-1	-1	1	1	-1	-1	1	1	1	-1	-1	1	1	-1	-1
-1	-1	1	1	1	1	-1	-1	1	1	-1	-1	1	1	-1	-1	1	1	-1	-1	1	-1	-1	1	1	-1	-1
-1	1	-1	-1	-1	1	-1	1	-1	-1	1	-1	1	-1	1	-1	1	1	-1	1	-1	1	-1	1	1	-1	-1
-1	1	-1	-1	1	-1	1	-1	1	1	-1	1	-1	1	-1	1	-1	-1	1	-1	-1	1	-1	1	1	-1	-1
-1	1	-1	1	-1	-1	1	-1	1	-1	1	-1	1	1	-1	1	-1	-1	1	-1	1	-1	1	-1	1	-1	-1
-1	1	-1	1	1	-1	1	-1	1	-1	1	-1	-1	-1	1	-1	1	-1	1	-1	1	-1	1	-1	1	-1	-1
-1	1	1	-1	1	1	-1	1	-1	1	-1	1	-1	-1	1	-1	1	-1	1	-1	1	-1	1	-1	1	-1	-1
-1	1	1	1	-1	1	-1	1	-1	1	-1	1	-1	1	-1	1	-1	1	-1	1	-1	1	-1	1	-1	1	-1
-1	1	1	1	1	1	-1	1	-1	1	-1	1	-1	1	-1	1	-1	1	-1	-1	-1	1	1	1	1	-1	-1
1	-1	-1	-1	-1	1	1	-1	-1	-1	-1	1	1	-1	-1	1	1	1	1	-1	-1	-1	1	1	1	1	1
1	-1	-1	-1	1	-1	-1	1	1	1	1	-1	-1	1	1	-1	-1	-1	-1	1	-1	-1	1	1	1	1	1
1	-1	-1	1	-1	-1	-1	1	1	-1	-1	1	1	1	1	-1	-1	-1	-1	1	1	1	-1	-1	-1	-1	-1
1	-1	-1	1	1	1	-1	-1	-1	-1	-1	1	1	1	1	-1	-1	-1	-1	1	1	1	1	-1	-1	-1	-1
1	-1	1	-1	-1	-1	-1	1	1	-1	-1	1	1	-1	-1	1	1	-1	-1	1	1	1	-1	-1	1	1	1
1	-1	1	-1	1	1	-1	-1	-1	1	1	-1	-1	-1	-1	1	1	-1	-1	1	-1	-1	1	1	-1	-1	-1
1	-1	1	1	-1	-1	-1	1	1	-1	-1	1	1	-1	-1	1	1	-1	-1	1	-1	-1	1	1	-1	-1	-1
1	-1	1	1	1	1	-1	-1	-1	1	1	1	1	1	-1	-1	-1	-1	1	1	1	1	1	1	1	-1	-1
1	1	-1	-1	1	1	1	1	1	-1	-1	-1	-1	-1	-1	-1	-1	1	1	1	1	1	1	1	1	-1	-1
1	1	-1	1	-1	1	1	1	1	-1	-1	-1	-1	1	1	1	1	-1	-1	-1	-1	-1	-1	-1	1	1	1
1	1	-1	1	1	-1	-1	-1	-1	1	1	1	1	-1	-1	-1	-1	1	1	1	1	-1	-1	-1	-1	1	1
1	1	1	-1	-1	1	1	1	1	1	1	1	1	-1	-1	-1	-1	-1	-1	-1	-1	-1	-1	-1	-1	-1	-1
1	1	1	1	1	-1	-1	-1	-1	-1	-1	-1	-1	-1	-1	-1	-1	-1	-1	-1	-1	1	1	1	1	1	1
1	1	1	1	1	1	1	1	1	1	1	1	1	1	1	1	1	1	1	1	1	1	1	1	1	1	1

